DNA 5379F

MATERIAL PROPERTIES OF NEVADA TEST SITE TUFF AND GROUT

Terra Tek, Inc.
420 Wakara Way
Salt Lake City, Utah 84108

1 May 1980

Final Report for Period 1 September 1978—31 August 1979

CONTRACT No. DNA 001-78-C-0395

THIS WORK SPONSORED BY THE DEFENSE NUCLEAR AGENCY
UNDER RDT&E RMSS CODE K400078462 J45GAXYX97310 H2590D.

Prepared for
Director
DEFENSE NUCLEAR AGENCY
Washington, D. C. 20305

Destroy this report when it is no longer needed. Do not return to sender.

PLEASE NOTIFY THE DEFENSE NUCLEAR AGENCY, ATTN: STTI, WASHINGTON, D.C. 20305, IF YOUR ADDRESS IS INCORRECT, IF YOU WISH TO BE DELETED FROM THE DISTRIBUTION LIST, OR IF THE ADDRESSEE IS NO LONGER EMPLOYED BY YOUR ORGANIZATION.

UNCLASSIFIED

SECURITY CLASSIFICATION OF THIS PAGE *(When Data Entered)*

19 REPORT DOCUMENTATION PAGE		READ INSTRUCTIONS BEFORE COMPLETING FORM
1. REPORT NUMBER (18) DNA 5379F	2. GOVT ACCESSION NO. AD-A094 220	3. RECIPIENT'S CATALOG NUMBER
4. TITLE *(and Subtitle)* (6) MATERIAL PROPERTIES OF NEVADA TEST SITE TUFF AND GROUT		5. TYPE OF REPORT & PERIOD COVERED (9) Final Report for Period 1 Sep 78—31 Aug 79
		6. PERFORMING ORG. REPORT NUMBER (14) TR-80-35
7. AUTHOR(s) (10) S. W. Butters, J. F. Patterson, J. M. Gronseth		8. CONTRACT OR GRANT NUMBER(s) (15) DNA 001-78-C-0395
9. PERFORMING ORGANIZATION NAME AND ADDRESS Terra Tek, Inc. 420 Wakara Way Salt Lake City, Utah 84108 (17) X973		10. PROGRAM ELEMENT, PROJECT, TASK AREA & WORK UNIT NUMBERS (16) Subtask J45GAXYX973-10
11. CONTROLLING OFFICE NAME AND ADDRESS Director Defense Nuclear Agency Washington, D.C. 20305 (12) 1210		12. REPORT DATE (11) 1 May 1980
		13. NUMBER OF PAGES 112
14. MONITORING AGENCY NAME & ADDRESS *(if different from Controlling Office)*		15. SECURITY CLASS *(of this report)* UNCLASSIFIED
		15a. DECLASSIFICATION/DOWNGRADING SCHEDULE

16. DISTRIBUTION STATEMENT *(of this Report)*

Approved for public release; distribution unlimited.

17. DISTRIBUTION STATEMENT *(of the abstract entered in Block 20, if different from Report)*

18. SUPPLEMENTARY NOTES

This work sponsored by the Defense Nuclear Agency under RDT&E RMSS Code K400078462 J45GAXYX97310 H2590D.

19. KEY WORDS *(Continue on reverse side if necessary and identify by block number)*

Nuclear Test	Tuff	Creep
Hydrostatic	Grout	
Uniaxial Strain	Pressure	
Triaxial Compression	Load	

20. ABSTRACT *(Continue on reverse side if necessary and identify by block number)*

The mechanical and physical properties of tuffs and grouts from the Nevada Test Site were determined. The tests performed include unconfined compression, triaxial compression, and uniaxial strain tests. More specialized tests such as cycled burst tests to study the phenomena of residual stress buildup and triaxial creep tests to study the viscoelastic properties of tuffs and grouts were performed. The relationships between fracturing and ultrasonic velocities were also investigated.

DD FORM 1 JAN 73 1473 EDITION OF 1 NOV 65 IS OBSOLETE

UNCLASSIFIED 38925

SECURITY CLASSIFICATION OF THIS PAGE *(When Data Entered)*

PREFACE

The authors would like to express their thanks for the guidance of Mr. J. W. LaComb (DNA, Mercury, Nevada). They would also like to thank Mr. A. W. Rae and Mr. P. Flynn for their assistance in conducting the laboratory tests and to Ms. J. Grant, Ms. C. Stevenson and Ms. J. Ruff for their effort in preparing the manuscript.

The mechanical and physical properties of various geological and man-made materials have been determined for the Defense Nuclear Agency Field Command. The testing was performed in support of the Nevada Test Site nuclear test program and covered the period from 1 September 1978 to 31 August 1979. The contract number was DNA001-78-C-0395 and Mr. J. W. LaComb was the Contracting Office Representative.

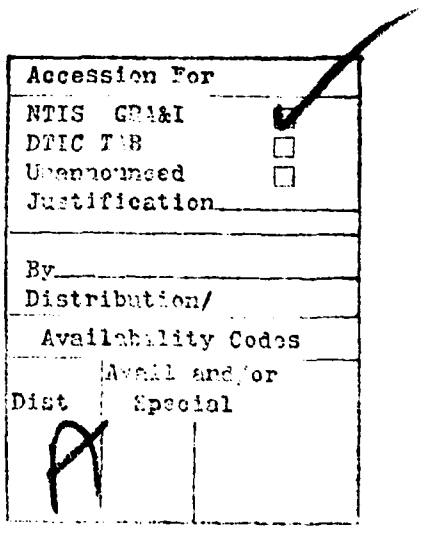

TABLE OF CONTENTS

LIST OF ILLUSTRATIONS

LIST OF TABLES

INTRODUCTION

The Defense Nuclear Agency (DNA) requires a knowledge of the mechanical and physical properties of the materials, both geological and man-made, which are used in conjunction with its underground testing program at the Nevada Test Site. This report summarizes the materials testing program conducted by Terra Tek from September 1978 through August 1979 for the Test Directorate, Field Command, DNA. The purpose of this testing program was materials characterization to be used in containment evaluation studies.

The mechanical properties of tuffs and grouts from various locations at the Nevada Test Site (NTS) were determined using standardized tests such as unconfined compression, triaxial compression and uniaxial strain tests, as well as more specialized tests to study creep behavior, residual stress buildup and ultrasonic velocity/fracturing interaction.

The areas and studies for which tuff and grout were characterized were:

Section I

- IA. U12n.11 Area
- IB. U12n.12 Area
- IC. U12e.20, U12G, and "TS" Samples

Section II

- Huron King Grout

Section III

- Residual Stress Studies

Section IV

- Time Dependent (Creep) Behavior

Section V

- Ultrasonic Velocity/Fracturing Interaction

SECTION I

MECHANICAL AND PHYSICAL PROPERTIES OF VARIOUS TUFFS

The mechanical and physical properties of tuffs from various locations at the NTS were determined. Mechanical properties were determined using unconfined compression tests, triaxial compression tests and uniaxial strain tests. The physical properties which were determined include wet and dry bulk densities, grain densities, moisture content by wet weight, porosity, percent saturation and percent air voids. The velocities of compressional and shear waves through tuff specimens were determined using ultrasonic techniques.

The results of the tests performed on these materials are given in the appropriate sections and the raw data from the individual tests are included as appendices. As a note, the "measured permanent compaction" reported throughout the text is the permanent volume decrease (percent of original volume) resulting from a uniaxial strain test to a confining pressure of 4 kilobars.

Sample handling and preparation techniques as well as the procedures which were followed for the mechanical properties, physical properties, and ultrasonic velocity determinations are described in Appendix D.

SECTION IA

AREA U12n.11 TUFF

U12n.11 UG-1 Tuffs

Table 1 shows the physical properties, measured permanent compactions, and ultrasonic velocities determined on specimens from drill hole U12n.11 UG-1. Figure 1 is a plot of measured permanent compaction versus location in hole U12n.11 UG-1. The individual test results are given in Appendix A.

U12n.11 GI Series

Table 2 gives the physical properties, measured permanent compactions and ultrasonic velocities determined on U12n.11 GI series tuffs. The individual test results are also given in Appendix A.

TABLE 1

Physical Properties, Measured Permanent Compaction, and Ultrasonic Velocities on Samples from U12n.11 UG-1

DRILL HOLE FOOTAGE (M/FT)	DENSITY (gm/cc) AS-RECEIVED	DRY	GRAIN	WATER BY WET WEIGHT (%)	POROSITY (%)	SATURATION (%)	CALC. AIR VOIDS (%)	MEAS. PERMANENT COMP. (%)	VELOCITY (km/sec) LONG	SHEAR
U12n.11 UG-1										
153.3/503	1.78	1.32	2.42	25.9	45.7	100.0	0.0	2.0	2.73	1.09
159.1/522	1.76	1.38	2.36	21.5	41.4	91.2	3.6	3.6	2.80	1.25
167.6/550	1.86	1.55	2.33	16.5	33.3	92.1	2.6	3.2	3.48	1.84
174.7/573	1.62	1.28	2.36	21.0	45.6	74.7	11.6	9.3	2.81	1.17
182.9/600	1.93	1.63	2.43	15.8	33.2	91.4	2.9	0.9	2.89	1.41
191.4/628	1.98	1.67	2.48	15.6	32.8	94.4	1.8	1.2	2.76	1.25
198.1/650	1.89	1.58	2.36	16.7	33.2	95.5	1.5	2.4	3.08	1.48
206.0/676	1.91	1.56	2.44	18.0	35.9	95.8	1.5	1.5*	3.17	1.50
213.1/699	1.93	1.60	2.33	17.2	31.5	100.0	0.0	2.3	3.29	1.68
220.7/724	1.88	1.54	2.45	18.2	37.3	92.0	3.0	3.2	2.95	1.34
228.3/749	1.91	1.58	2.43	17.7	35.1	96.6	1.2	3.4	2.78	1.24
235.0/774	1.92	1.60	2.43	16.9	34.3	94.9	1.7	1.9	3.05	1.50
243.5/799	1.97	1.67	2.39	15.4	30.3	99.8	0.1	1.9	3.53	1.76
250.9/823	1.84	1.49	2.43	19.2	38.7	91.3	3.4	4.6	2.53	1.06
258.2/847	1.81	1.37	2.39	24.1	42.6	100.0	0.0	0.9	2.67	1.22
328.9/874	1.77	1.35	2.38	23.9	43.2	98.0	0.9	1.9	2.85	1.46
274.3/900	1.94	1.55	2.52	19.9	38.6	99.9	0.0	0.2	2.77	1.25
281.3/923	1.76	1.36	2.38	23.6	43.0	97.5	1.1	3.0	2.51	1.12
288.6/947	1.91	1.56	2.30	18.3	32.3	100.0	0.0	4.5	2.70	1.30
296.9/974	1.92	1.61	2.47	16.0	34.6	88.8	3.9	1.7	3.15	1.55
305.1/1001	1.87	1.54	2.34	17.9	34.4	97.6	0.8	5.5	2.95	1.53

* Force limit

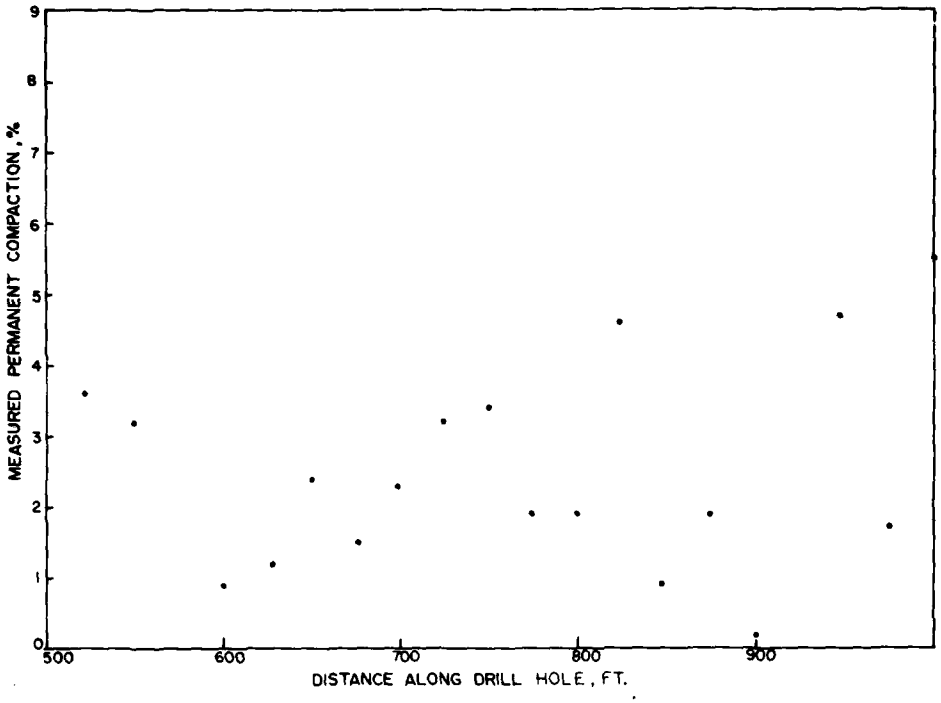

Figure 1. Measured permanent compaction versus drill hole footage for U12n.11 UG-1.

TABLE 2

Physical Properties, Measured Permanent Compaction, and Ultrasonic Velocities on Samples from the U12n.11 GI Series

SAMPLE DESIGNATION	DENSITY (gm/cc)			WATER BY WET WEIGHT (%)	POROSITY (%)	SATURATION (%)	CALC. AIR VOIDS (%)	MEAS. PERMANENT COMP. (%)	VELOCITY (km/sec)	
	AS-RECEIVED	DRY	GRAIN						LONG	SHEAR
U12n.11										
GI#1	1.94	1.60	2.39	17.7	33.2	100.0	0.0	---	3.69	2.15
GI#2	1.93	1.56	2.45	19.3	36.4	100.0	0.0	1.8	3.13	1.42
GI#3	1.86	1.52	2.40	18.1	36.5	92.2	2.8	2.1	2.95	1.43
GI#4	1.98	1.70	2.49	14.2	31.8	88.6	3.6	3.2	3.03	1.29
GI#5	1.91	1.53	2.52	19.9	39.3	96.6	1.3	7.7	2.94	1.42
GI#6	1.87	1.55	2.41	17.4	35.9	90.5	3.4	0.9	3.08	1.55
GI#7	1.75	1.32	2.39	24.4	44.6	95.6	2.0	2.2	2.46	1.04
GI#8	1.93	1.62	2.43	15.9	33.2	92.6	2.5	2.2	2.90	1.49
GI#9	1.87	1.53	2.42	18.0	36.7	91.9	2.9	3.4	2.96	1.47
GI#10	1.78	1.42	2.39	20.0	40.5	88.2	4.8	2.2	3.00	1.52
GI#11	1.94	1.61	2.45	17.1	34.5	96.5	1.2	2.3	2.95	1.41
GI#12	1.98	1.67	2.44	15.7	31.6	98.4	0.5	2.6	2.99	1.47
GI#13	1.90	1.54	2.45	18.7	37.0	96.3	1.4	3.7	2.67	1.26

SECTION IB

AREA U12n.12 TUFF

The physical properties, measured permanent compactions and ultrasonic velocities determined on cores from drill hole U12n.12 UG-1 are given in Table 3. A plot of measured permanent compactions as a function of position in the drill hole is shown in Figure 2. Results of the individual tests are given in Appendix B.

As noted in Table 3, several specimens contained gravel inclusions which made it virtually impossible to perform a uniaxial strain test without puncturing the urethane jackets. A picture of one of these specimens is shown in Figure 3.

To assist in understanding the shear strength of tuffs as suggested by the uniaxial strain curves versus triaxial compression tests, triaxial compression tests (at 4 kbars confining pressure) were run on specimens which had been tested in uniaxial strain to 4 kbars. The maximum stress differences developed during the triaxial compression tests were plotted as a function of the stress difference at 4 kbars from the uniaxial strain tests (Figure 4). As can be seen from this plot, the failure strength for the triaxial compression tests, even after the sample had been subjected to uniaxial strain loading, were greater by about 10 percent than the stress difference at 4 kbars for the uniaxial strain tests.

TABLE 3

Physical Properties, Ultrasonic Velocities and Measured Permanent Compaction on Samples from U12n.12 UG-1

DRILL HOLE (M)	DRILL HOLE (ft)	DENSITY (gm/cc) AS-RECEIVED	DENSITY (gm/cc) DRY	DENSITY (gm/cc) GRAIN	WATER BY WET WEIGHT (%)	POROSITY (%)	SATURATION (%)	CALC. AIR VOIDS (%)	MEAS. PERMANENT COMP. (%)	VELOCITY (km/sec) LONG	VELOCITY (km/sec) SHEAR
61.9	203	1.79	1.38	2.38	23.0	41.9	98.1	0.8	6.8	2.42	1.03
65.6	215	1.81	1.41	2.44	22.0	42.1	94.8	2.2	2.3	2.59	1.24
69.3	227	1.88	1.52	2.41	19.0	37.1	96.3	1.4	4.2	3.35	1.77
72.5	238	1.88	1.52	2.42	19.2	37.1	97.1	1.1	1.5	2.77	1.47
78.8	252	1.91	1.59	2.41	16.8	34.1	94.0	2.0	2.9	2.99	1.46
81.2	267	1.85	1.44	2.48	22.2	41.9	98.1	0.8	1.1	2.84	1.29
83.3	273	1.99	1.73	2.39	13.3	27.6	96.1	1.1	--	3.18	1.75
87.7	288	1.98	1.65	2.51	16.6	34.2	96.4	1.2	1.3	2.95	1.38
90.9	298	1.83	1.43	2.47	21.9	42.0	95.1	2.1	7.4	2.63	1.14
94.6	310	1.81	1.40	2.44	22.4	42.5	95.1	2.1	2.1	2.87	1.34
99.2	325	1.86	1.50	2.40	19.7	37.8	96.5	1.3	--	2.90	1.47
102.5	336	1.84	1.46	2.45	20.8	40.5	94.5	2.2	1.9	3.06	1.48
107.8	354	2.08	1.90	2.37	8.4	19.6	89.5	2.1	2.8	2.84	1.42
112.0	367	1.99	1.71	2.39	14.0	28.2	98.7	0.4	0.7	3.06	1.52
114.8	377	1.91	1.59	2.42	16.7	34.3	92.7	2.5	2.5	3.06	1.64
118.1	387	1.95	1.65	2.39	15.5	31.0	97.7	0.7	**	3.60	1.83
122.4	402	2.08	1.90	2.37	8.6	19.8	90.2	1.9	0.2	4.32	2.37
127.2	417	1.82	1.43	2.44	21.6	41.4	95.2	2.0	1.5	2.90	1.25
131.1	430	1.85	1.47	2.48	20.7	41.0	93.3	2.8	0.3	2.83	1.30
135.3	444	1.96	1.65	2.41	15.9	31.7	98.7	0.4	1.9	3.21	1.52
138.4	454	1.89	1.57	2.39	17.5	34.4	96.3	1.3	0.6	3.26	1.71
142.3	467	1.95	1.65	2.44	15.4	32.4	92.6	2.4	1.6	2.99	1.40
145.7	478	2.05	1.76	2.49	13.8	29.2	97.0	0.9	0.2	3.25	1.56
150.6	494	2.03	1.78	2.41	12.4	26.2	95.5	1.2	1.6	3.62	1.88
153.6	504	1.95	1.65	2.43	15.4	31.9	94.3	1.8	2.4	3.14	1.61
155.8	511	1.92	1.60	2.43	16.8	34.3	94.1	2.0	1.3	4.06	2.21
159.1	522	2.00	1.74	2.39	13.1	27.4	95.7	1.2	0.4*	3.41	1.92
162.2	532	1.87	1.51	2.40	19.4	37.2	97.9	0.8	1.1	3.12	1.32
164.9	541	1.97	1.65	2.49	16.2	33.6	95.5	1.5	1.7	2.96	1.33
167.3	549	1.94	1.63	2.41	15.9	32.4	95.5	1.5	1.7*	3.48	1.73
170.7	560	1.89	1.52	2.42	19.3	37.1	98.4	0.6	1.4	2.70	--
174.3	572	1.93	1.59	2.48	17.7	35.8	95.7	1.5	1.6	2.93	1.30
175.6	576	1.86	1.46	2.46	21.4	40.6	97.9	0.8	3.1	2.69	1.29
178.0	584	1.94	1.59	2.46	18.1	35.6	98.3	0.6	0.6	2.65	1.14
180.4	592	1.87	1.50	2.43	20.1	38.4	98.0	0.8	1.9	2.85	1.35
183.5	602	1.96	1.63	2.49	16.8	34.7	94.6	1.9	2.1	3.08	1.48
185.6	609	2.03	1.74	2.47	14.1	29.5	96.8	1.0	1.8	3.27	1.52
188.4	618	1.97	1.70	2.42	13.9	29.9	91.8	2.5	0.7*	3.75	2.06
190.5	625	2.06	1.86	2.36	9.7	21.2	94.4	1.2	1.0*	4.17	2.19
193.9	636	1.89	1.55	2.48	18.3	37.7	91.6	3.2	1.4	3.27	1.73
196.6	645	1.91	1.59	2.38	16.9	33.4	96.8	1.1	4.1	2.89	1.32
199.6	655	1.81	1.40	2.47	22.7	43.2	95.4	2.0	1.6	2.68	1.31
202.7	665	1.97	1.69	2.39	14.5	29.6	96.2	1.1	0.4*	3.60	1.73
205.7	675	1.94	1.59	2.50	17.8	36.3	95.3	1.7	2.1	3.04	--
209.1	686	1.92	1.56	2.46	18.8	36.6	98.4	0.6	1.9	2.90	1.30
212.1	696	1.85	1.45	2.44	21.7	40.6	99.0	0.4	2.1	2.61	1.13
216.4	710	1.95	1.61	2.52	17.5	36.2	94.1	2.1	2.0	2.84	1.24
219.8	721	1.95	1.59	2.42	18.2	34.1	100.0	0.0	1.9	2.64	1.21
223.1	732	1.97	1.64	2.41	16.7	32.0	100.0	0.0	2.1	3.29	1.47
225.6	740	1.89	1.54	2.41	18.6	36.1	97.3	1.0	2.0	3.80	1.61
228.0	748	1.88	1.52	2.41	19.1	37.0	97.1	1.1	**	3.07	1.49
231.3	759	1.85	1.46	2.41	21.3	39.6	99.4	0.3	2.2	3.10	1.39

* Force limit

** Tests were unsuccessful because gravel in the samples punctured the jackets.

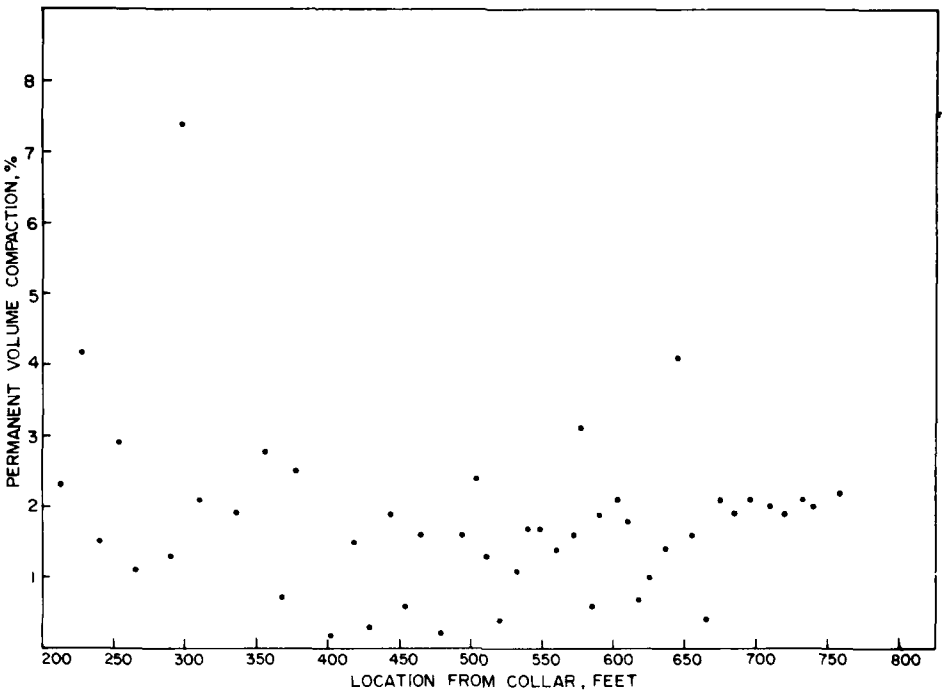

Figure 2. Uniaxial strain test permanent volume compaction versus drill hole footage for samples from U12n.12 UG-1.

Figure 3. Photograph of specimen with gravel inclusions.

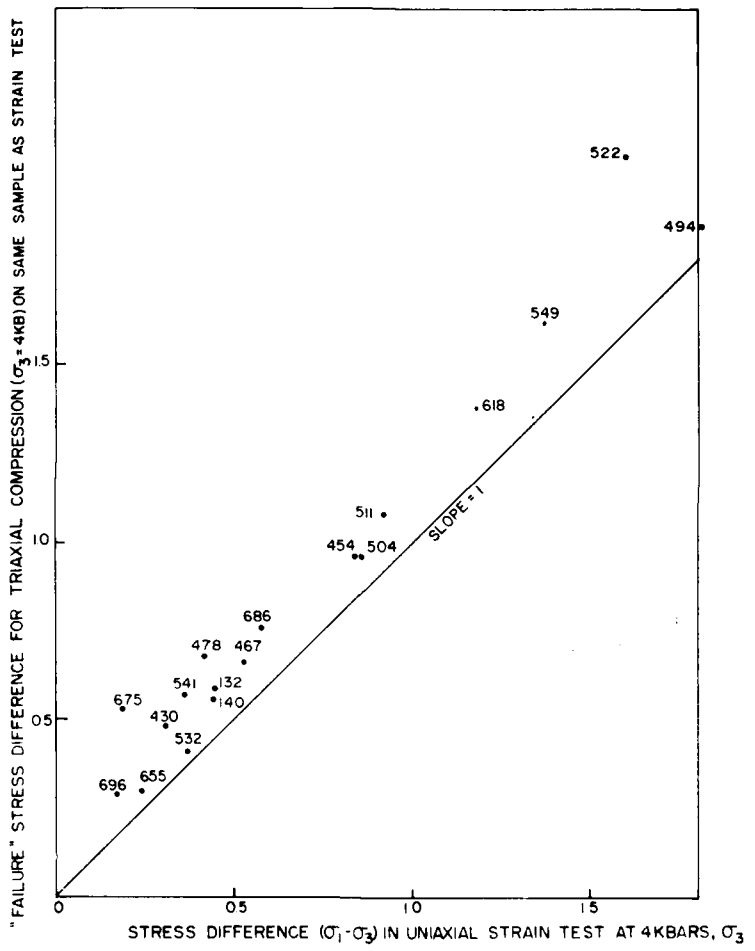

Figure 4. Stress difference of triaxial compression versus uniaxial strain test.

SECTION IC

MISCELLANEOUS CORE SAMPLES

U12e.20 DNRE#3, #5, #6 and U12G DNEX#3, #4 Tuffs

The physical properties, measured permanent compaction, ultrasonic velocities and gas permeabilities for the aforementioned tuffs are given in Table 4. Permeabilities were determined on dry specimens at steady state conditions. The results of the individual tests are given in Appendix C.

TS-1-15 Tuffs

Table 5 gives the physical properties, measured permanent compactions and ultrasonic velocities determined on TS-1-15 tuffs. The individual test results are given in Appendix C.

TABLE 4

Physical Properties, Measured Permanent Compaction, Ultrasonic Velocities and Permeabilities for Miscellaneous Tuffs

DRILL HOLE FOOTAGE (M/FT)	DENSITY (gm/cc) AS-RECEIVED	DRY	GRAIN	WATER BY WET WEIGHT (%)	POROSITY (%)	SATURATION (%)	CALC. AIR VOIDS (%)	MEAS. PERMANENT COMP. (%)	VELOCITY (km/sec) LONG	SHEAR	DRY PERMEABILITY (GAS) mdarcy
U12e.20 DNRE#3											
71.1/233	1.74	1.27	2.41	26.8	47.3	98.6	0.67	1.65	2.28		97.74
72.3/237	2.35	2.67	2.50	3.6	9.4	89.8	0.95	0.40	5.47	3.16	0.0035
80.5/264	2.01	1.73	2.46	14.0	29.8	94.0	1.77	2.10	3.26	1.65	0.325
81.4/267	1.95	1.62	2.46	16.7	33.8	96.5	0.17	1.40	3.69	1.40	6.43
84.5/277	2.05	1.74	2.55	15.2	31.7	97.9	0.65	2.30	2.65	1.02	0.345
U12e.20 DNRE#5											
68.9/226	1.79	1.36	2.45	24.0	44.4	97.0	1.33	2.24	2.55	0.98	3.28
70.5/231	1.78	1.35	2.40	24.0	43.6	97.9	0.91	2.10	2.28	0.83	0.922
76.9/252	1.77	1.36	2.40	23.6	43.6	96.2	1.65	2.00	2.41	0.81	69.42
78.4/257	1.83	1.45	2.36	20.7	38.7	97.6	0.91		2.61	1.15	6.79
U12e.20 DNRE#6											
46.4/152	1.92	1.57	2.53	18.4	38.0	93.2	2.58	2.00	1.85	0.51	278.29
32.6/107	1.85	1.45	2.47	21.8	41.4	97.4	1.07	1.70	1.59	0.43	4.10
U12G DNEX#3											
20.1/66	1.89	1.54	2.55	18.5	39.5	88.8	4.41	6.75	2.94	1.22	2.82
24.7/81	1.80	1.45	2.45	19.7	40.9	86.6	5.47	4.95	2.77	1.30	2.81
26.2/86	1.79	1.37	2.51	23.5	45.5	92.6	3.36	1.70	2.55	1.10	2.55
U12G DNEX#4											
93.3/306	1.92	1.56	2.61	18.6	40.1	88.6	4.59	3.20	2.36	1.18	10.37
94.6/310	1.88	1.53	2.58	18.6	40.5	86.6	5.44	4.80	2.81	1.35	7.78
95.8/314	1.81	1.39	2.58	23.3	46.4	91.0	4.18	2.00	2.81	1.57	0.255

TABLE 5

Physical Properties, Measured Permanent Compaction and Ultrasonic Velocities for TS-1-15 Tuffs

SAMPLE DESIGNATION	DENSITY (gm/cc) AS-RECEIVED	DRY	GRAIN	WATER BY WET WEIGHT (%)	POROSITY (%)	SATURATION (%)	CALC. AIR VOIDS (%)	MEAS. PERMANENT COMP. (%)	VELOCITY (km/sec) LONG	SHEAR
TS-1	1.90	1.59	2.38	16.2	33.1	93.1	2.3	1.0	2.95	1.48
TS-2	1.94	1.62	2.39	16.8	32.4	100.0	0.0	1.2	2.90	1.47
TS-3	1.96	1.67	2.40	14.6	30.3	94.6	1.6	1.3*	3.78	2.16
TS-4	1.93	1.58	2.47	18.2	36.1	97.3	1.0	1.4	2.70	1.18
TS-5	1.89	1.53	2.34	19.0	34.6	100.0	0.0	2.6	3.17	1.62
TS-6	2.04	1.78	2.47	13.0	28.1	94.0	1.7	1.6	2.87	1.31
TS-7	1.93	1.57	2.48	18.5	36.6	97.6	0.9	1.6	2.93	1.42
TS-8	1.88	1.55	2.35	17.4	33.9	96.5	1.2	2.0	3.10	1.62
TS-9	1.73	1.28	2.37	26.1	46.1	98.1	0.9	2.8	--	--
TS-10	1.91	1.59	2.40	16.7	33.7	94.6	1.8	1.0	3.14	1.46
TS-11	1.89	1.53	2.42	19.1	36.8	98.0	0.7	2.3	3.13	1.54
TS-12	1.80	1.42	2.42	21.3	41.5	92.5	3.1	2.7	2.91	1.12
TS-13	1.92	1.60	2.39	16.5	32.9	96.2	1.3	--	--	--
TS-14	1.95	1.61	2.35	17.3	31.4	100.0	0	1.8	2.91	1.41
TS-15	1.88	1.52	2.45	19.3	38.1	93.3	1.8	2.6	2.33	1.03

* Load Limit

SECTION II

HURON KING GROUT

A series of physical properties determinations, hydrostatic compression tests, uniaxial strain tests and ultrasonic velocity determinations were performed on Huron King grout [HK-SLR-SL-1(10)].

The physical properties, permanent compactions measured from uniaxial strain tests and ultrasonic velocities determined on specimens of Huron King grout are given in Table 6.

The results of the hydrostatic compression tests are given in Figures 5 to 7. As can be seen from these figures, the permanent compactions after hydrostatic compression were from 4 percent to 5 percent by volume. The volumetric strain at confining pressures of 4 kbars averaged 7 percent.

The results of the uniaxial strain tests are shown in Figures 8 to 11. As can be seen from these figures, the measured permanent compactions after the uniaxial strain tests ranged from 8.5 percent to 10 percent.

One problem that was encountered during these tests was that voids opened up on the surfaces of the specimens during testing and resulted in the specimen jackets leaking at the higher confining pressures. Pictures of tested specimens showing these voids are shown in Figures 12 and 13.

TABLE 6

Physical Properties, Measured Permanent Compaction and Ultrasonic Velocities for Huron King Grout

SAMPLE DESIGNATION	DENSITY (gm/cc)			WATER BY WET WEIGHT (%)	POROSITY (%)	SATURATION (%)	CALC. AIR VOIDS (%)	MEAS. PERMANENT COMP. (%)	VELOCITY (km/sec)	
	AS-RECEIVED	DRY	GRAIN						LONG	SHEAR
878-862	1.65	1.11	2.49	32.6	55.3	97.2	1.6	10.0	2.14	1.01
1032-995(4A)	1.72	1.18	2.61	31.2	54.7	98.2	1.0	8.4	2.15	1.07
1032-995(4)	1.67	1.16	2.91	30.7	60.2	85.1	9.0	9.1	2.13	1.07
Stage 2 1063-1103	1.77	1.26	2.94	28.7	57.1	89.2	6.2	9.0	--	--

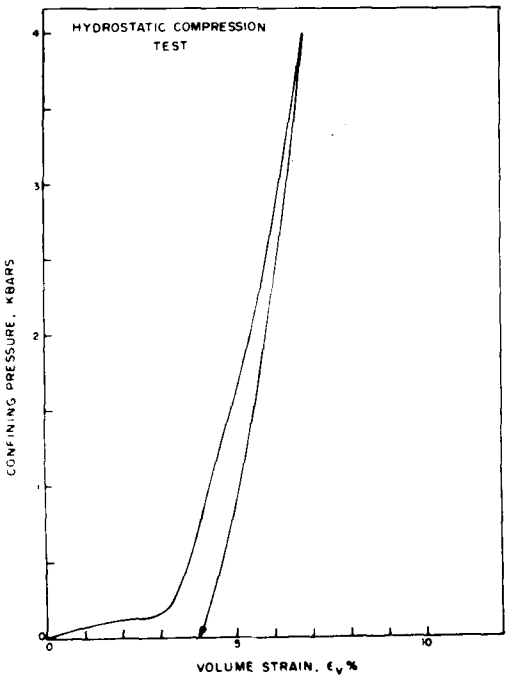

Figure 5. Hydrostatic compression test stress-strain response on Huron King grout HK SLR SL1 10, 878-862.

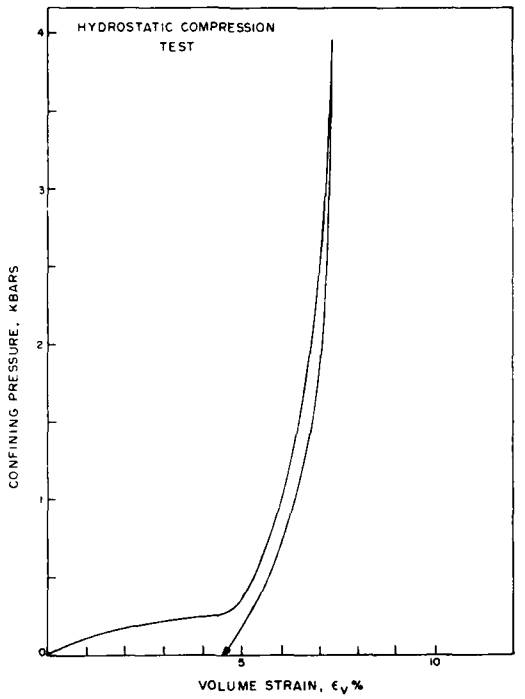

Figure 6. Hydrostatic compression test stress-strain response on Huron King grout HK SLR SL1 10, 1032-995(4A).

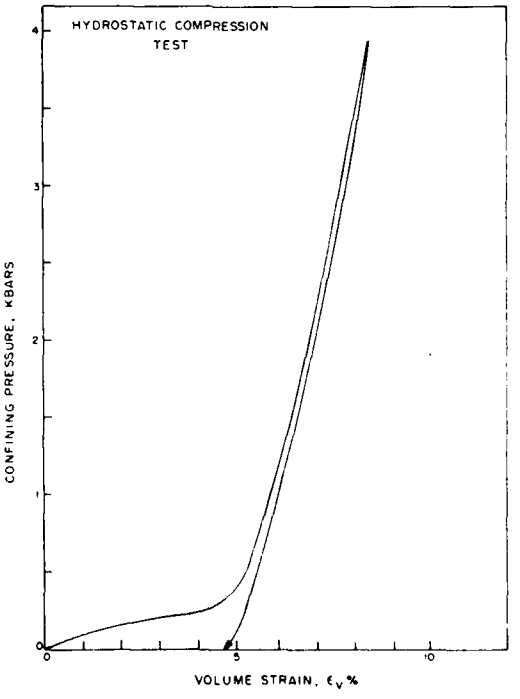

Figure 7. Hydrostatic compression test stress-strain response on Huron King grout HK SLR SL1 10, 1032-995(4).

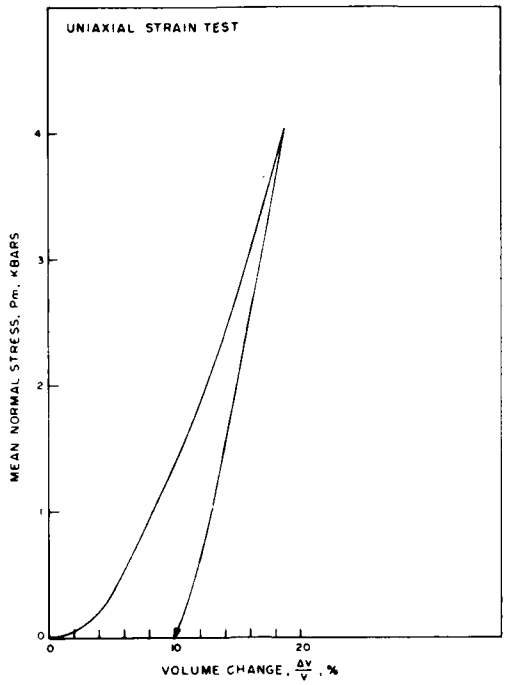

Figure 8a. Uniaxial strain test stress-strain response on Huron King grout HK SLR SL1 10, 878-862.

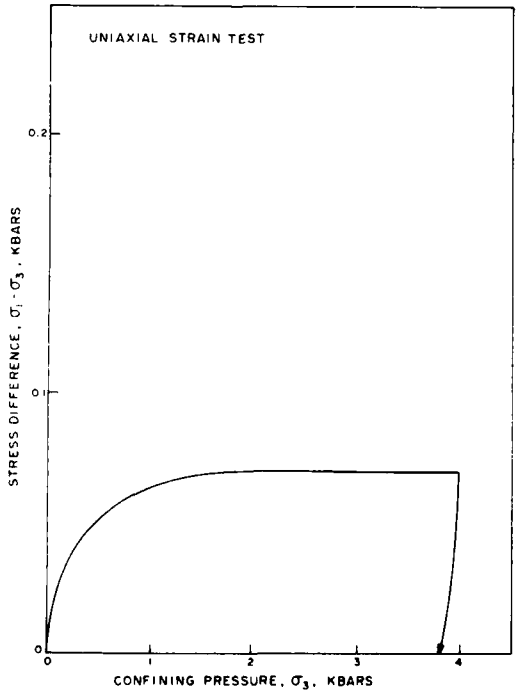

Figure 8b. Uniaxial strain test stress-stress response on Huron King grout HK SLR SL1 10, 878-862.

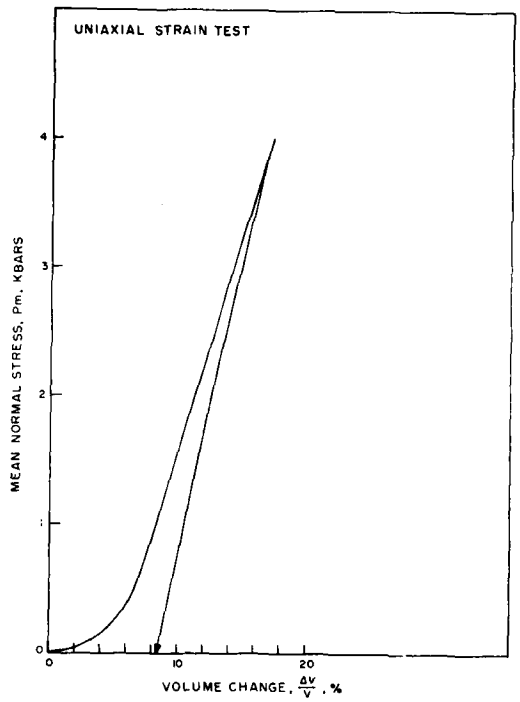

Figure 9a. Uniaxial strain test stress-strain response on Huron King grout HK SLR SL1 10, 1032-995(4A).

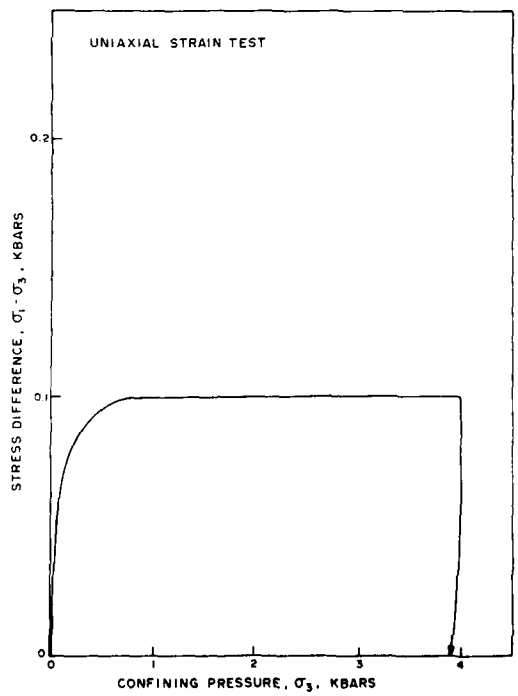

Figure 9b. Uniaxial strain test stress-stress response on Huron King grout HK SLR SL1 10, 1032-995(4A).

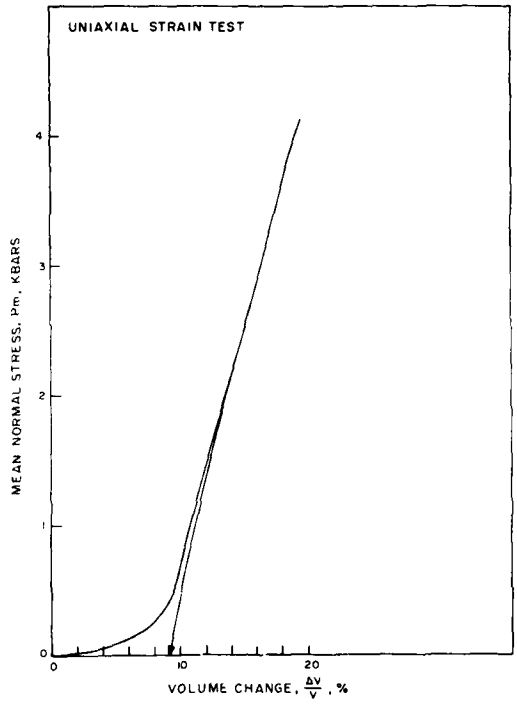

Figure 10a. Uniaxial strain test stress-strain response on Huron King grout HK SLR SL1 10, 1032-995(4).

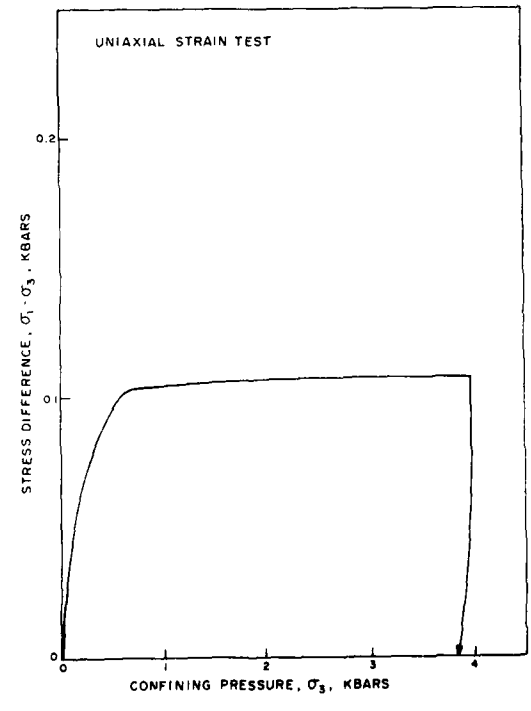

Figure 10b. Uniaxial strain test stress-stress response on Huron King grout HK SLR SL1 10, 1032-995(4).

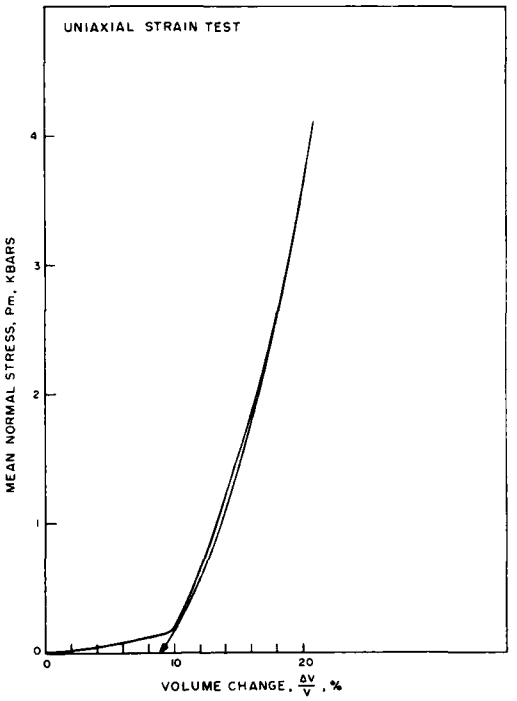

Figure 11a. Uniaxial strain test stress-strain response on Huron King grout, stage 2, 1063-1103.

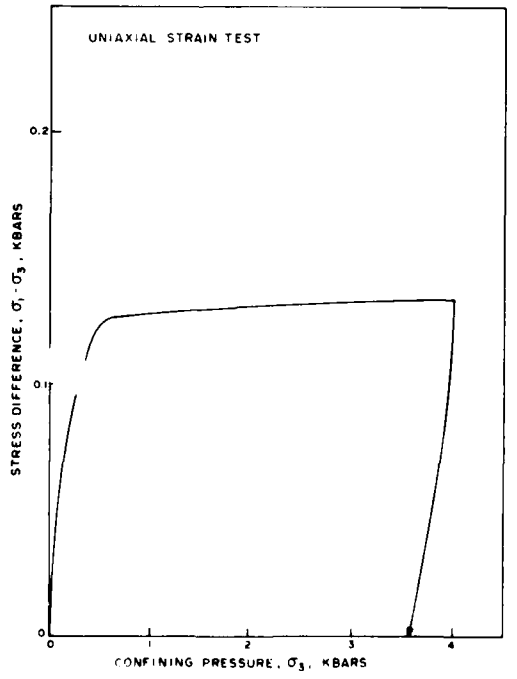

Figure 11b. Uniaxial strain test stress-stress response on Huron King grout, stage 2, 1063-1103.

Figure 12. Huron King grout sample showing voids after testing.

Figure 13. Huron King grout sample showing voids after testing.

SECTION III

RESIDUAL STRESS

Residual Stress Buildup in Thick Walled Cylinders of Ash Fall Tuff Subjected to Cycled Internal and External Pressurization

In situ stress determinations at the NTS suggest that residual stresses can be found in the rock material surrounding the cavity formed by an underground event and that these residual compressive stresses aid in the containment of the gases formed during these events. Since the ability of the rock mass to form these residual stress fields can be an important factor in the siting of the events, a test to investigate residual stress buildup was devised.

This test is called the cycled burst test and it was performed on thick walled cylinders of ash-fall tuff and grout. The test consists of applying a confining pressure to a jacketed specimen, then applying pressure to the interior (also jacketed) of the specimen. These pressures are removed, and after a period of time the specimen is burst by the application of internal pressure to the specimen. By comparing this burst pressure to the pressure required to burst an uncycled specimen, it was thought that a qualitative measure of any residual stress buildup could be obtained. Specimens were burst at various time intervals following the removal of the internal and external pressures to investigate any stress relaxation with time. Figure 14 outlines the procedures used during these tests.

Cycled and uncycled burst tests were performed on tuff from hole U12n.11 UG-2. The tests were performed, as much as possible, on specimens which were taken from the same approximate location in that hole to

minimize scatter due to difference in material properties. The results of the uncycled and cycled burst tests are given in Tables 7 and 8, respectively.

As can be seen from these tables, there appears to be no appreciable difference between the burst pressures of the uncycled and cycled specimens. If residual stresses were indeed built up in the specimen due to yielding and if these stresses decay with time, then the effect of residual stresses on the burst pressures would be most apparent on those specimens which were burst a short time after the pressures were cycled. Inspection of Table 8 reveals that, if anything, the specimens were weakened by the cycling.

While the burst tests followed a relatively simple procedure, the rock mechanic aspects of these tests is quite complex. Research on thick walled cylinders subjected to axial loads and external pressure (Robertson, 1955) revealed that yielding of the interior region of the cylinders was accompanied by spalling of a thin layer of rock at the inner surface of the cylinder. It has also been found that the magnitude of burst pressures is dependent upon the rate of pressurization (Haimson, 1968). It is also quite possible that the magnitudes of the burst pressures are dependent upon any damage to the inner surface of the cylinder due to spalling. These findings suggest that if these "burst tests" advance beyond the qualitative approach thus far that more attention is due an analytical study of the phenomena.

Previous work (TR 77-96 and TR 78-78) on grout has resulted in evidence that a residual stress can be reproduced in the grout and is

TABLE 7

Uncycled Burst Test Data

Sample	Internal Pressure at Failure, Bars
1	26
2	20
3	40

$\bar{X}$ = 28.66 bars
s = 10.26 bars

TABLE 8

Cycled Burst Test Data

Sample	Cycled Pressure, bars		Internal Pressure at Failure, Bars	Time After Pressure Release
	External	Internal		
1	500	675	16	30 sec.
2	500	675	8	30 sec.
3	500	675	27	1 min.
4	500	675	20	1 min.
5	500	675	18	2 min.
6	500	675	90	2 min.
7	500	675	12	5 min.
8	500	675	40	5 min.
9	500	675	6	10 min.
10	500	675	20	10 min.
11	500	675	10	30 min.
12	500	675	36	30 min.
13	500	675	406	60 min.
14	500	675	26	60 min.
15	500	675	30	120 min.
16	500	675	30	120 min.

$\bar{X}$ = 25.93 excluding Sample 13
s = 20.41

time dependent. Tests on tuff from U12n.11 UG#2 drill hole have produced, however, little or no evidence of residual stress in the burst samples. Data presented at a DNA meeting during 1979 suggested a residual stress. Since the data contained considerable scatter, however, further scrutiny located an anomaly in the laboratory test equipment which invalidated the results.

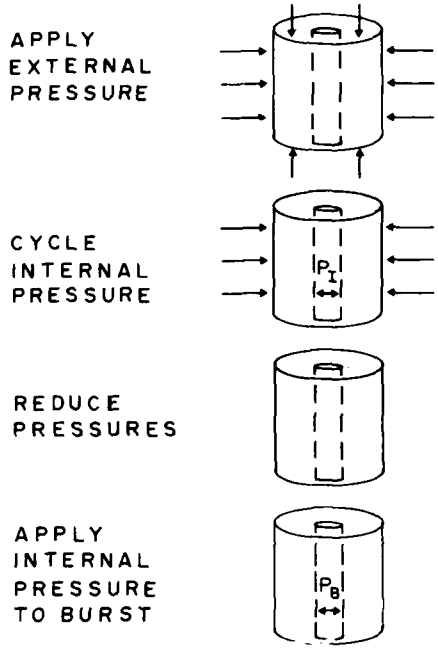

Figure 14a. Procedures for the cycled burst test.

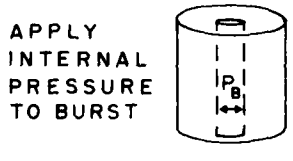

Figure 14b. Uncycled burst test.

Figure 14. Procedures used to investigate residual stress buildup in thick walled cylinders of ash-fall tuff.

SECTION IV

TIME DEPENDENT (CREEP) BEHAVIOR

High pressure gases are generated during a nuclear event and it is imperative that these gases be contained in the cavity formed by the detonation. These gases persist for a period of time, during which time they exert stresses on the surrounding materials. Nearly all materials will deform with time when subjected to this type of loading (i.e. constant stress), and in order to adequately assess the containment potential for a given site it is necessary to know the time dependent material behavior.

Deformation with time of materials subjected to constant loads is called creep. The creep behavior of materials is studied with a creep test which consists of measuring the deformations occurring with time for specimens subjected to constant stress conditions. An idealized deformation-time (creep) curve is shown in Figure 15. When the load is first applied, the material undergoes an immediate elastic strain (A). Primary creep occurs after the loading (B). Primary creep (or viscoelasticity) is characterized by a rapid, then decreasing strain rate. This primary creep may be recoverable or it may be partially or totally unrecoverable. After the primary creep stage the strain rate becomes fairly constant (C), this is termed secondary creep. Plastic deformation may occur during this stage and if the load is removed during this phase the specimen may be permanently strained. The final stage of creep is called tertiary creep (D). During this stage the strain rates increase until specimen failure occurs.

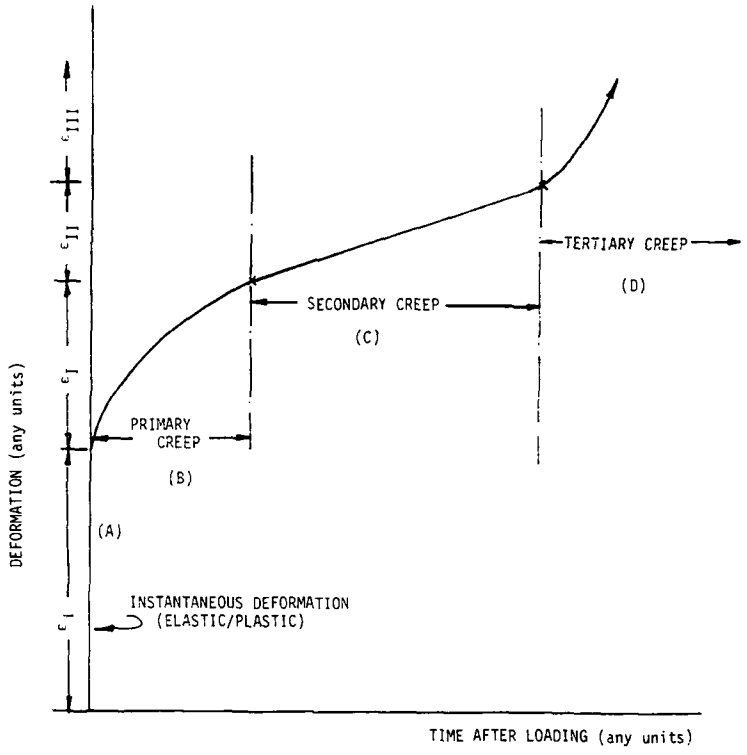

Figure 15. Idealized stages in the time-dependent response due to the application of constant load, termed creep.

The inverse behavior of creep is called relaxation. If a constant strain is maintained on a viscoelastic material, the stress in that material will decrease or relax with time. A relaxation test consists of straining a specimen and then maintaining that strain while monitoring the stress in the specimen.

To aid in the understanding of the time dependent behavior of the materials used in conjunction with underground nuclear events, a series of triaxial compression tests, triaxial creep tests, relaxation tests and creep/relaxation tests were performed on tuff from borehole U12n.11 UG-2 and on Stanford Research Institute (SRI) 2C4 grout. The grout

used for these tests was cast on 9-6-78 at SRI and had as-received densities of 2.19 ± 0.07 gm/cc. The test matrix which was followed is shown in Figure 16. All tests were conducted at ages greater than 28 days.

Triaxial Compression Tests

A series of drained and undrained triaxial compression tests were performed on U12n.11 UG-1 tuffs and on 2C4 grout to define the strengths of these materials at a confining pressure of 0.5 kbars. The results of these triaxial tests are shown in Figures 17 to 20. These results were used to define the loading conditions for the subsequent tests. The strain rates were 10^{-4} in/in/sec.

Triaxial Creep Tests

A series of drained and undrained triaxial creep tests were performed using confining pressures of 0.25 kbar, 0.5 kbar and 1.0 kbar. These tests were performed using several different axial stresses which were percentages of the failure loads defined by the triaxial compression tests. The axial shear stress was applied with a servocontrolled actuator so that a constant stress could be maintained.

After approximately 30 minutes of constant stress difference, the axial loads were rapdily removed while the confining pressure was maintained. The recovery of the specimen was monitored for another 30 minutes. After the 30 minute recovery period the specimen was loaded to the next highest axial load. This procedure was repeated until all tests for a given confining pressure were completed.

Triaxial Compression Tests
σ_3 = 0.5 Kbars

	Tuff	Grout
Drained	2	3
Undrained	2	3

Triaxial Creep Tests

Confining Pressure	Tuff		Grout	
	Drained	Undrained	Drained	Undrained
0.25 Kbars	-	1	-	1
0.5 Kbars	1	2	1	1
1.0 Kbar	-	1	-	1

Triaxial Undrained-Drained Creep
σ_3 = 0.5 Kbar

Tuff	Grout
1	1

Triaxial Relaxation Tests
σ_3 = 0.5 Kbar

Tuff	Grout
1	1

Traxial Creep - Relaxation (Undrained) Tests
σ_3 = 0.5 Kbar

Tuff	Grout
1	1

Figure 16. Test Matrix for Investigation of the Time Dependent Behavior of Tuff and Grout.

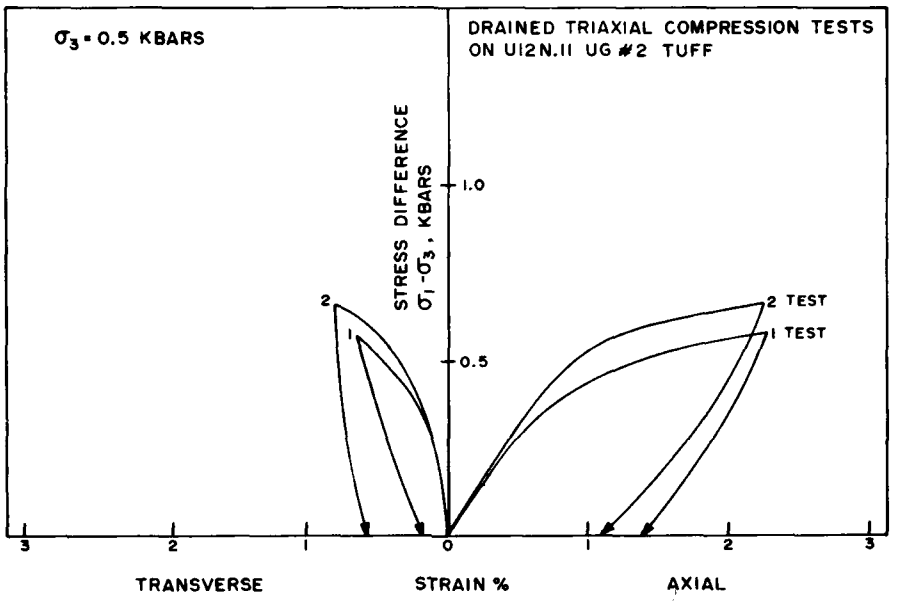

Figure 17. Drained triaxial compression on U12n.11 UG#2 tuff.

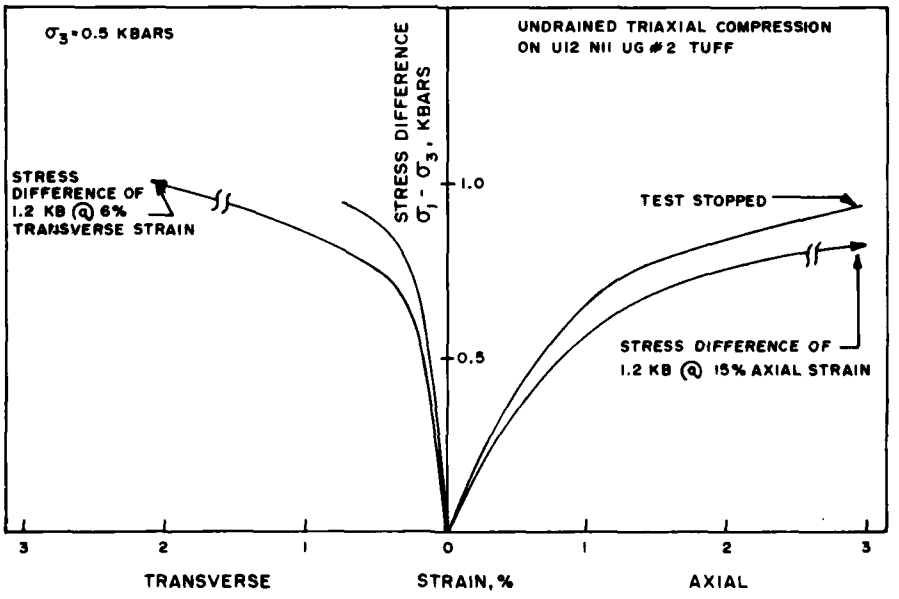

Figure 18. Undrained triaxial compression on U12n.11 UG#2 tuff.

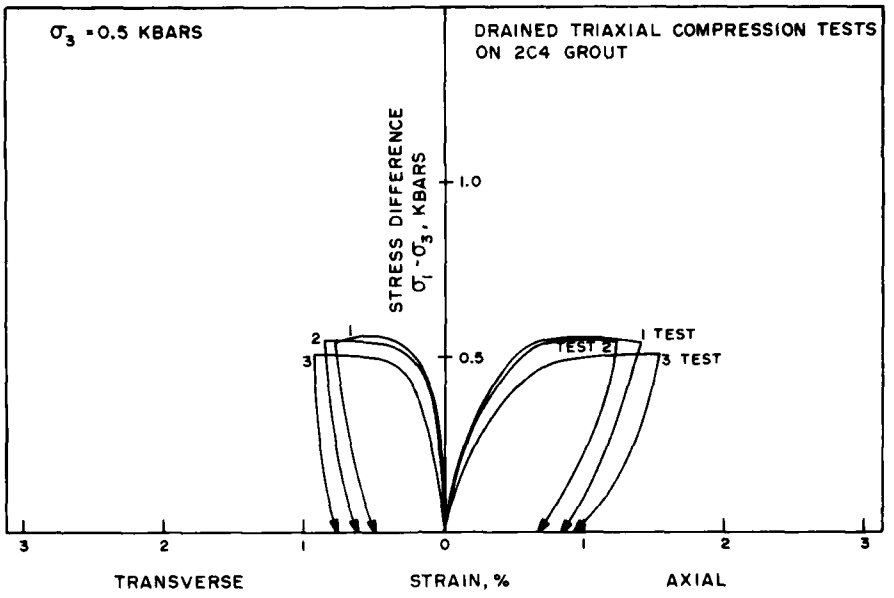

Figure 19. Drained triaxial compression on 2C4 grout.

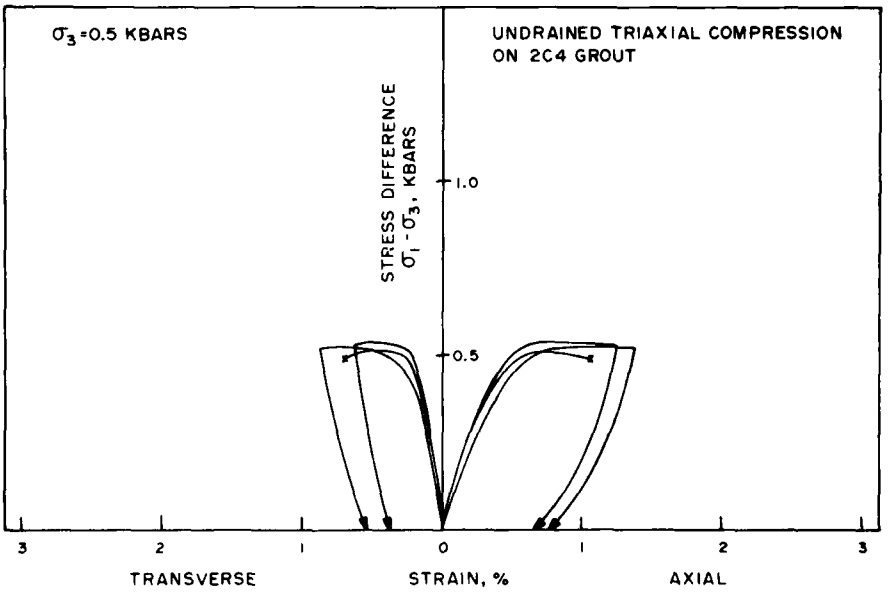

Figure 20. Undrained triaxial compression on 2C4 grout.

It is noted in each figure caption the sequence of testing since single sample were used to generate several curves. For example, in Figure 21, sample 1 was first subjected to a stress difference of 0.10 kbars and unloaded, then 0.2 kbars and unloaded and finally 0.30 kbars. A second sample generated the curves at stress differences of 0.25, 0.35 and 0.45 kbars.

The strain-time records from the triaxial creep tests are shown in Figures 21 to 29. As can be seen from these figures, all of the specimens had progressed to the secondary creep stage by the end of 30 minutes. This is evidenced by the fairly constant slope of the strain time curves and also by the incomplete strain recovery after the axial stresses were removed. It can also be seen from these figures that some specimens had entered the tertiary creep stage. This is evidenced by the increase in strain rate following secondary creep and sample failure.

The following generalizations can be made from this data:

1. Drained specimens creep more than undrained specimens.
2. For a given stress difference, the specimens tested at higher confining pressures creep more than those at lower confining pressures.

For all of the creep and relaxation tests the strain resulting from the hydrostatic compression is not included.

Some features of Figures 21 through 29 warrant explanation or comment at this time. The apparent Young's moduli (stress difference divided by apparent axial strain) in Figure 23 increases from about

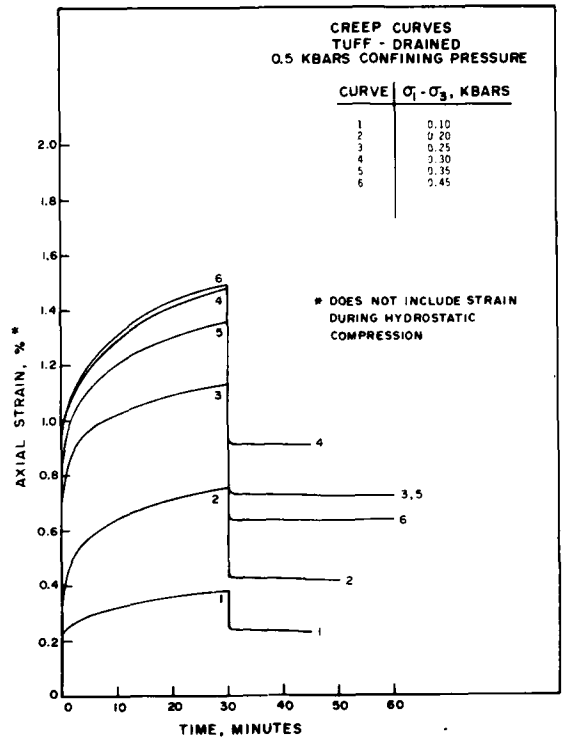

Figure 21. Drained creep tests on tuff at 0.5 kilobars confining pressure; sample 1 produced curves 1, 2 and 4, and sample 2 produced curves 3, 5 and 6.

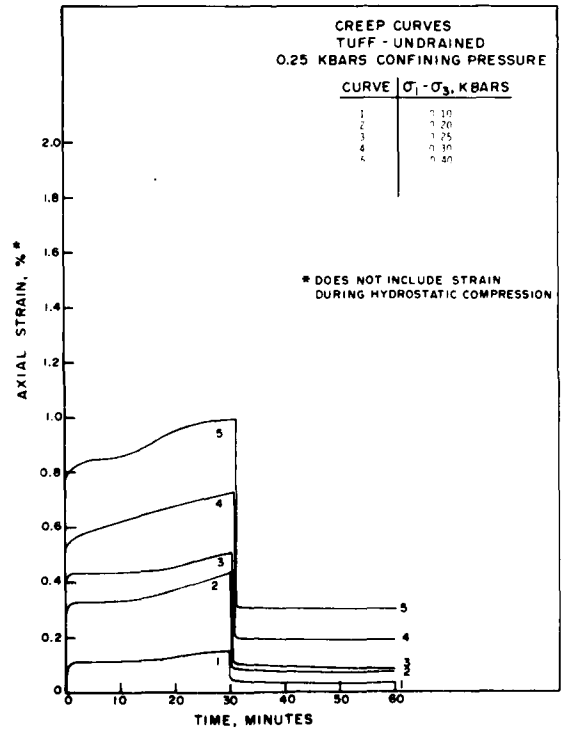

Figure 22. Undrained creep tests on tuff at 0.25 kilobars confining pressure; sample 1 produced curves 1-5.

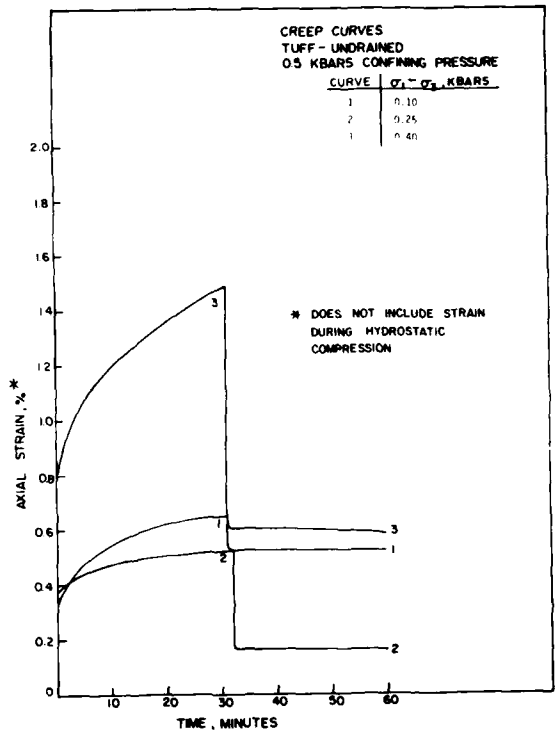

Figure 23. Undrained creep tests on tuff at 0.5 kilobars confining pressure; sample 1 produced curves 1-3.

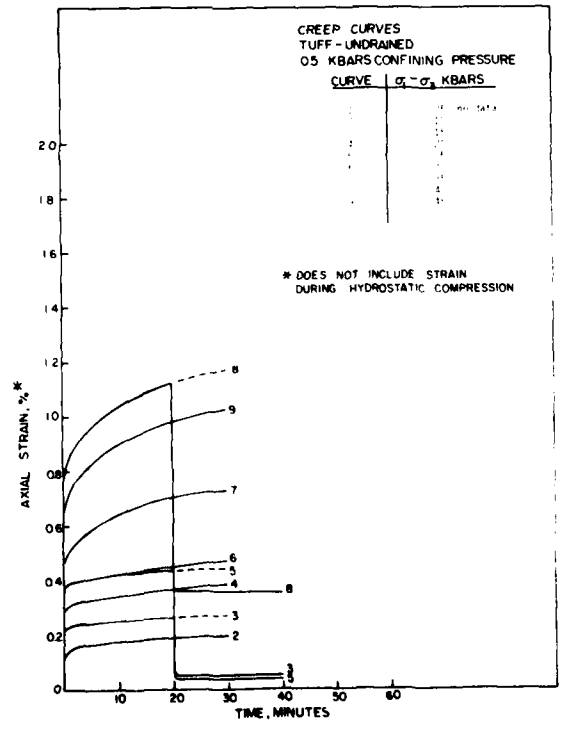

Figure 24. Undrained creep tests on tuff at 0.5 kilobars confining pressure; sample 1 produced 2, 5 and 8, sample 2 produced curves 3, 6 and 9, and sample 3 produced curves 4 and 7.

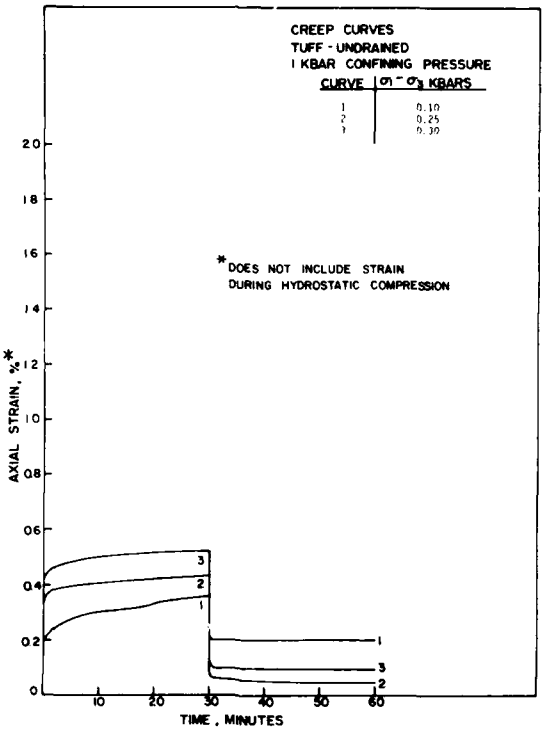

Figure 25. Undrained creep tests on tuff at 1 kilobar confining pressure; sample 1 produced curves 1-3.

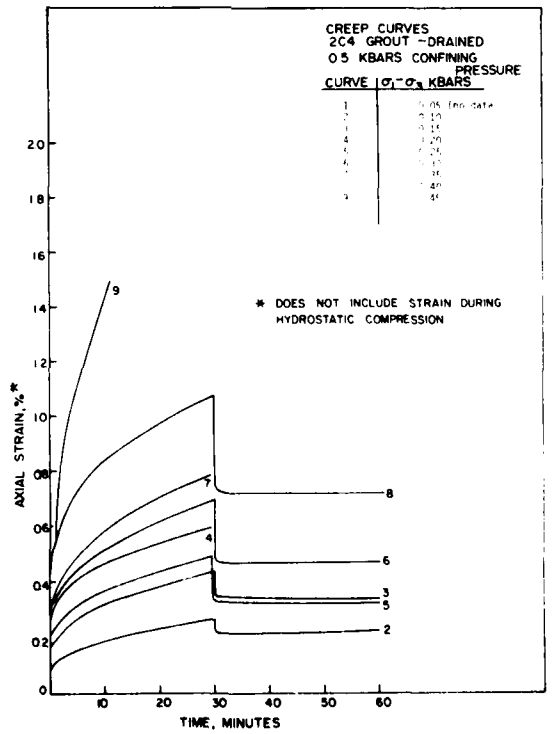

Figure 26. Drained creep tests on 2C4 grout at 0.5 kilobars confining pressure; sample 1 produced curves 2, 5 and 8, sample 2 produced curves 3, 6 and 9, and sample 3 produced curves 4 and 7.

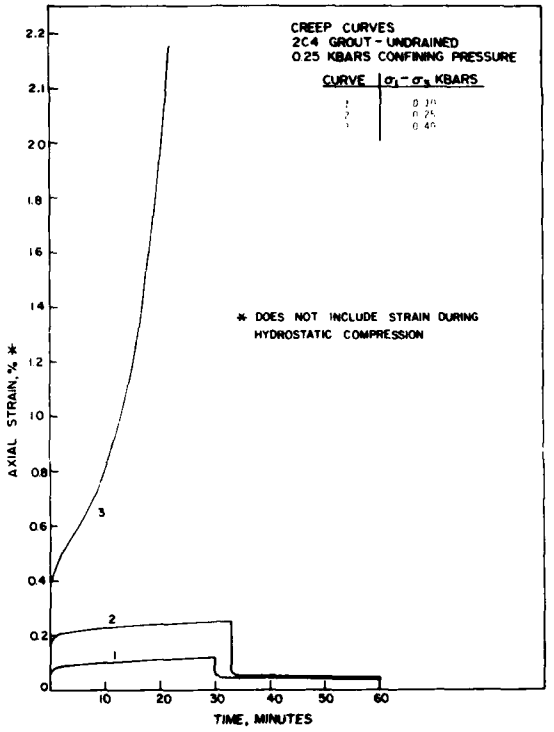

Figure 27. Undrained creep tests on 2C4 grout at 0.25 kilobars confining pressure; sample 1 produced curves 1-3.

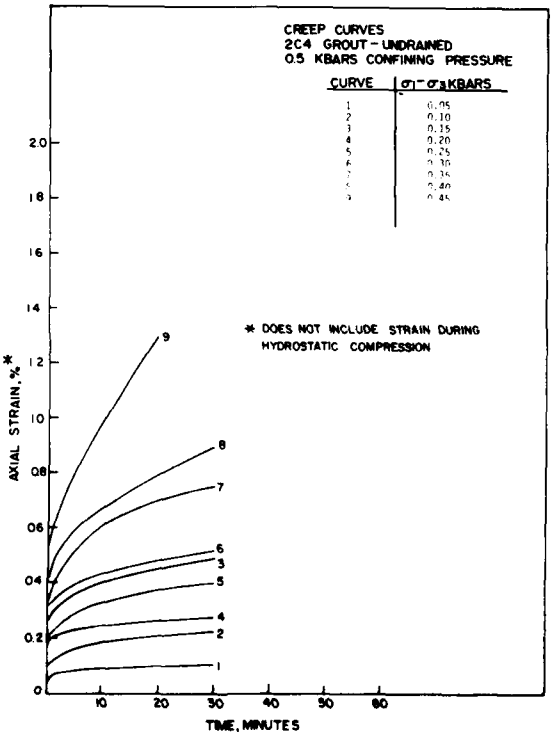

Figure 28. Undrained creep tests on 2C4 grout at 0.5 kilobars confining pressure; sample 1 produced curves 1, 4 and 6, sample 2 produced curves 2, 5 and 8, and sample 3 produced curves 3, 6 and 9.

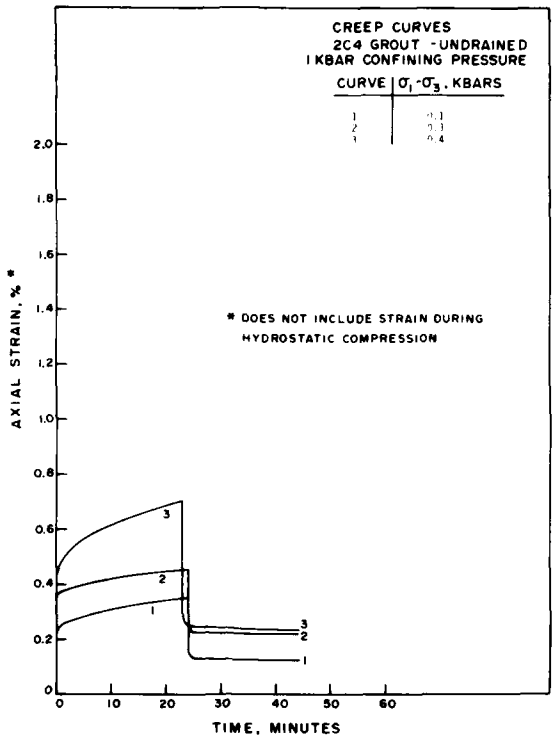

Figure 29. Undrained creep tests on 2C4 grout at 1 kilobar confining pressure; sample 1 produced curves 1-3.

30 kbars to 70 kbars as a result of stress difference increases of 0.10 and 0.25 kbars, respectively. This change is not unexpected since the strain associated with the 0.10 kbars stress difference step likely included some pore collapse and a "foot" on the stress-strain response. The subsequent decrease from 70 kbars to about 50 kbars associated with the 0.25 and 0.4 kbars steps, however, suggests that the creep unloading (i.e. recovery) is affecting the total strain upon reloading. Without the actual stress-strain curves (rather than just the end points and assuming linearity) the reasons behind the "apparent" varying behavior are unclear.

Figures 23 and 24 show the same types of tests (at σ_3 = 0.5) but the tests were conducted at different times. In Figure 24, the data at the stress difference step of 0.1 was not recovered. Unloading behavior was obtained only on the 0.15, 0.25 and 0.4 steps and after only 20 minutes (the dashed lines extrapolate the curves out to 30 minutes). It should be noted for scaling purposes that all curves have been reproduced identical to the continuous trace obtained during testing. No interpretation has been applied.

In Figure 26, curves 4 and 7 do not include unloading and no test data was obtained at the 0.05 kbar stress difference step.

In Figure 27, the testing procedure is identical to other creep tests even though the unloading data is not shown.

Triaxial Undrained-Drained Creep Tests

An undrained-drained creep test differs only from a regular creep test in that after 30 minutes of being creeped undrained a valve was opened and the test was continued as a drained creep test. One test each at a confining pressure of 0.5 kbars and a stress difference (σ_1-σ_3) of 0.4 kbars was performed on tuff and 2C4 grout.

The results of these tests are shown in Figures 30 and 31. As can be seen from these figures, it appears that the grout creeped slightly more than the tuff and that there is not apparent difference in the undrained and drained portions of either curve.

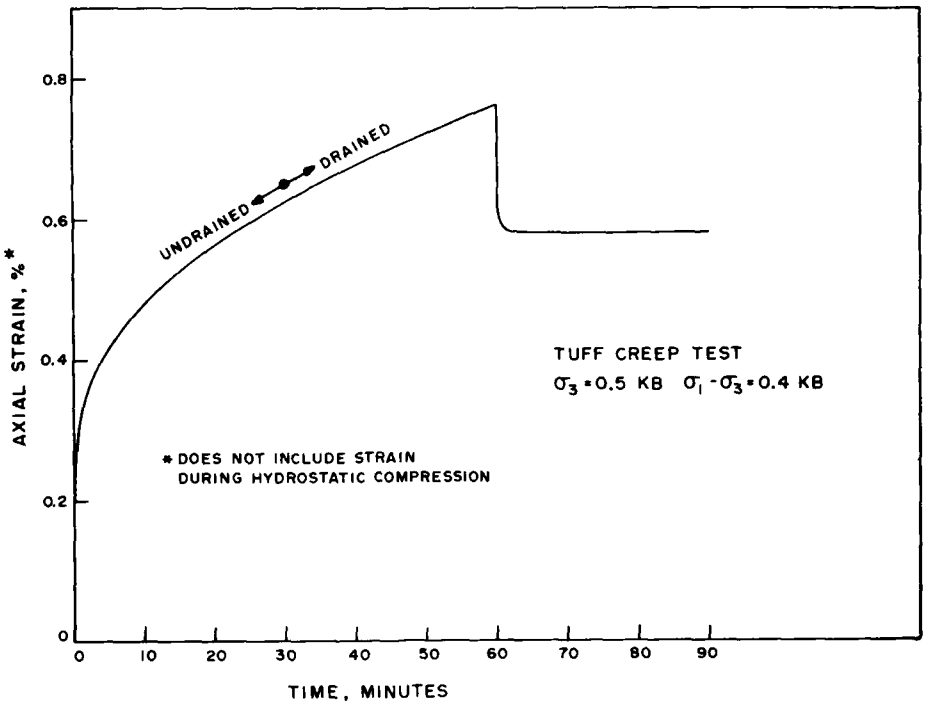

Figure 30. Creep test on tuff at 0.5 kilobars confining pressure; combined undrained and drained.

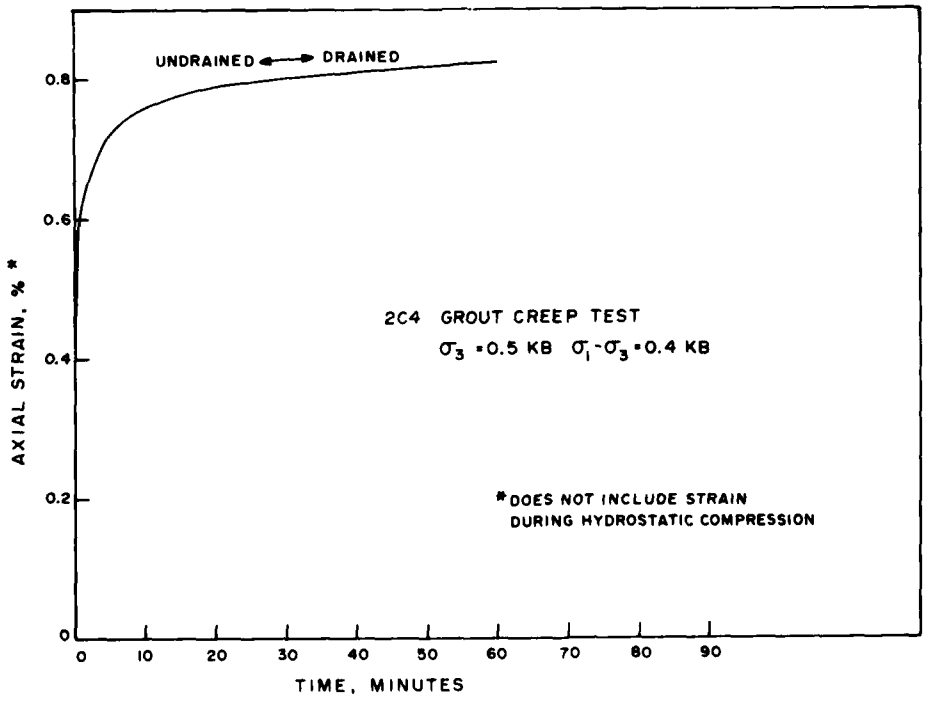

Figure 31. Creep test on 2C4 grout at 0.5 kilobars confining pressure; combined undrained and drained.

Triaxial Relaxation Test

Undrained triaxial relaxation tests were performed on tuff and 2C4 grout specimens. Confining pressures of 0.5 kbars were used for these tests. The test consisted of applying the confining pressure to the specimen and then applying an axial stress difference of 0.4 kbars to the specimen. The displacement corresponding to an initial stress difference of 0.4 kbars was then maintained for the duration of the test. The stress difference was then monitored as a function of time.

The stress difference versus time curves for the tuff and grout are shown in Figures 32 and 33, respectively. As can be seen from these two figures, the grout relaxed faster than the tuff. The stress difference at the end of the test was 0.2 kbars for the grout and 0.24 kbars for the tuff.

Triaxial Creep/Relaxation Test

Undrained triaxial creep/relaxation tests were performed on tuff and 2C4 grout specimens. These tests were again performed using confining pressures of 0.5 kbars and the stress difference was 0.4 kbars.

As the name implies, a triaxial creep/relaxation test is a combination of the two previously described tests. The specimens were creeped for approximately 30 minutes, at which time a constant axial strain was maintained and the stress relaxation of the specimens was monitored.

The strain versus time and stress difference versus time records for the triaxial creep/relaxation tests performed on the tuff and grout

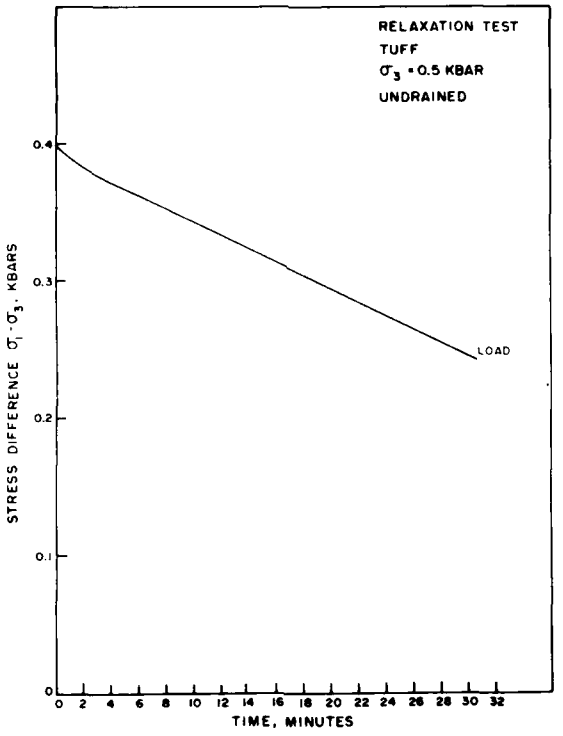

Figure 32. Stress difference versus time for triaxial relaxation test on tuff.

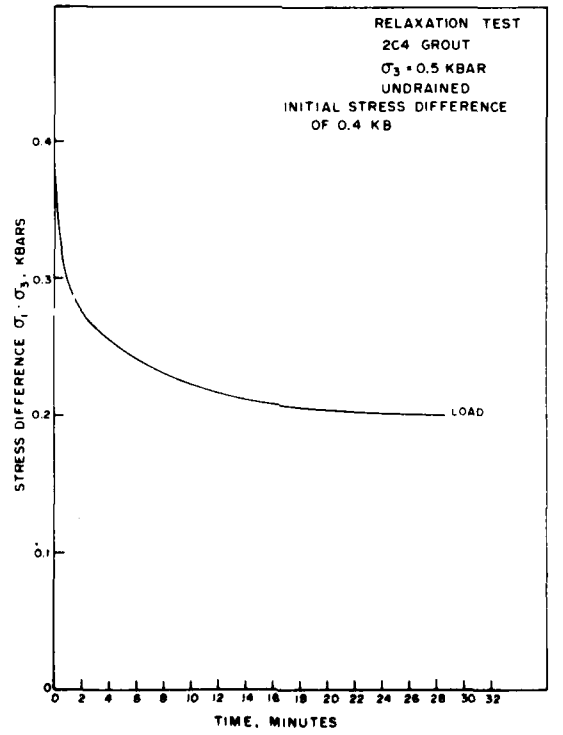

Figure 33. Stress difference versus time for triaxial relaxation test on 2C4 grout.

specimens are shown in Figures 34 and 35. As can be seen from these figures, the tuff displayed more creep and relaxed faster than the grout. It is interesting to note that even though the tuff relaxed faster than the grout (i.e. just the opposite of the previous "relaxation" tests), the final stress difference was approximately the same for the two materials.

General Comments

Previous tests conducted (July, 1977) on the 2C4 grout from SRI are shown in Appendix E. That previous data indicated a slightly lower strength (i.e. about 0.3 kb at 0.5 kb pressure as compared to 0.5 kb at 0.5 kb pressure). The previous tests were run at 14 days age as compared to 28 days plus for the tests shown herein. As a note, the cure being used by SRI for their 14 day test has been thought to simulate a 28 day age at 14 days. However the cure (per Ralph Bendinelli, Vicksburg, Mississippi) only simulates the curing of a mass pour and does not accelerate the curing process.

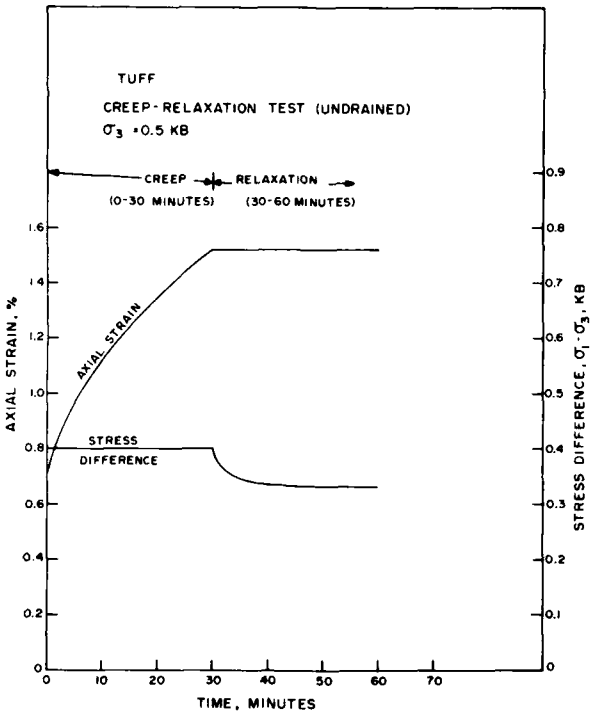

Figure 34. Undrained creep-relaxation test on tuff at 0.5 kilobars confining pressure.

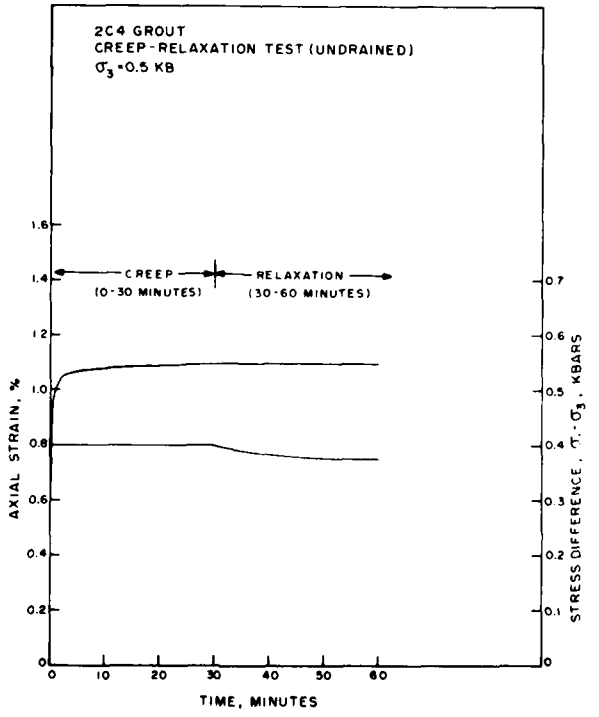

Figure 35. Undrained creep-relaxation test on 2C4 grout at 0.5 kilobars confining pressure.

SECTION V

ULTRASONIC VELOCITIES/FRACTURING INTERACTION

Ultrasonic velocity measurements were made on a tuff specimen from U12n.05 UG#4 subjected to confining pressure with an additional axial load superimposed (see configuration in Figure 36). Figure 37 shows the p-wave and s-wave (polarized parallel and perpendicular to the plane of the applied stress) velocities as a function of the stress difference (i.e. one-half the shear stress).

The specimen was first loaded hydrostatically to 2500 psi and then a stress difference was applied until the rock began "failing" (i.e. deviating from a straight line in stress-strain space). The confining pressure was then slightly increased (i.e. point 10) to prevent abrupt failure and stress difference was increased until an approximately 10 percent change was observed in the p-wave velocity. The stress difference and the confining pressures were then reduced simultaneously from point 19, maintaining a constant ratio between the two. Unfortunately, at one point the confining pressure was removed faster than the stress difference and additional failure occured in the specimen. At points 21 and 23 the ultrasonic signal amplitude decreased to the point where a reliable reading could not be obtained. Following the removal of the stress difference, a confining pressure of 1000 psi was maintained on the sample for 18 hours. During this time the ultrasonic velocities did not change (point 25).

Figure 38 is a plot of relative signal amplitudes and Poisson's ratios versus stress difference while the velocity ratios as function of stress

differences are shown in Figure 39 for the same test shown in Figure 37.

It is interesting to note that the velocity ratio of p-wave to s-wave polarized perpendicular to the plane of the applied stress increases during loading while the ratio of the p-wave velocity to s-wave velocity polarized parallel to the plane of the axial stress decreased during this phase. This trend was reversed during unloading.

An explanation of this phenomena is that the fractures which were initially formed were predominantly vertical and that the fractures which formed during the subsequent loading were inclined at 45° to the applied axial stress. This explanation is substantiated in part by observations made on the tested specimen which show that both vertical and 45° fractures were present. A longitudinal cross-section of the specimen showing these fractures is shown in Figure 40.

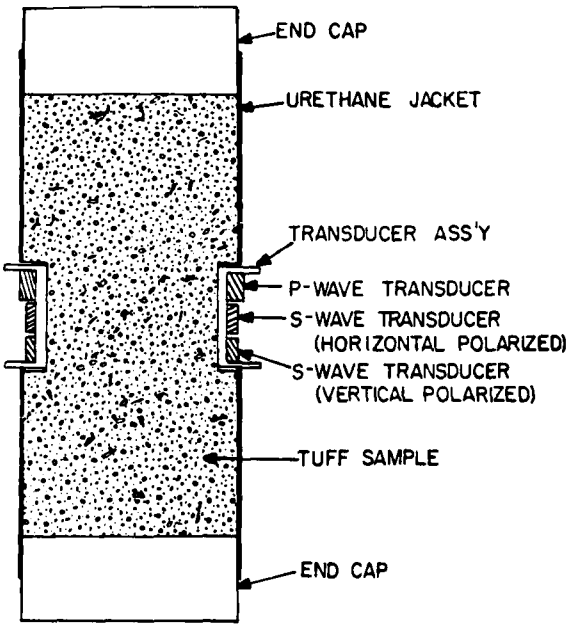

Figure 36. Sample configuration.

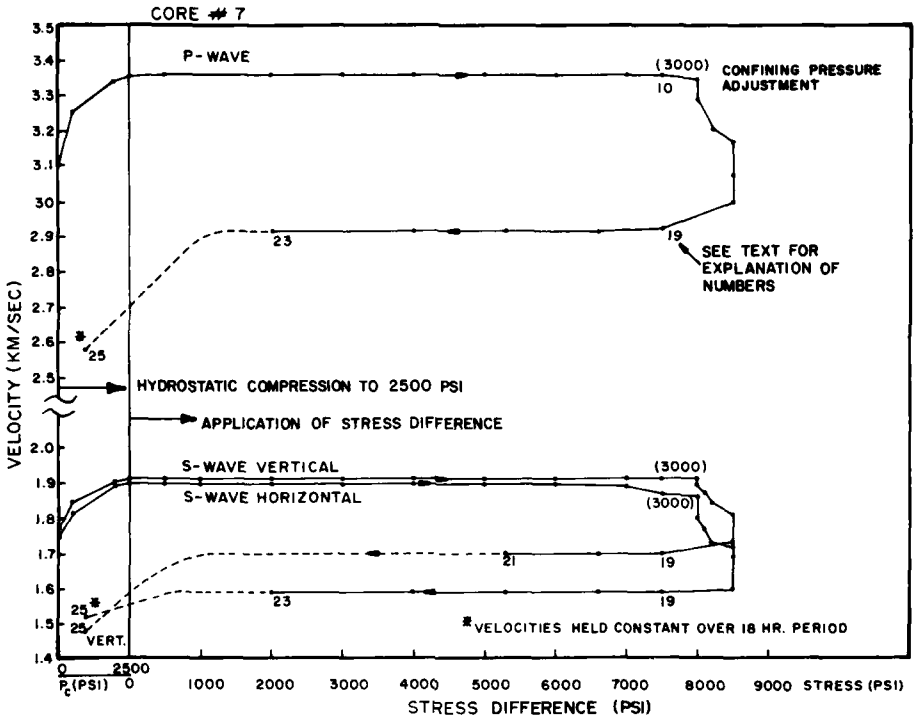

Figure 37. Wave velocity versus stress difference and confining pressure.

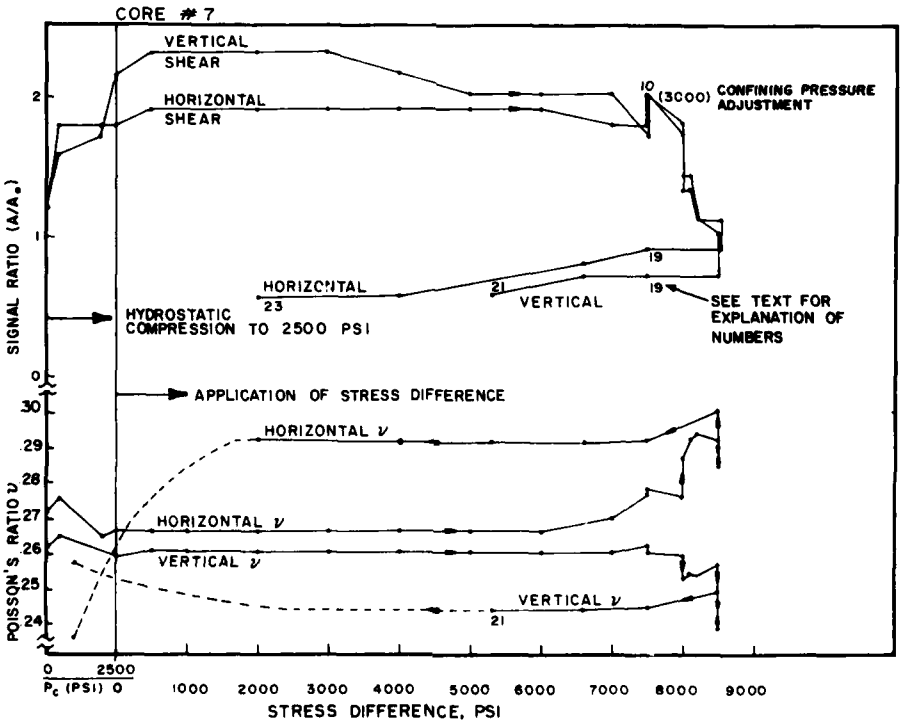

Figure 38. Signal attenuation versus stress difference.

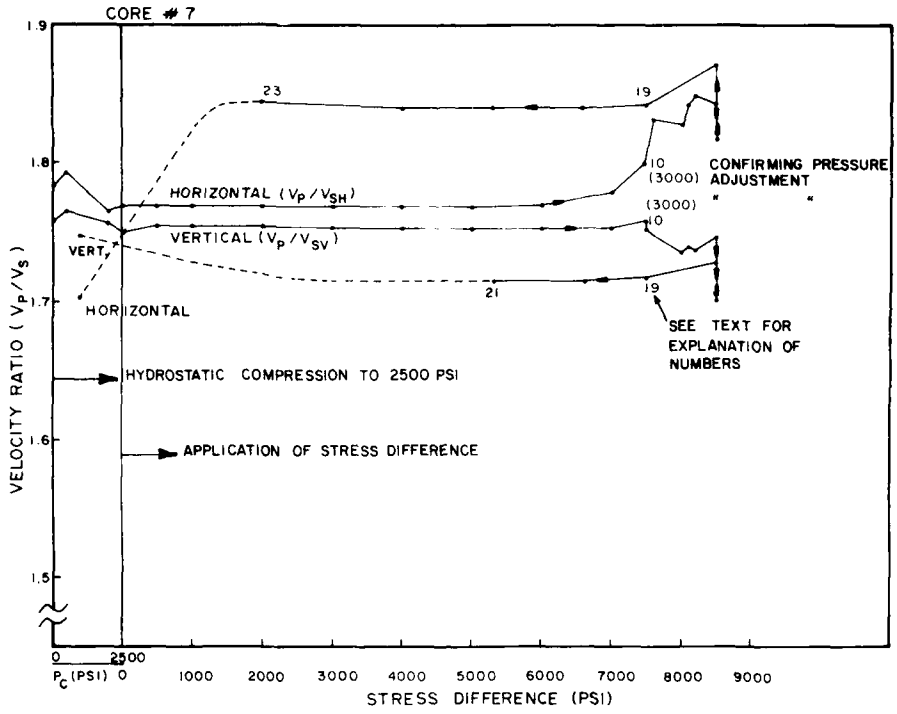

Figure 39. Velocity ratios versus stress difference.

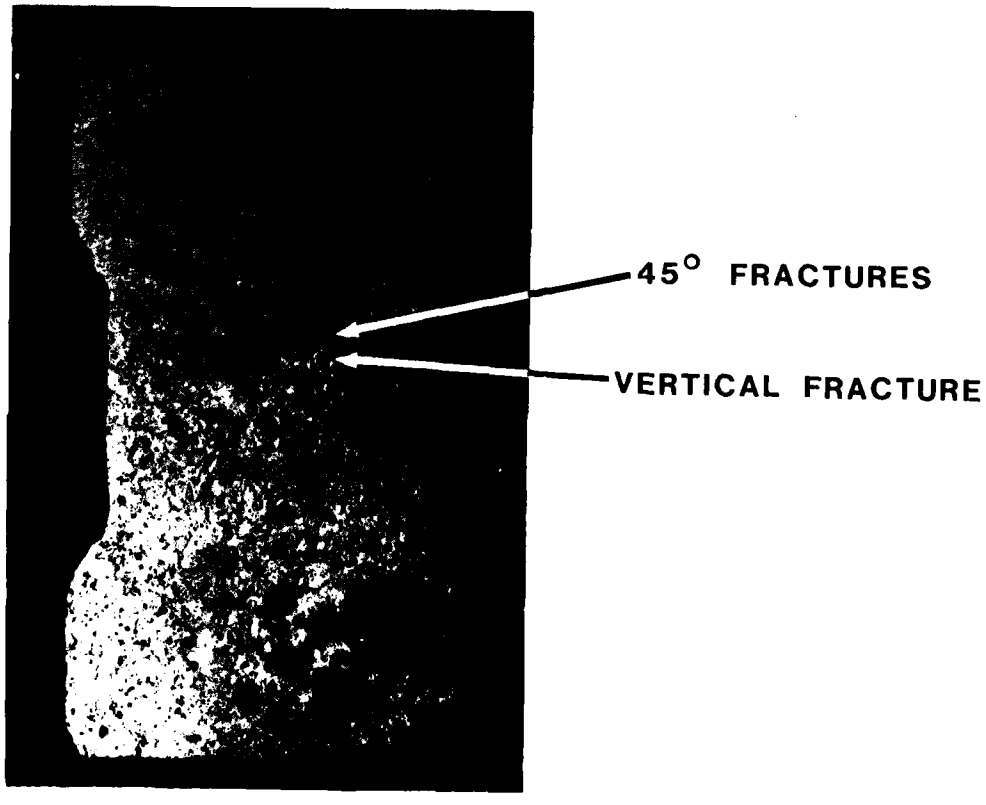

Figure 40. Longitudinal cross section of specimen showing vertical and 45° fractures.

APPENDIX A

TEST RESULTS ON U12n.11 TUFF SAMPLES

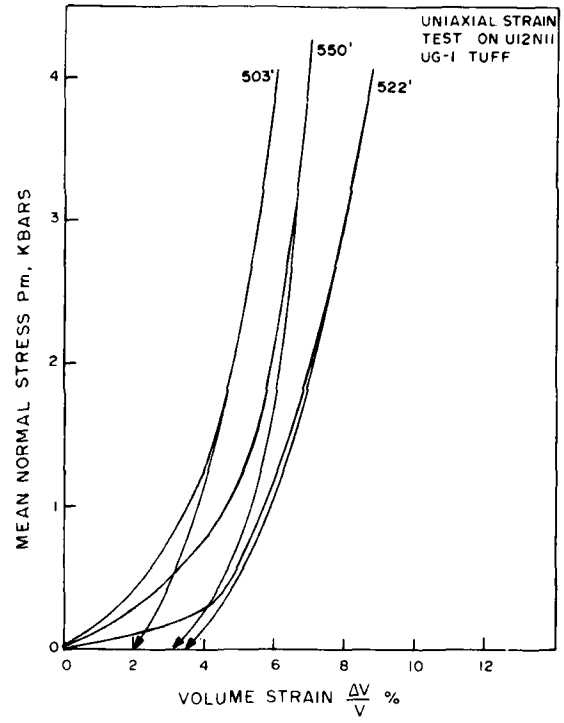

Figure A1a.

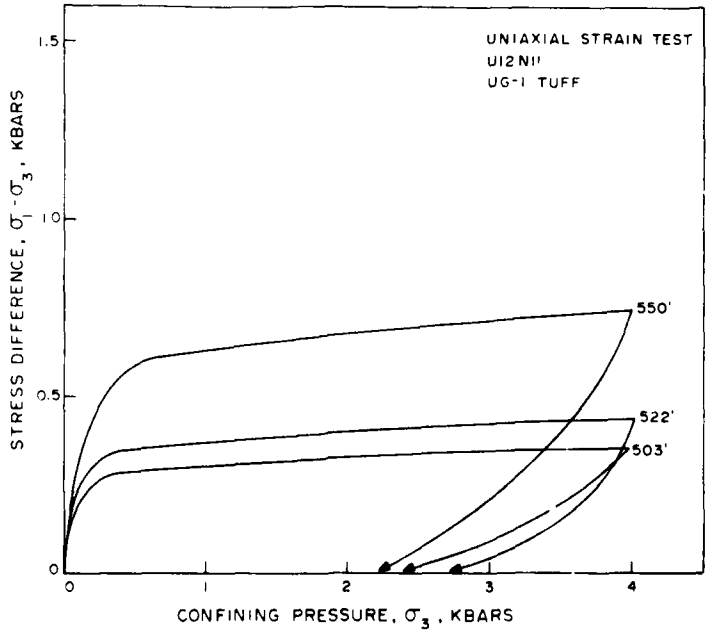

Figure A1b.

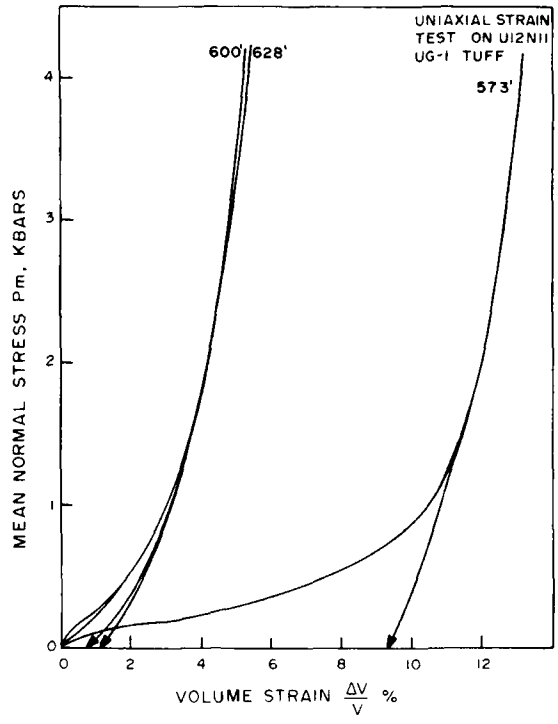

Figure A2a.

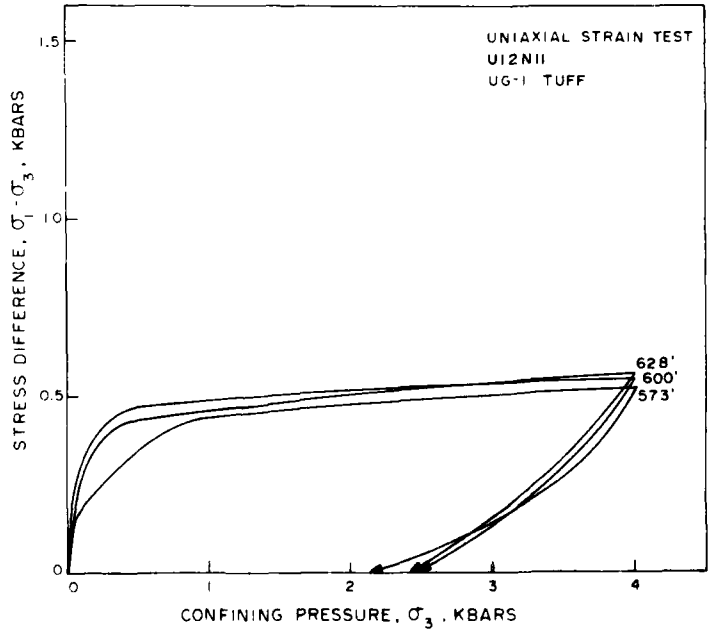

Figure A2b.

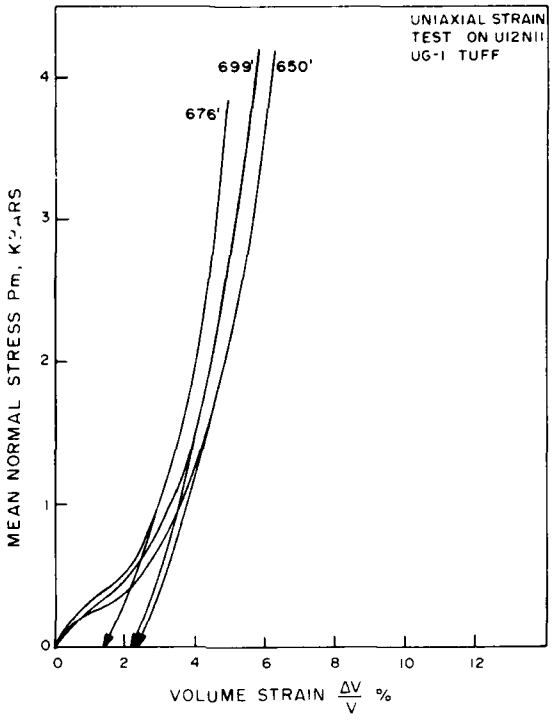

Figure A3a.

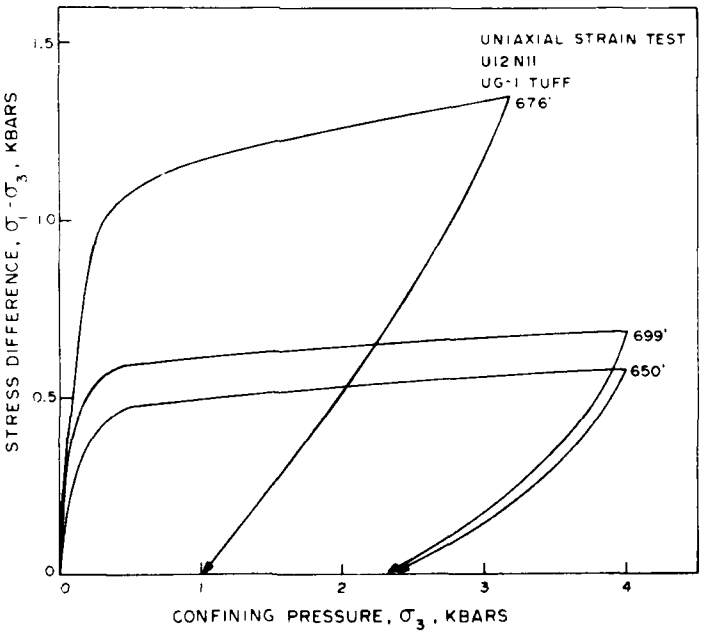

Figure A3b.

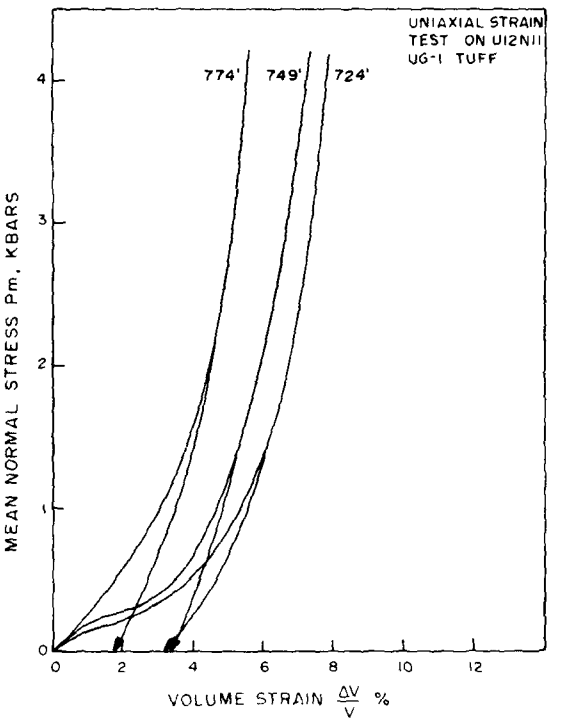

Figure A4a.

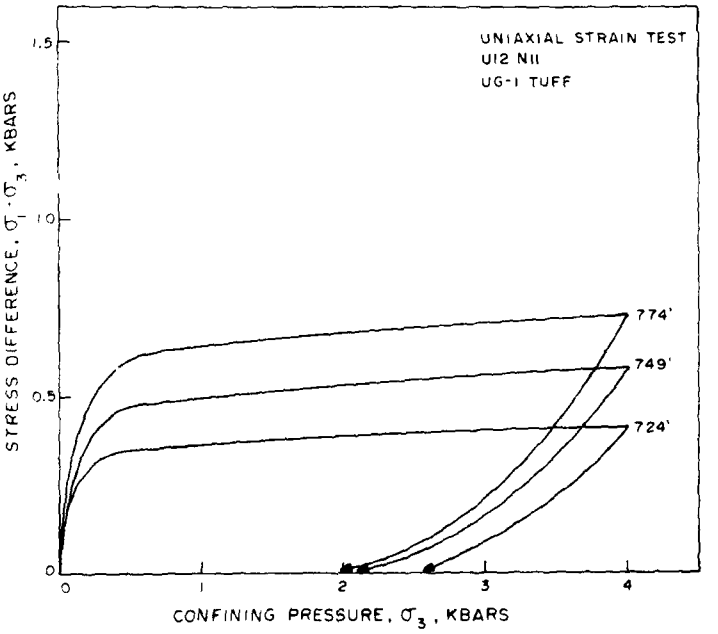

Figure A4b.

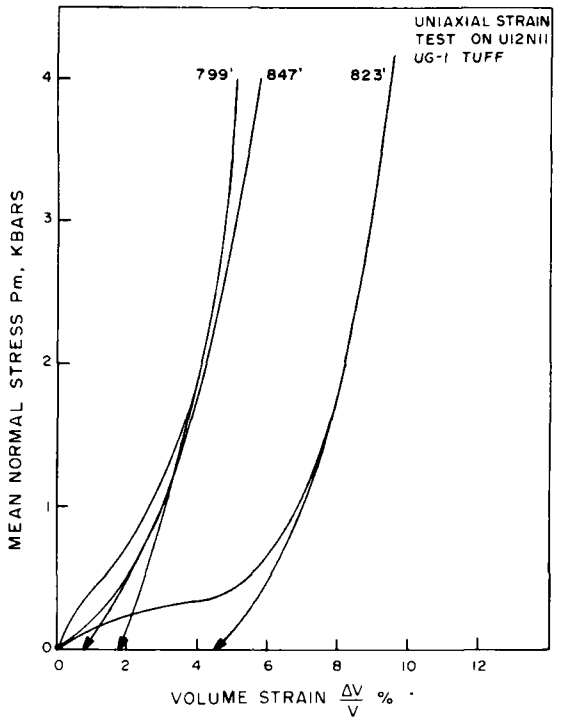

Figure A5a.

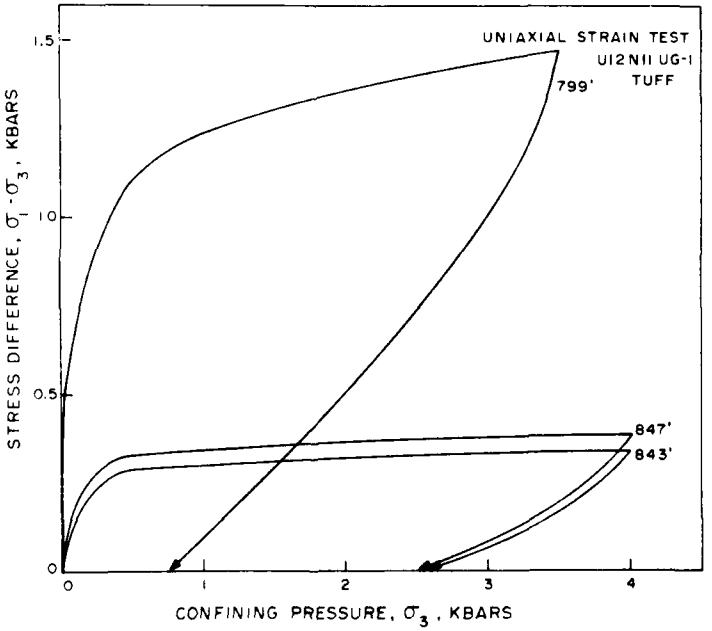

Figure A5b.

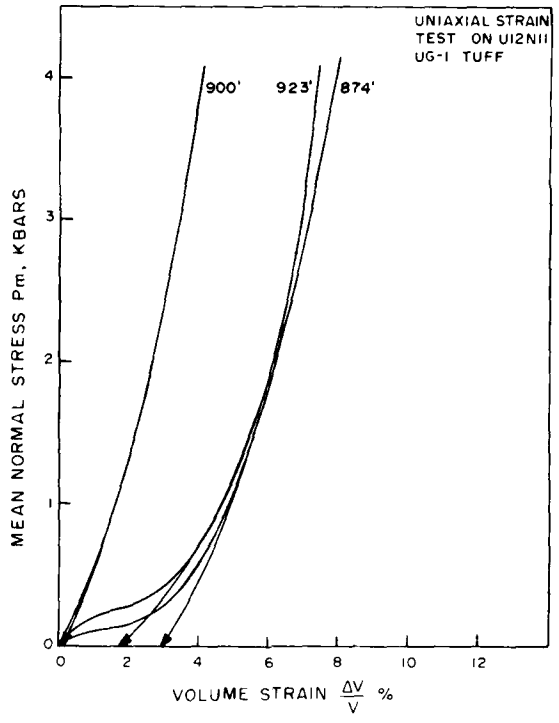

Figure A6a.

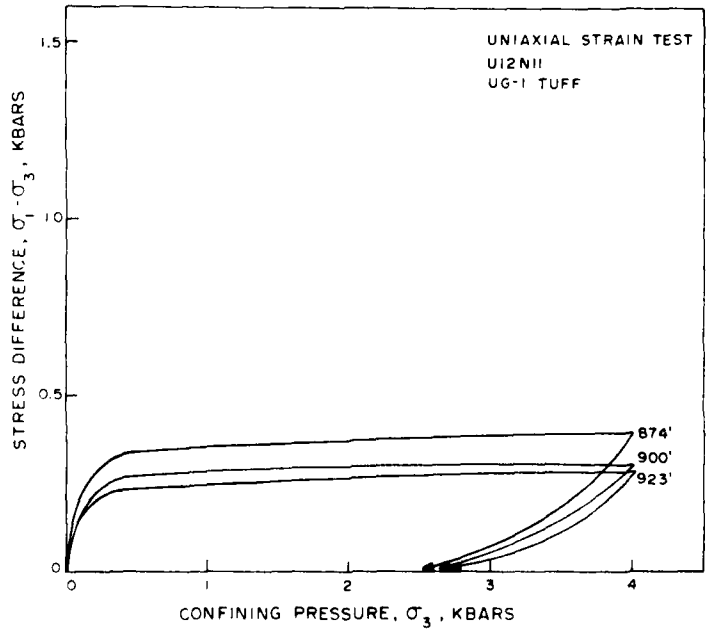

Figure A6b.

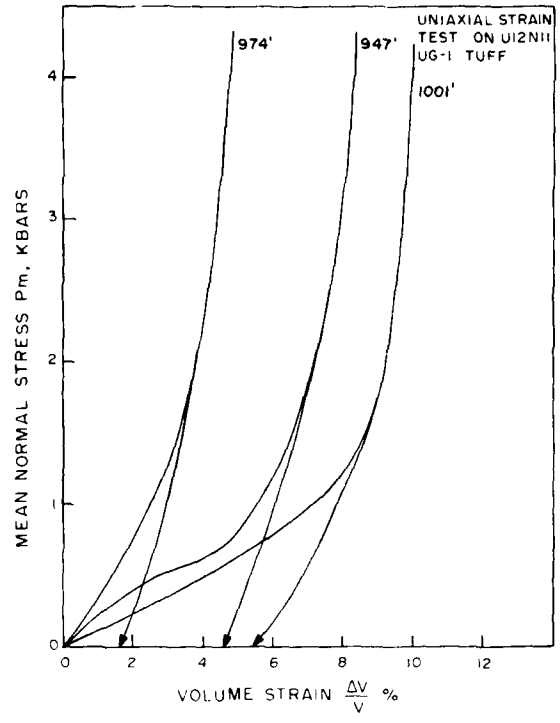

Figure A7a.

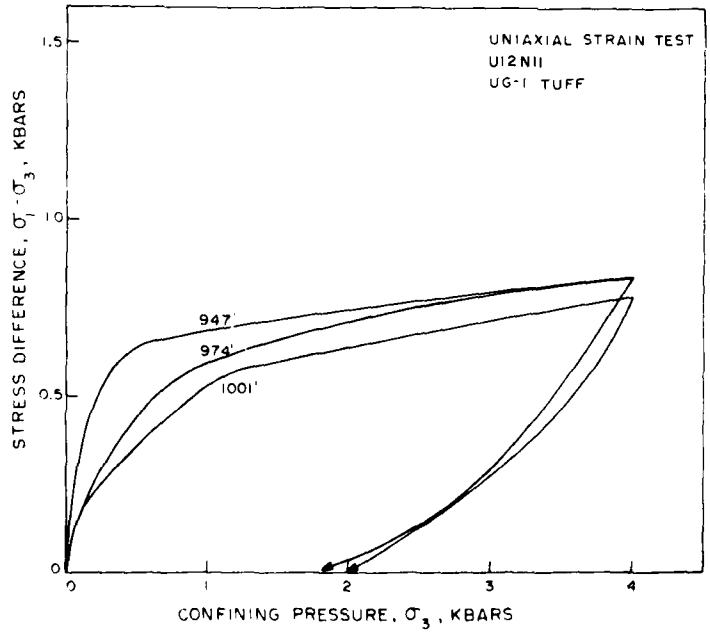

Figure A7b.

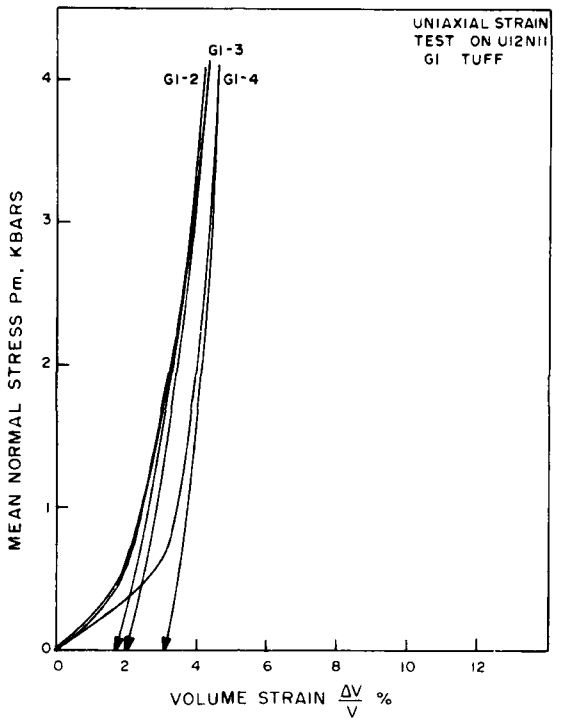

Figure A8a.

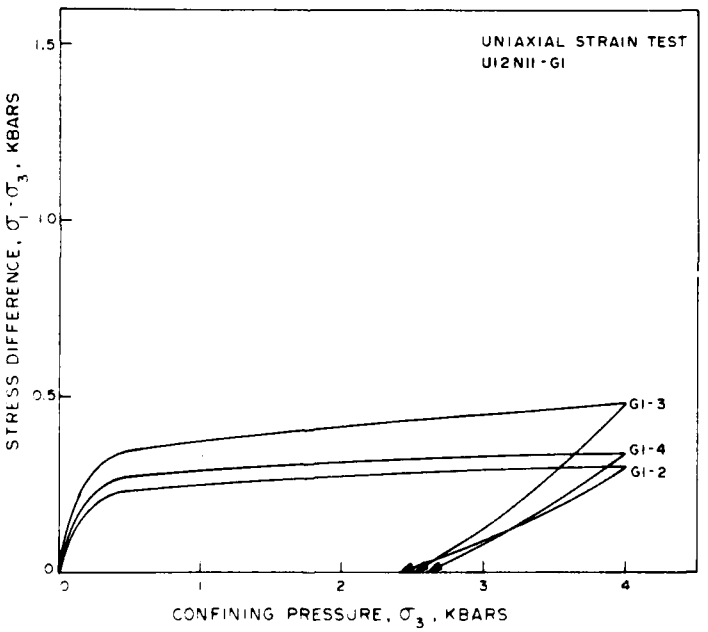

Figure A8b.

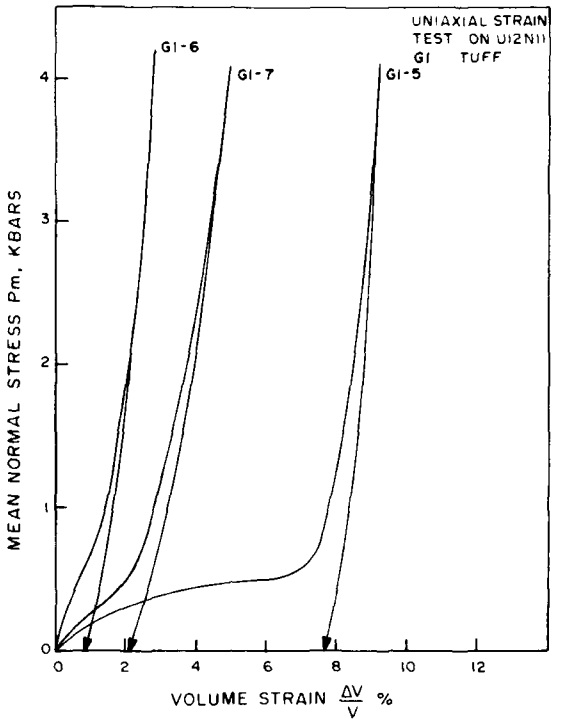

Figure A9a.

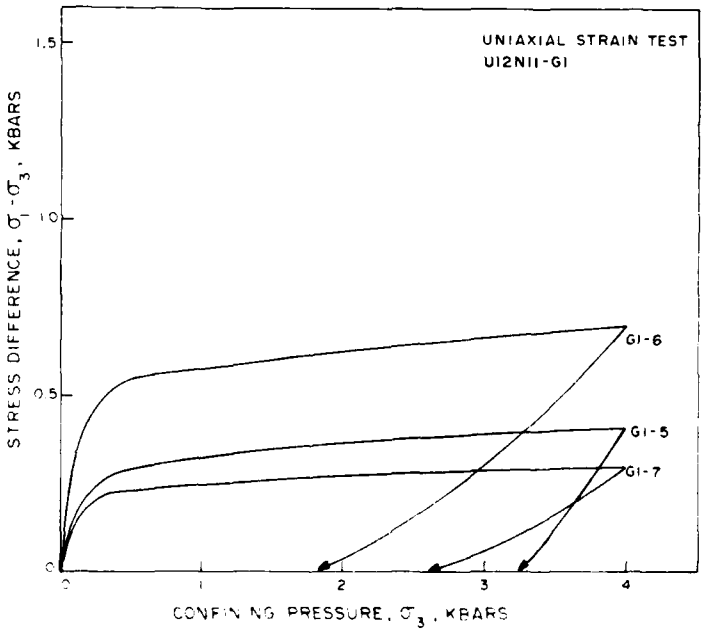

Figure A9b.

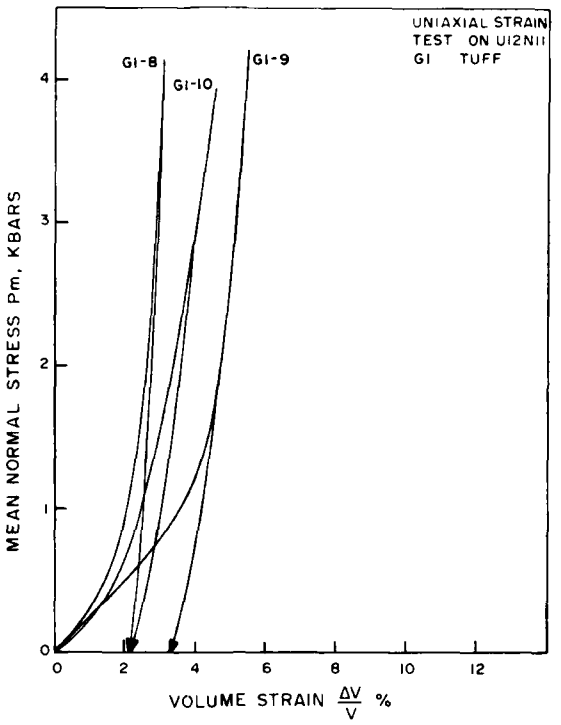

Figure A10a.

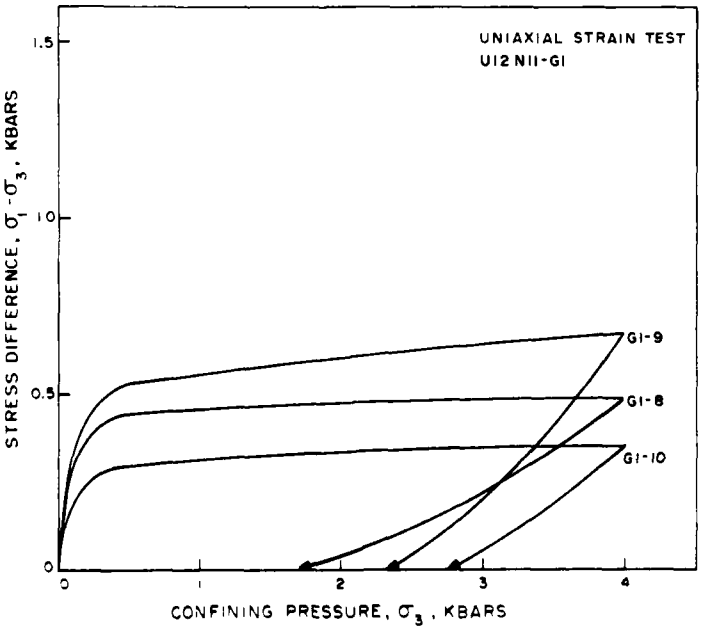

Figure A10b.

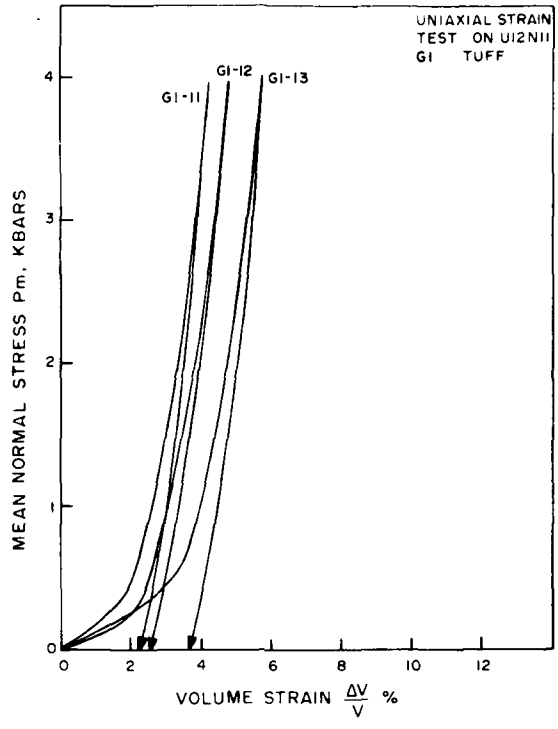

Figure A11a.

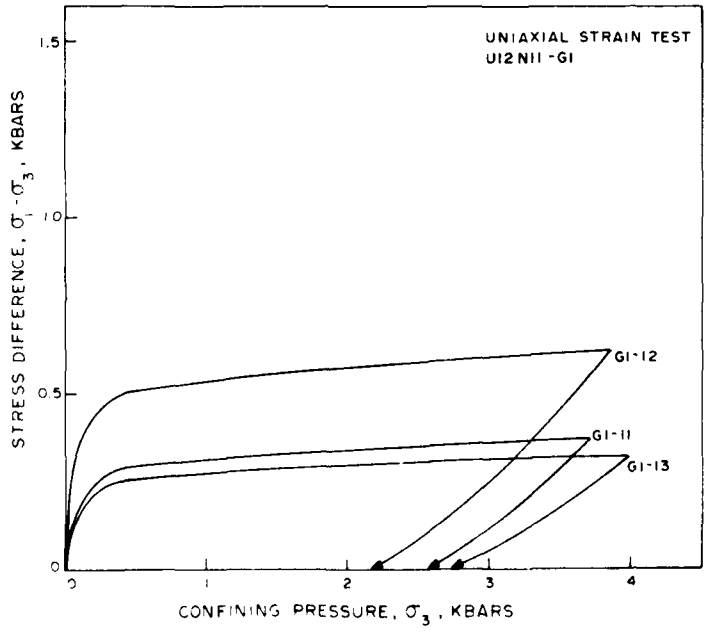

Figure A11b.

APPENDIX B

TEST RESULTS ON U12n.12 TUFF SAMPLES

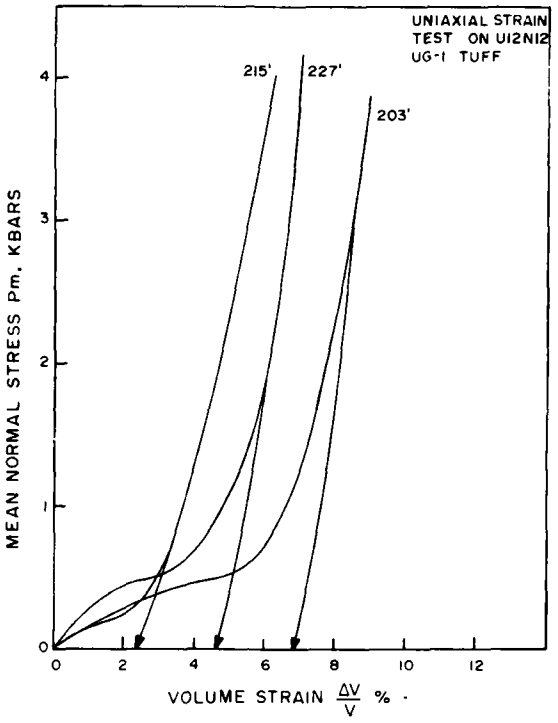

Figure B1a.

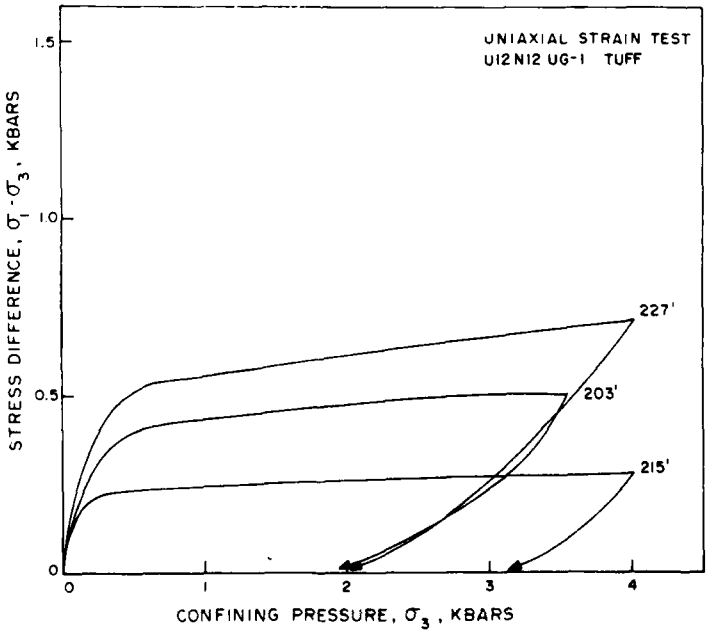

Figure B1b.

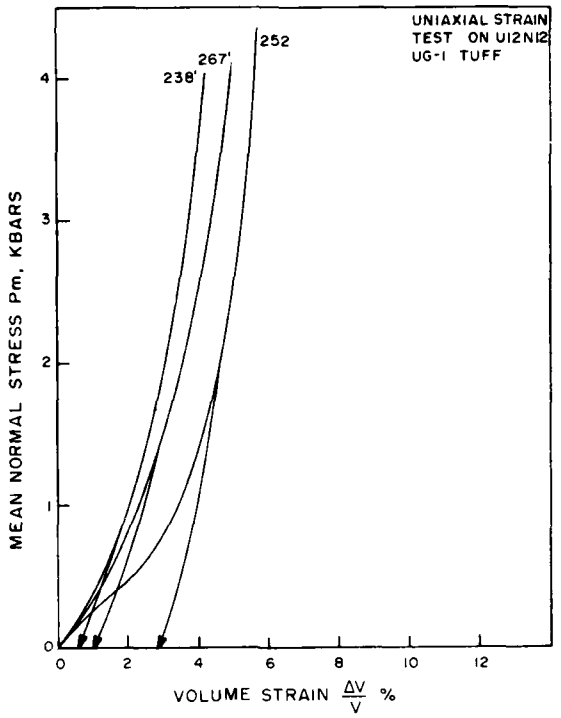

Figure B2a.

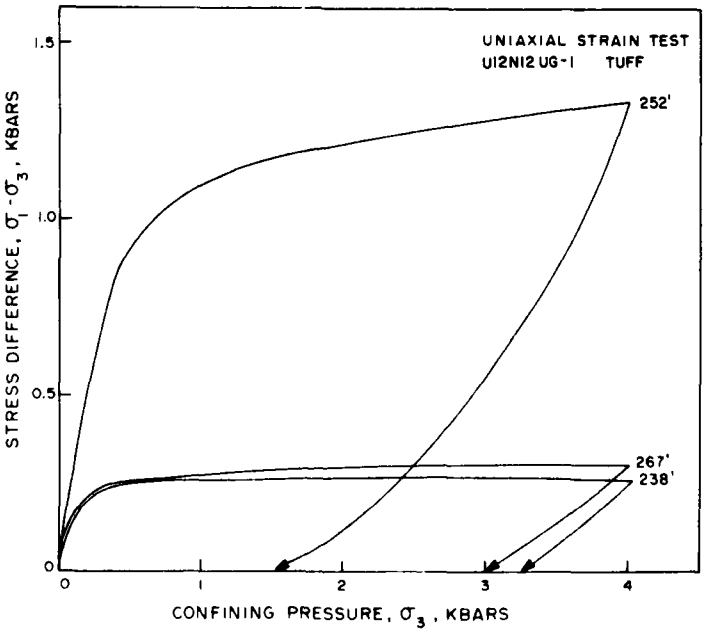

Figure B2b.

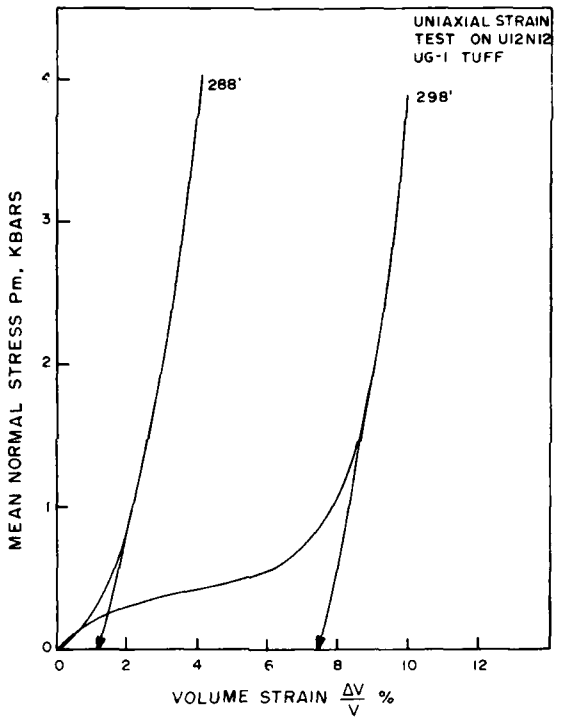

Figure B3a.

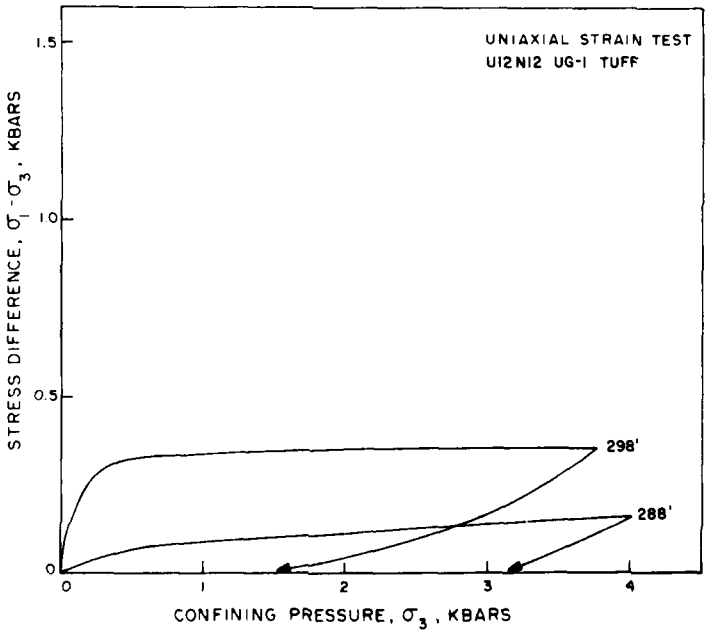

Figure B3b.

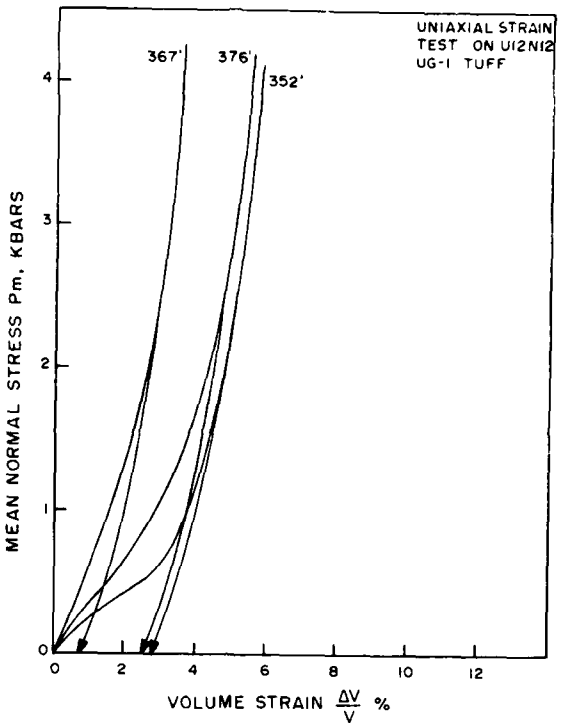

Figure B4a.

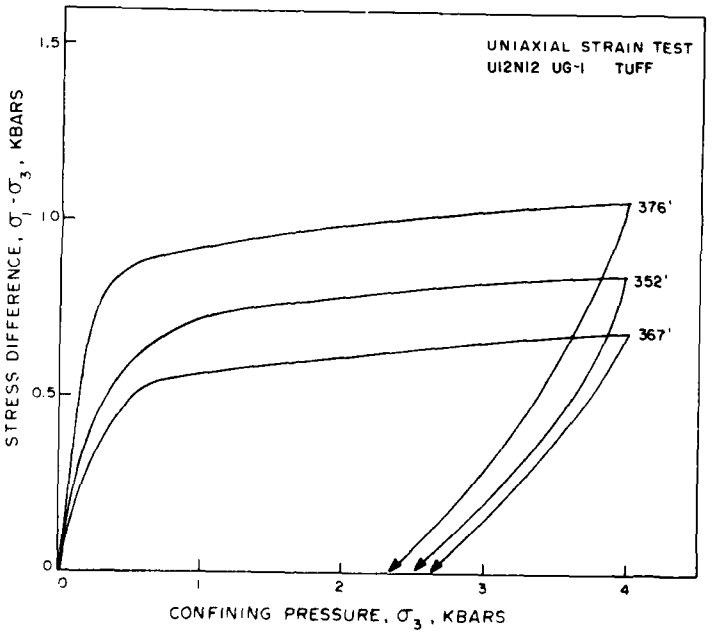

Figure B4b.

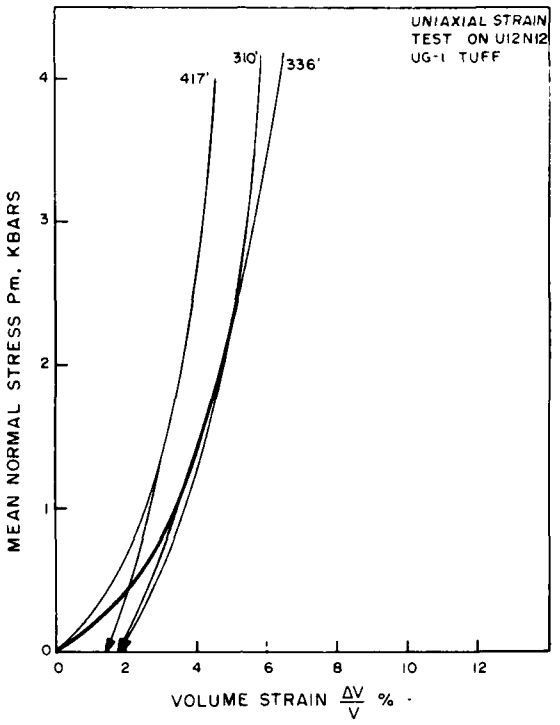

Figure B5a.

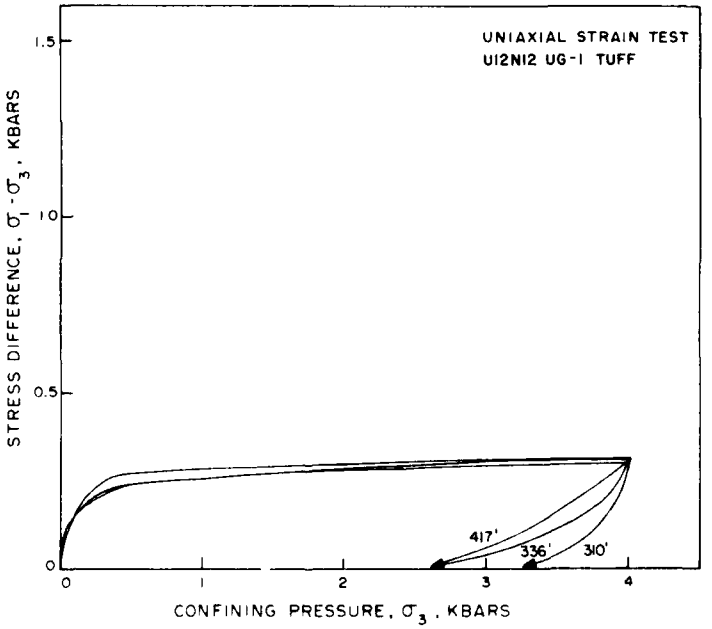

Figure B5b.

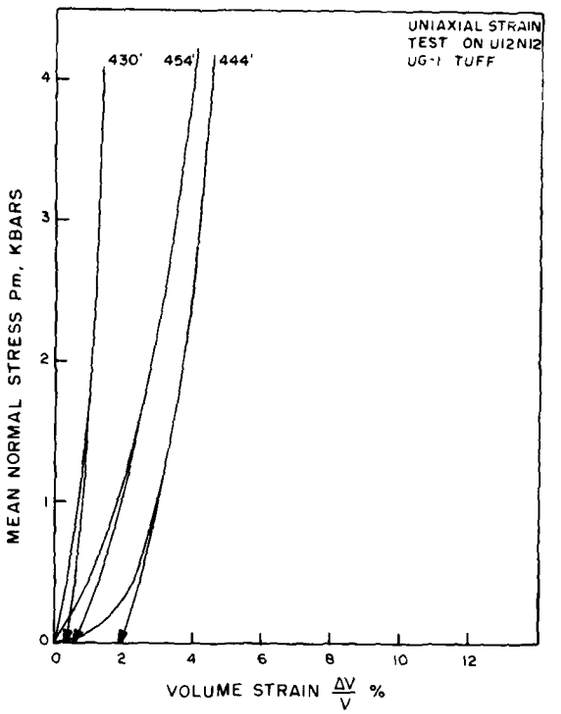

Figure B6a.

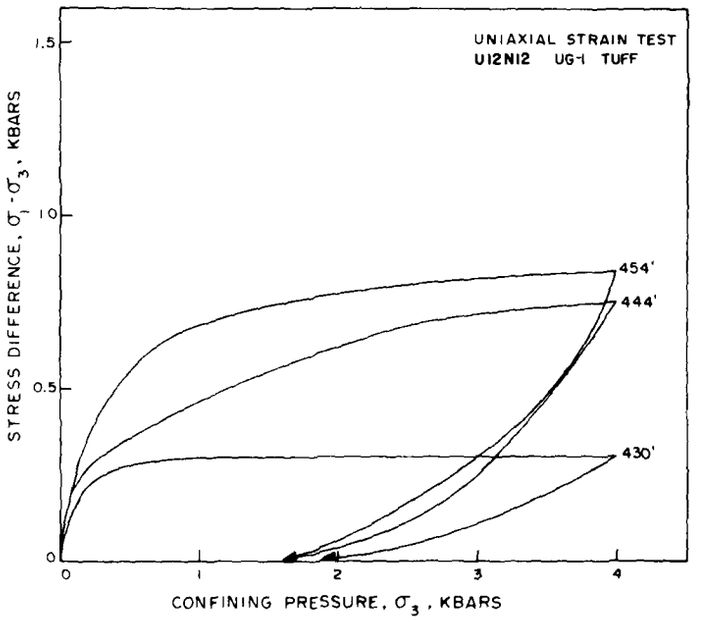

Figure B6b.

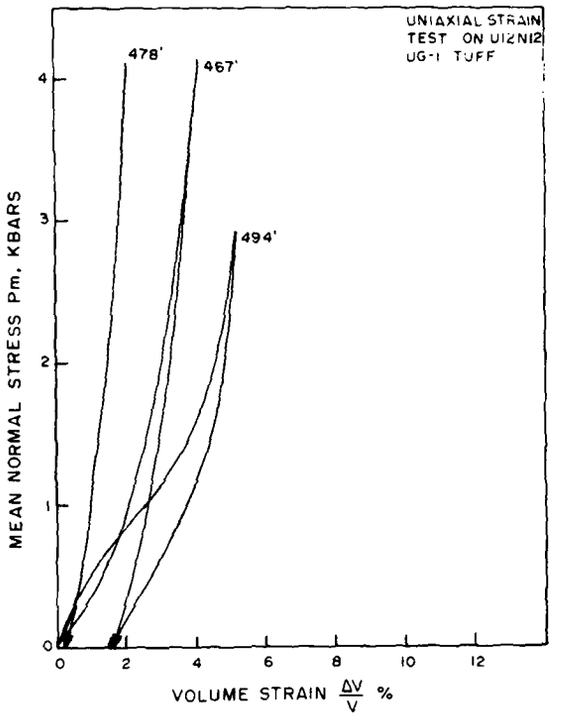

Figure B7a.

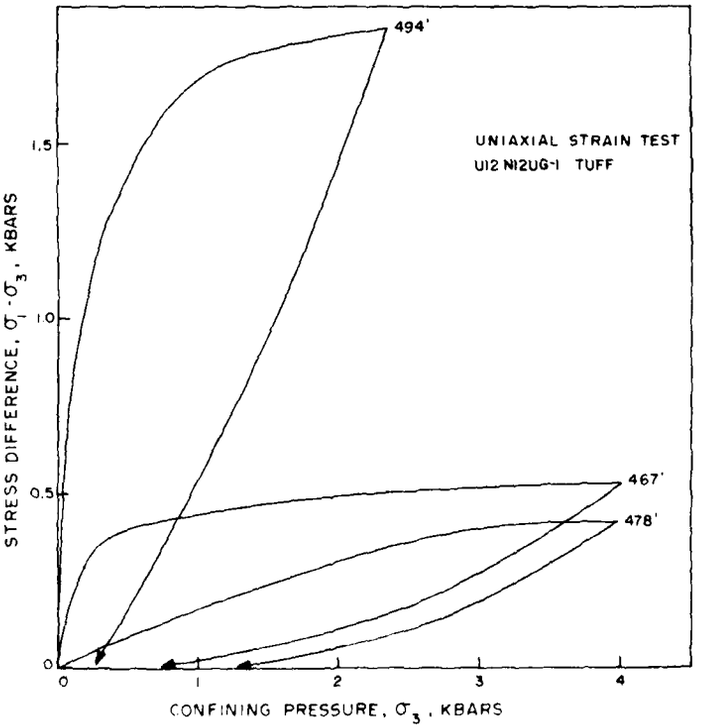

Figure B7b.

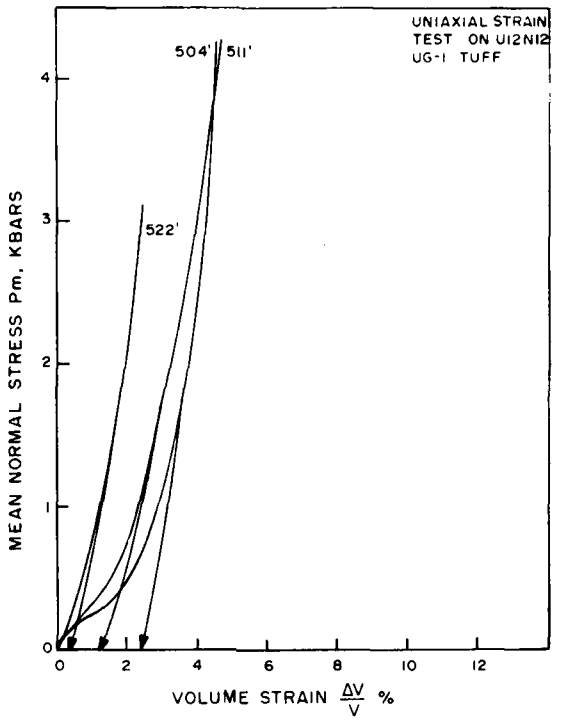

Figure B8a.

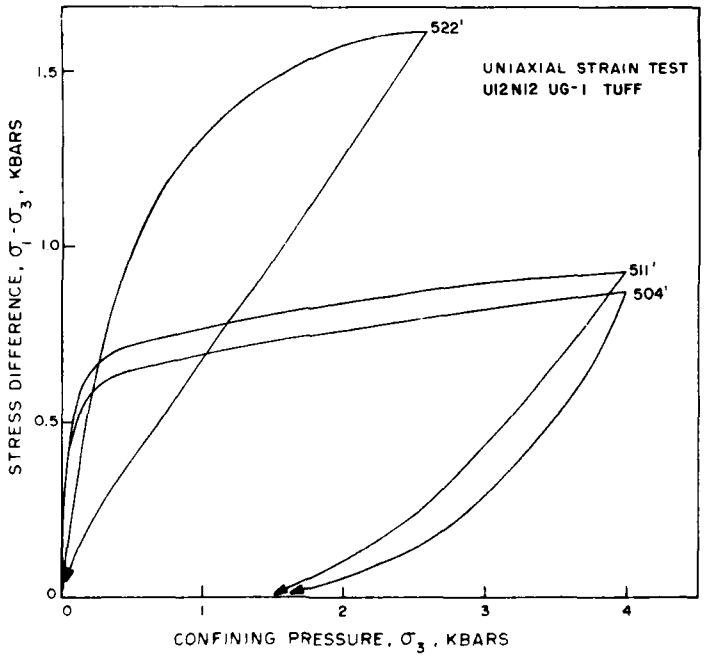

Figure B8b.

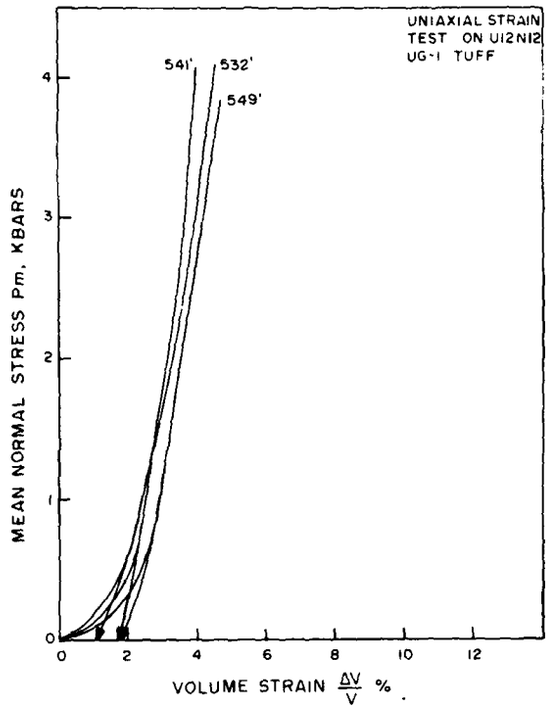

Figure B9a.

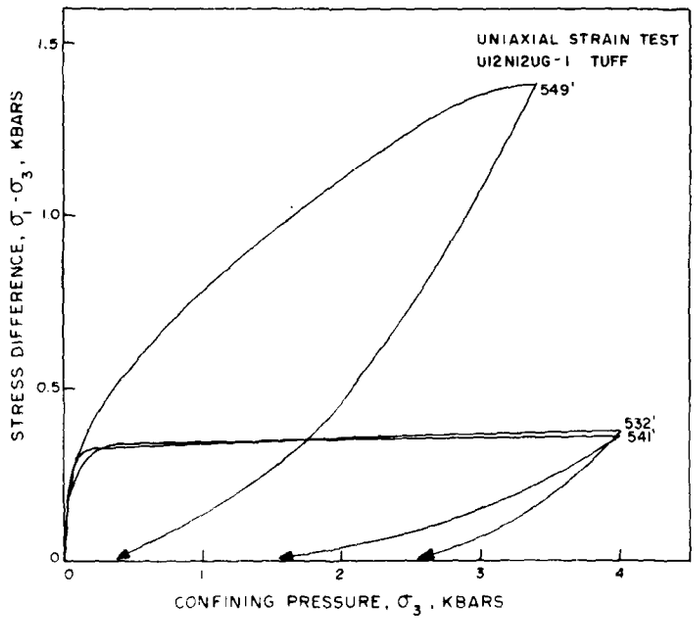

Figure B9b.

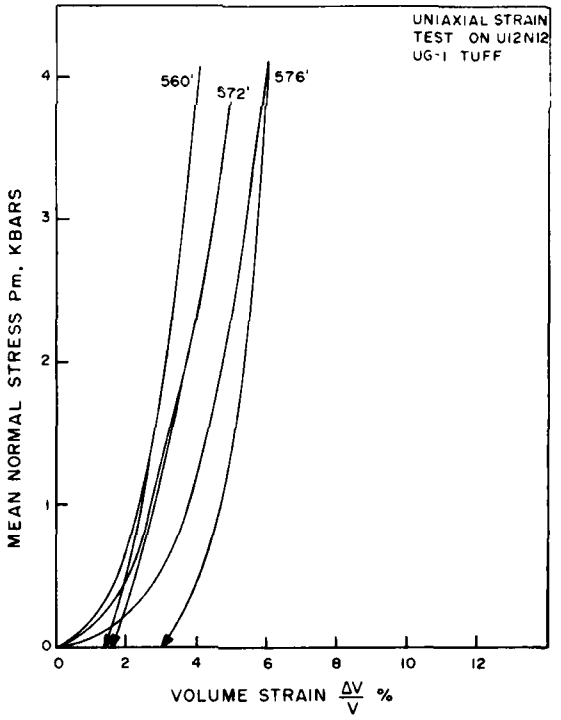

Figure B10a.

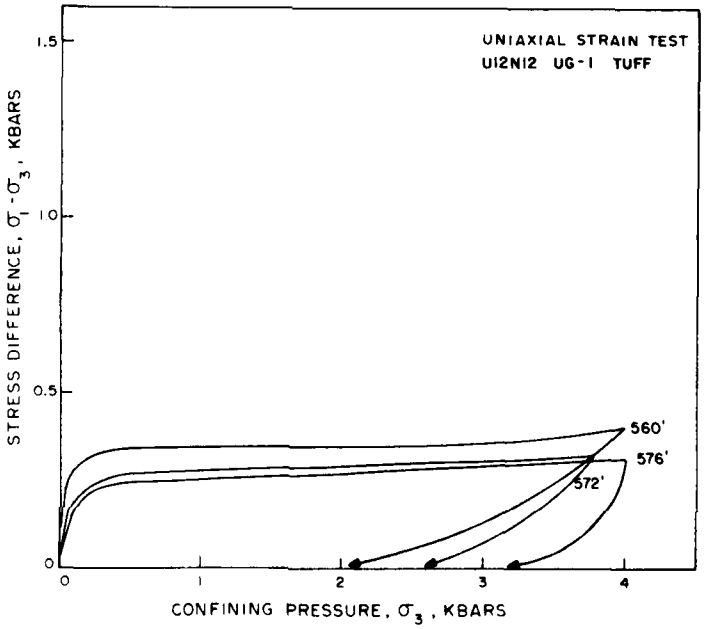

Figure B10b.

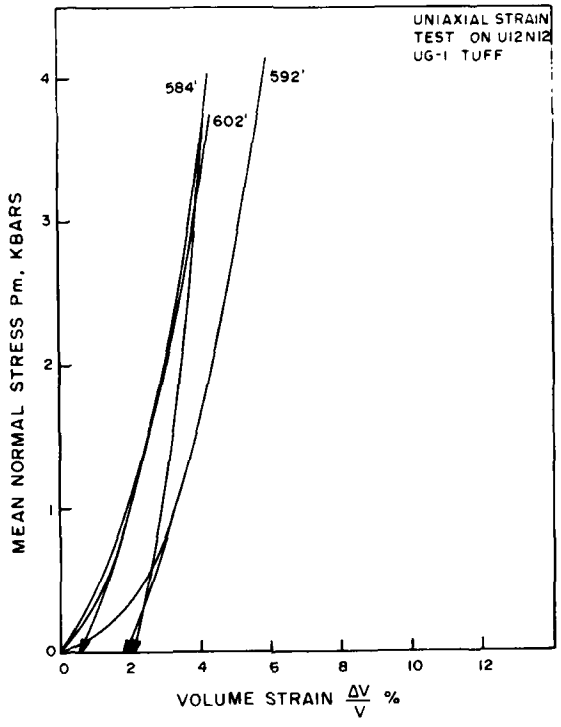

Figure B11a.

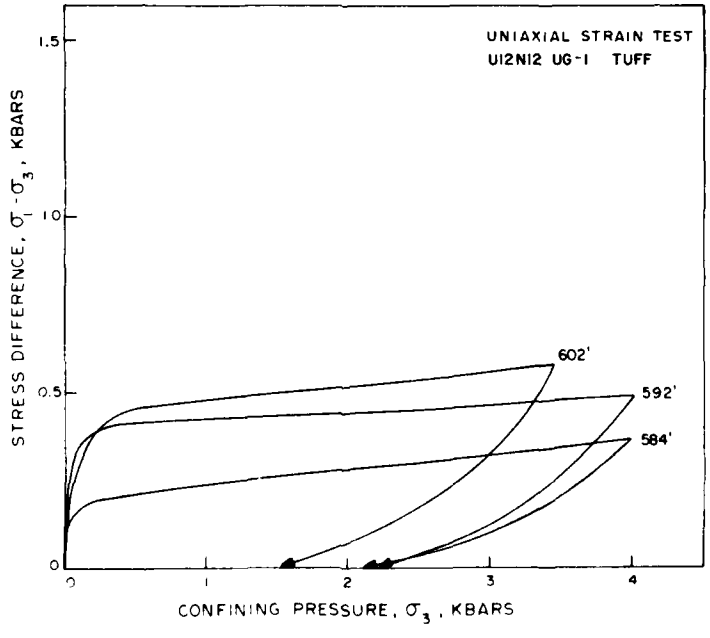

Figure B11b.

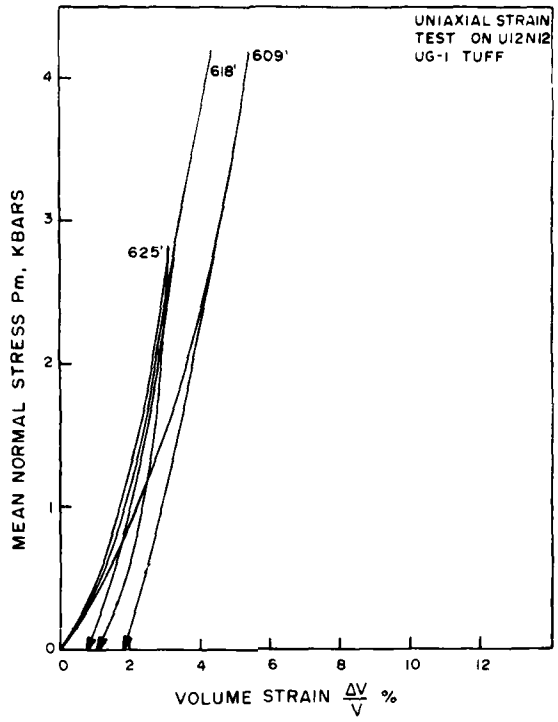

Figure B12a.

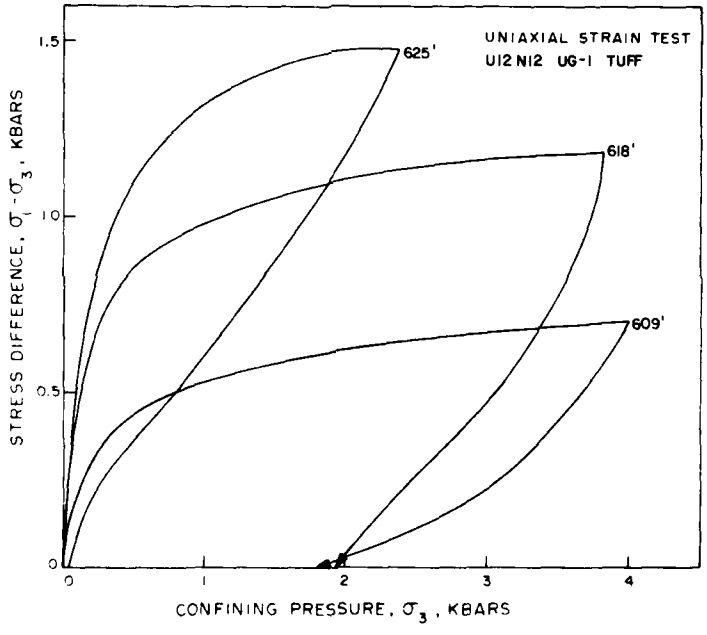

Figure B12b.

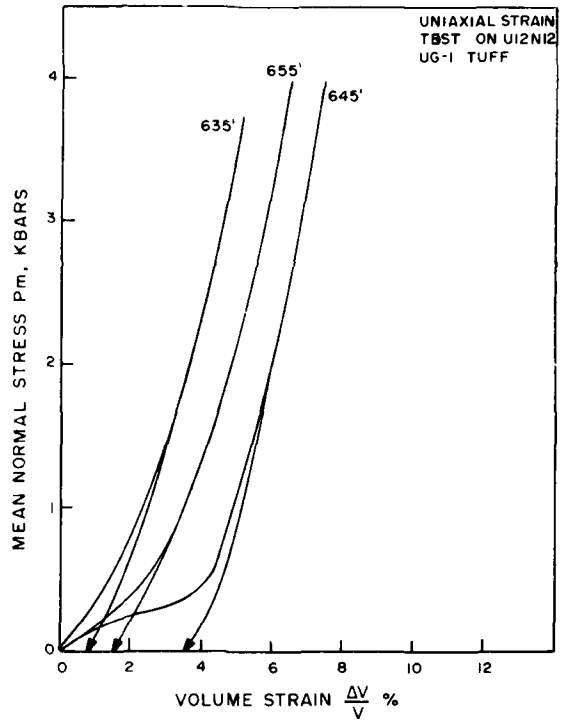

Figure B13a.

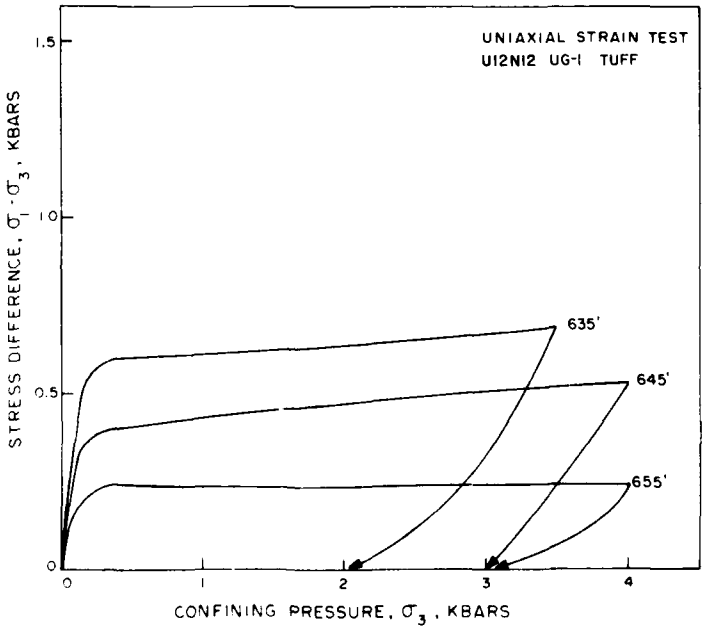

Figure B13b.

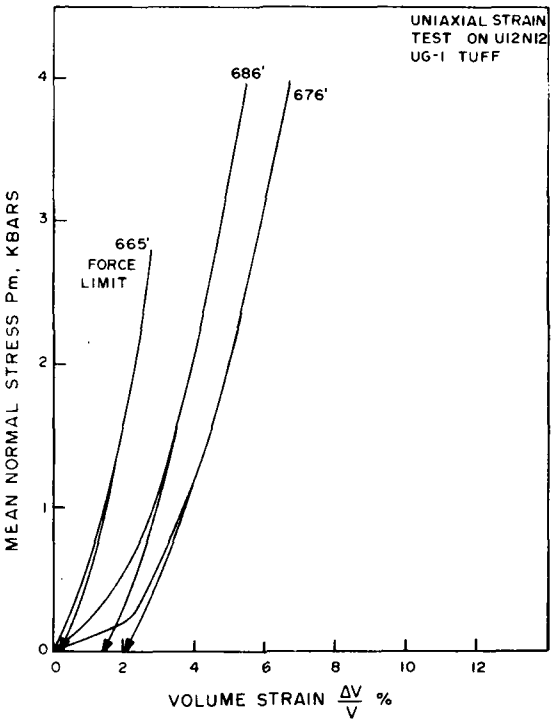

Figure B14a.

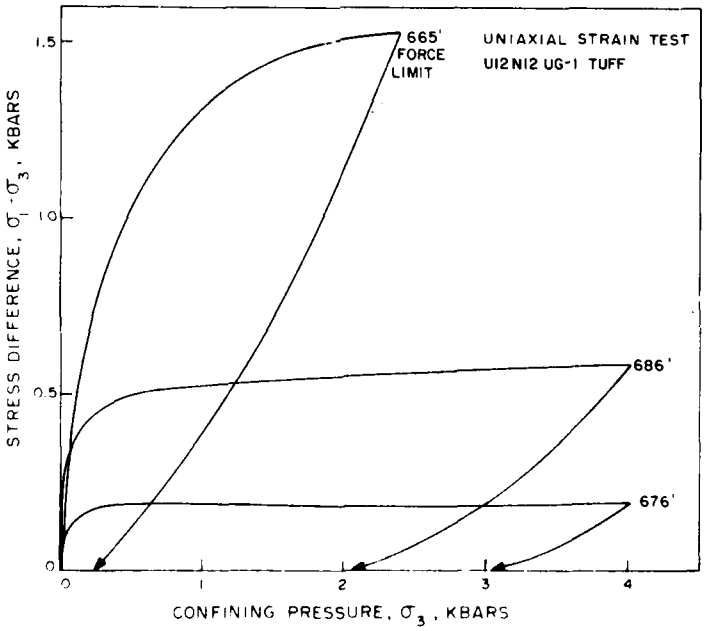

Figure B14b.

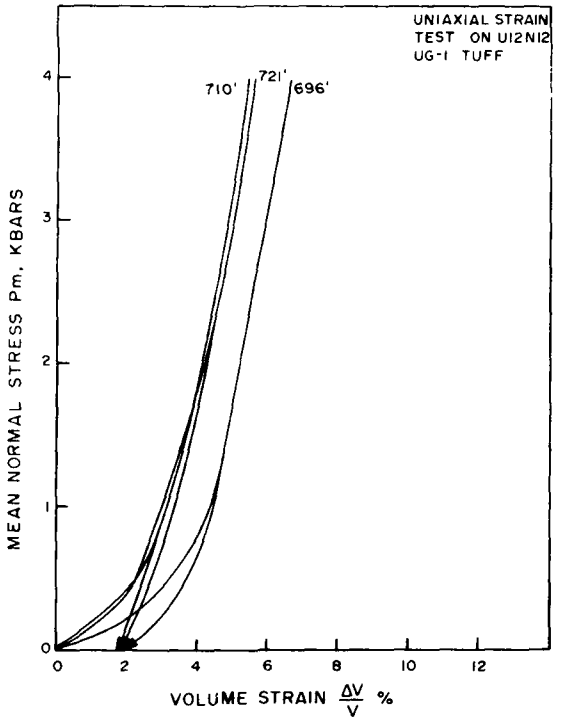

Figure B15a.

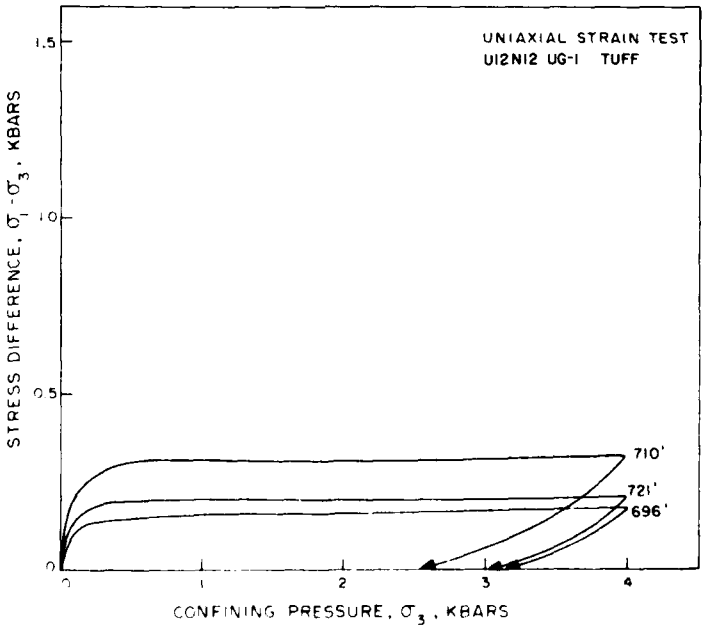

Figure B15b.

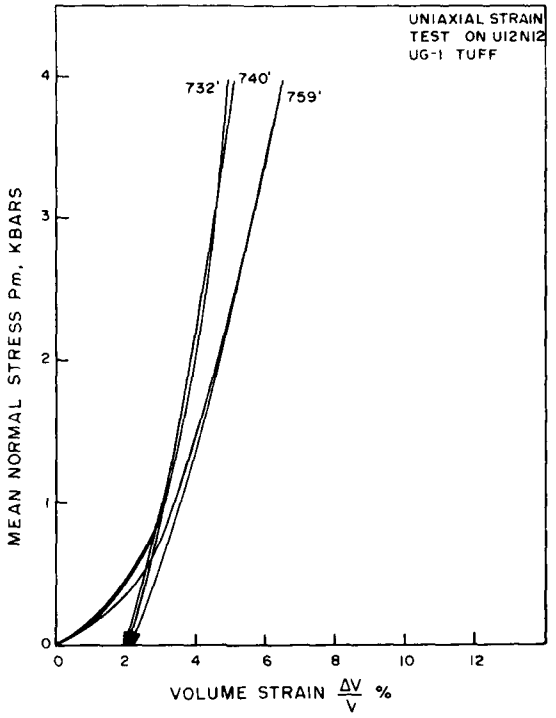

Figure B16a.

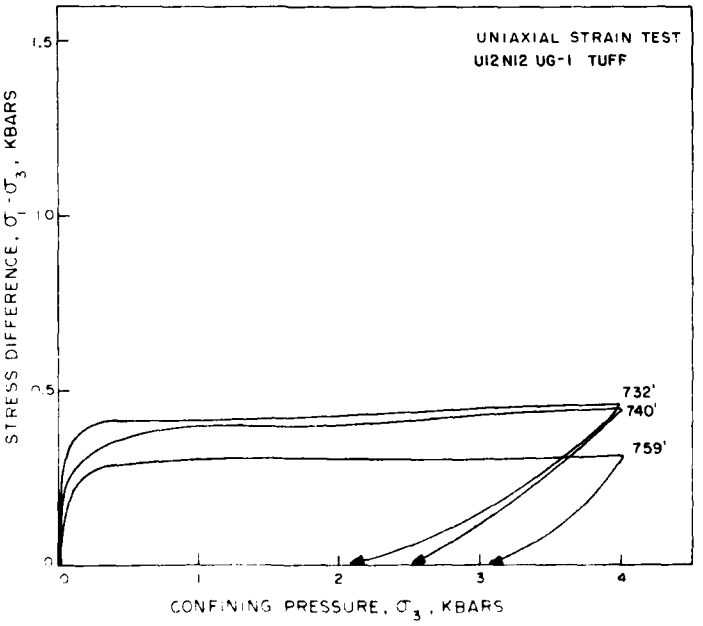

Figure B16b.

APPENDIX C

TEST RESULTS ON MISCELLANEOUS TUFF SAMPLES

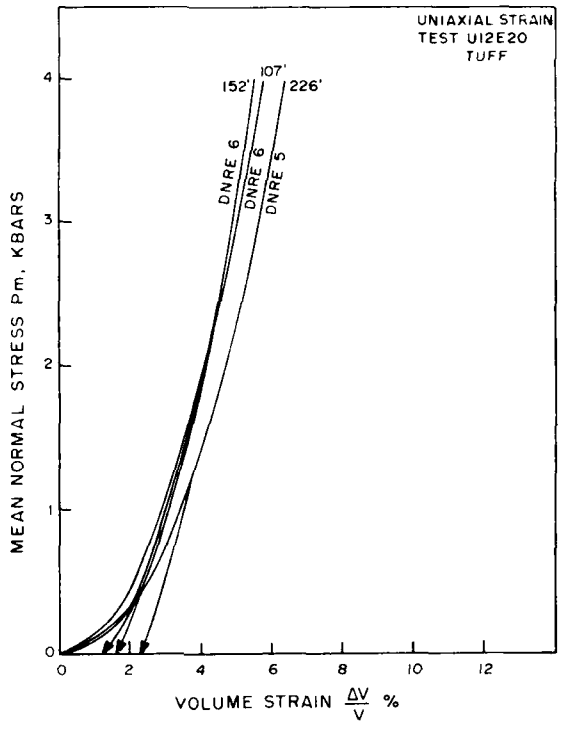

Figure C1a.

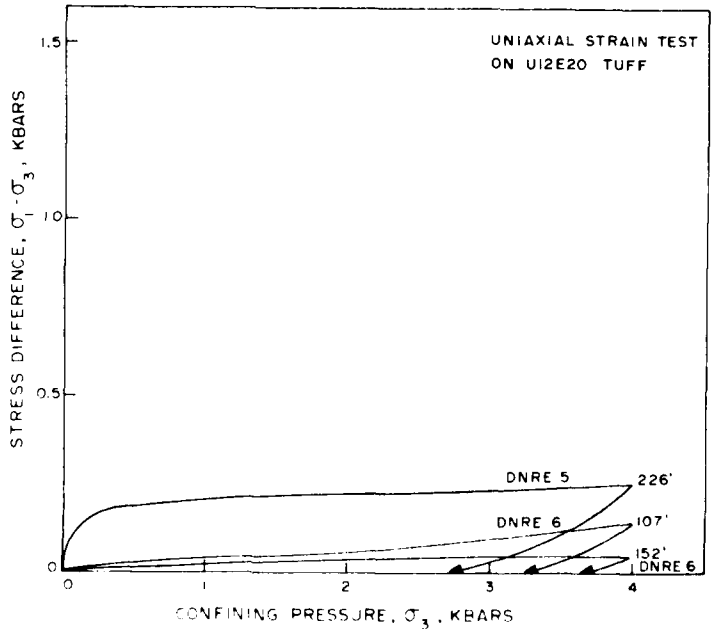

Figure C1b.

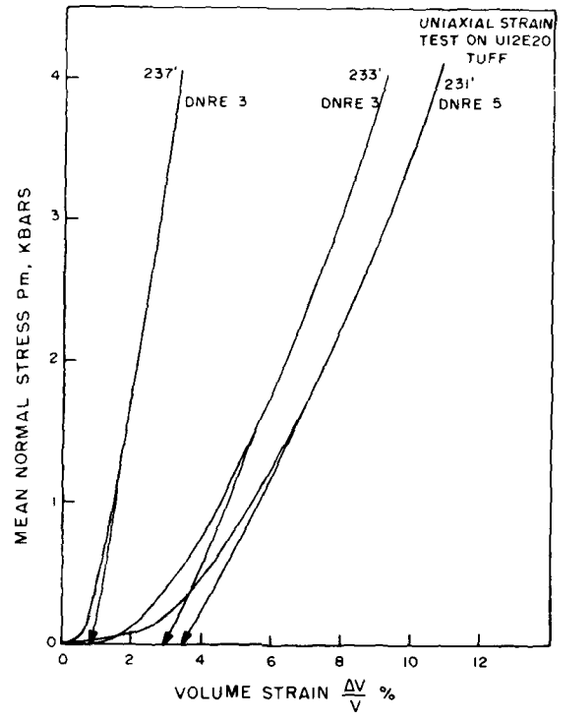

Figure C2a.

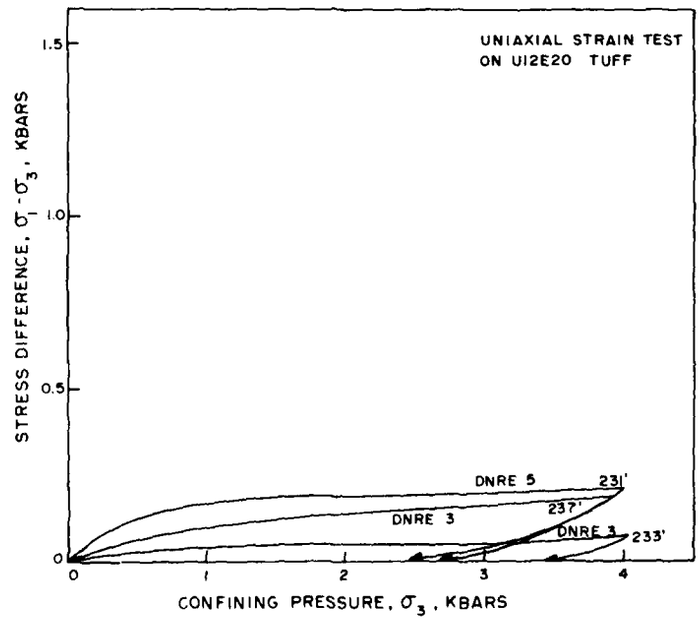

Figure C2b.

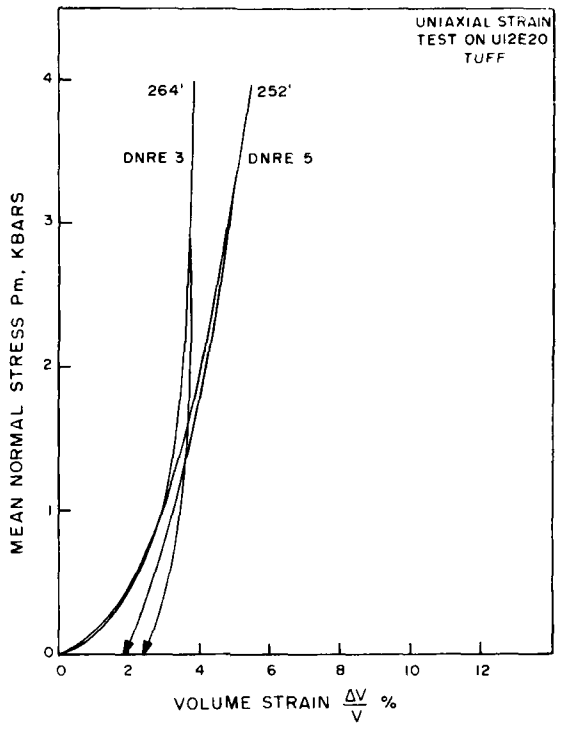

Figure C3a.

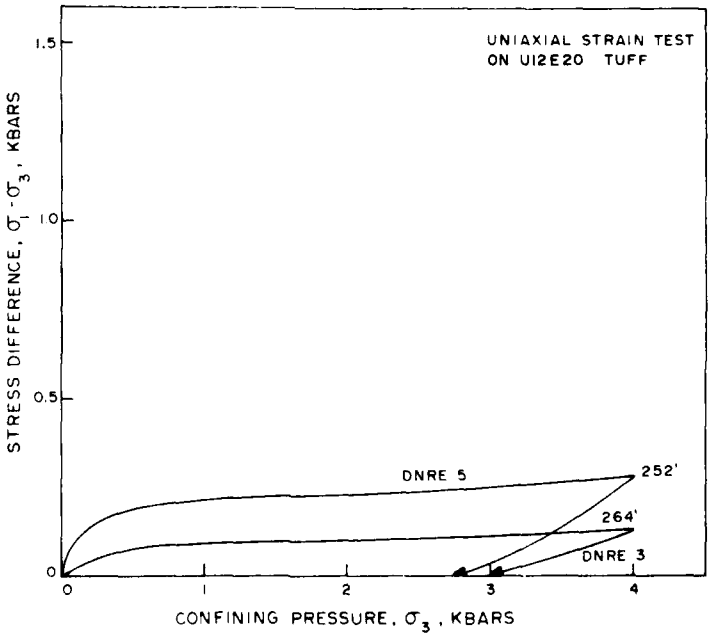

Figure C3b.

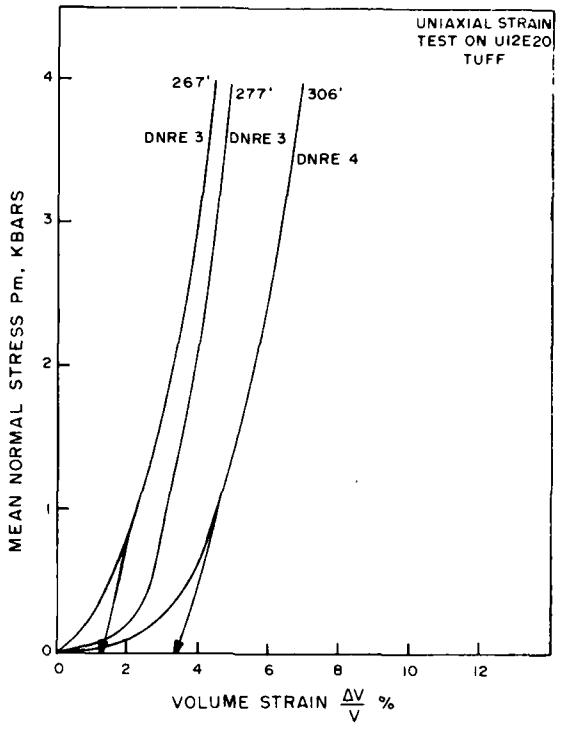

Figure C4a.

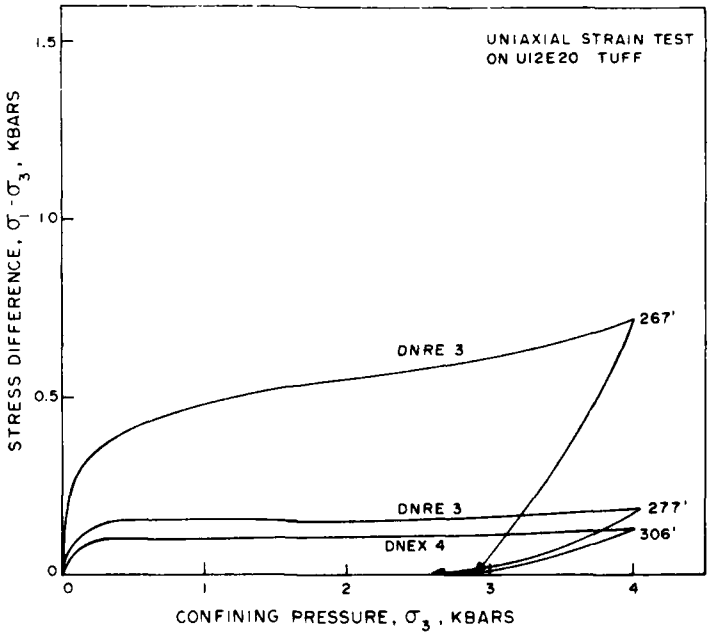

Figure C4b.

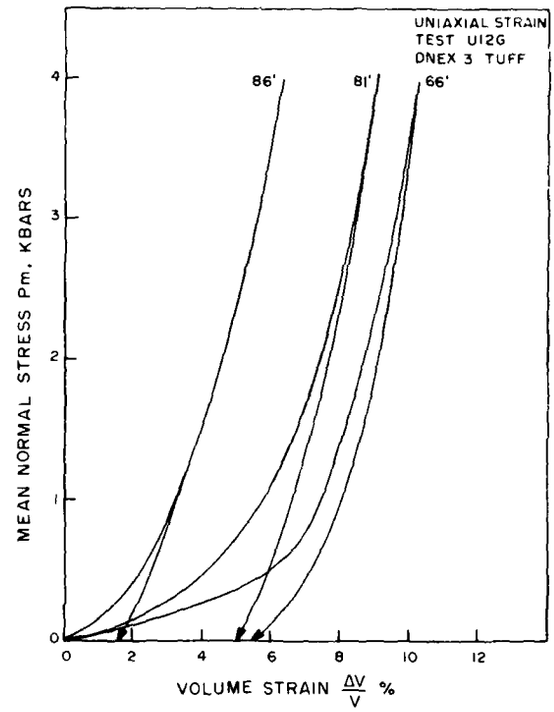

Figure C5a.

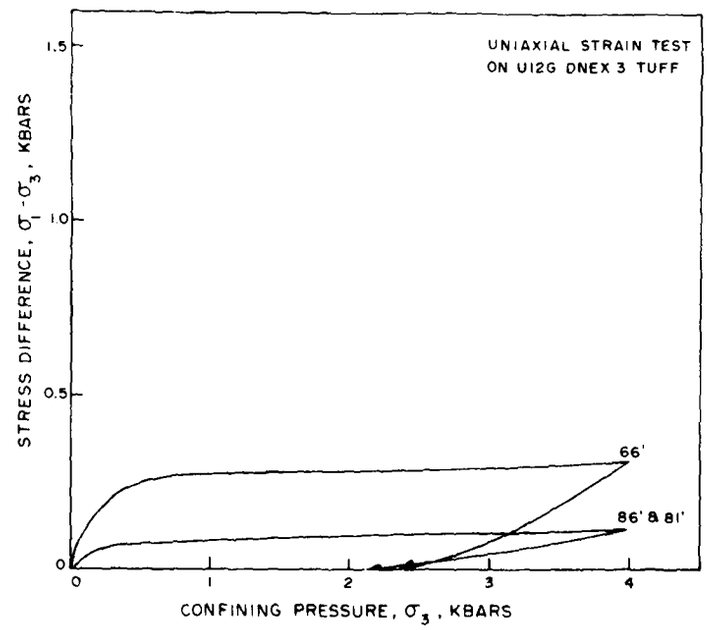

Figure C5b.

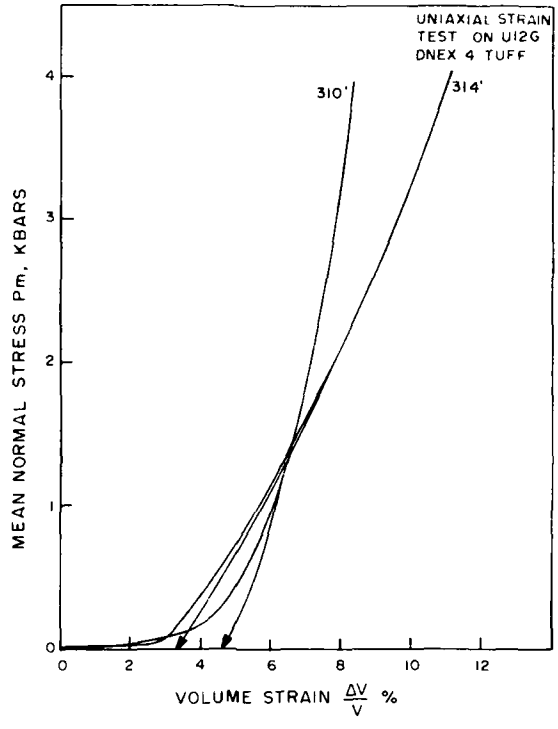

Figure C6a.

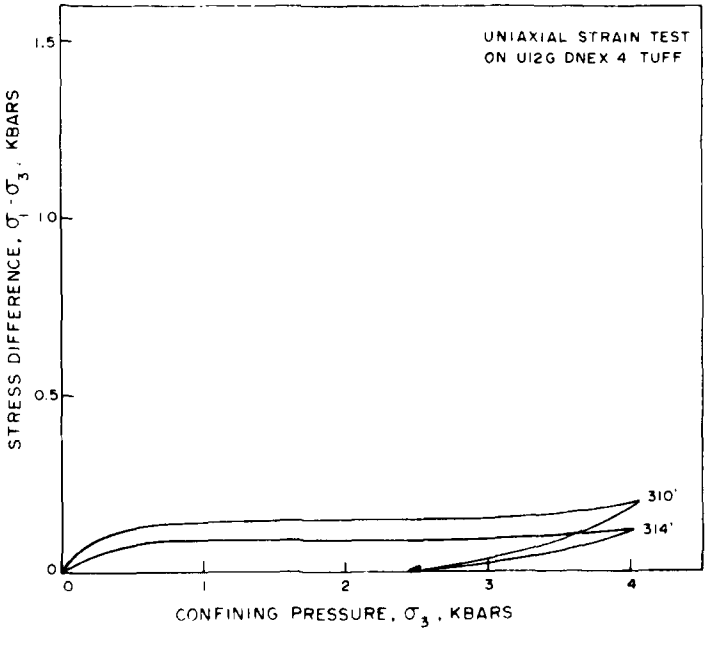

Figure C6b.

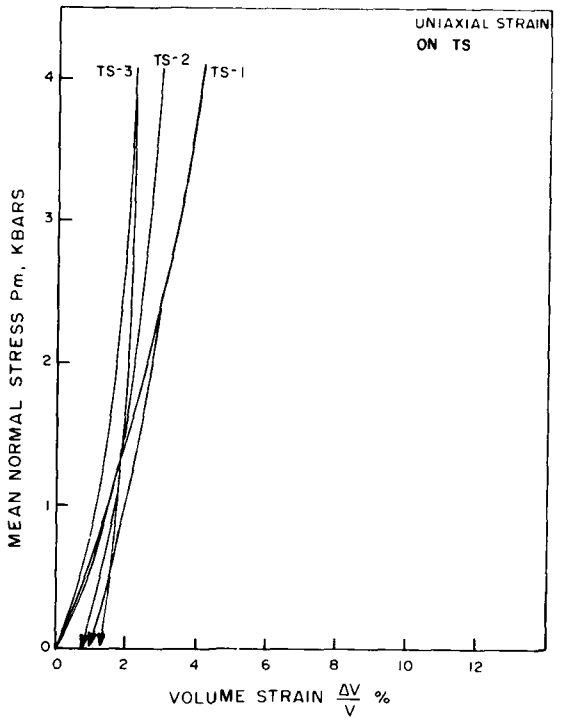

Figure C7a.

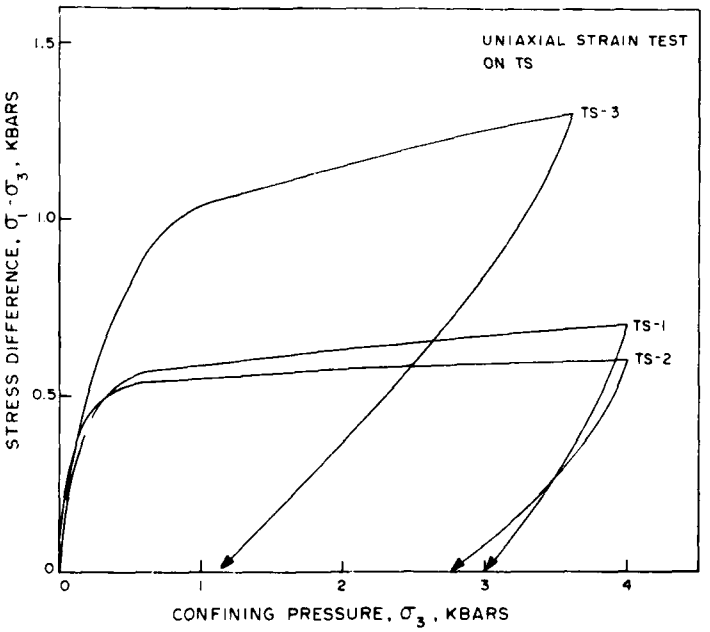

Figure C7b.

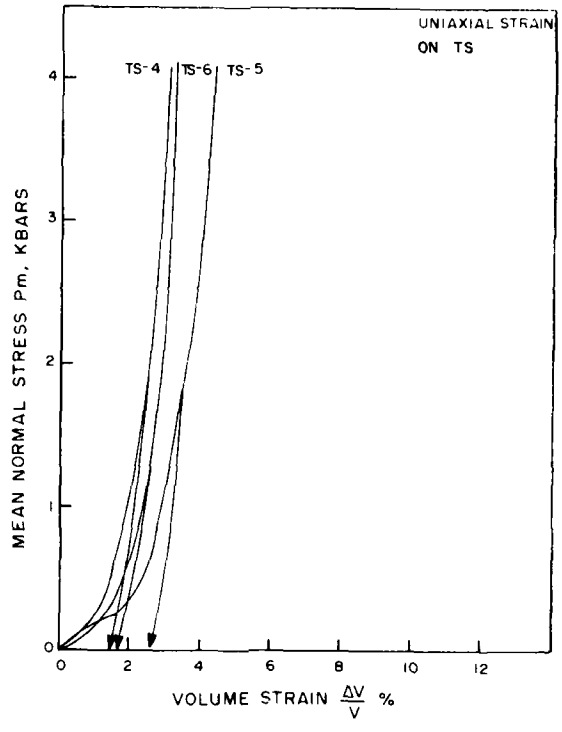

Figure C8a.

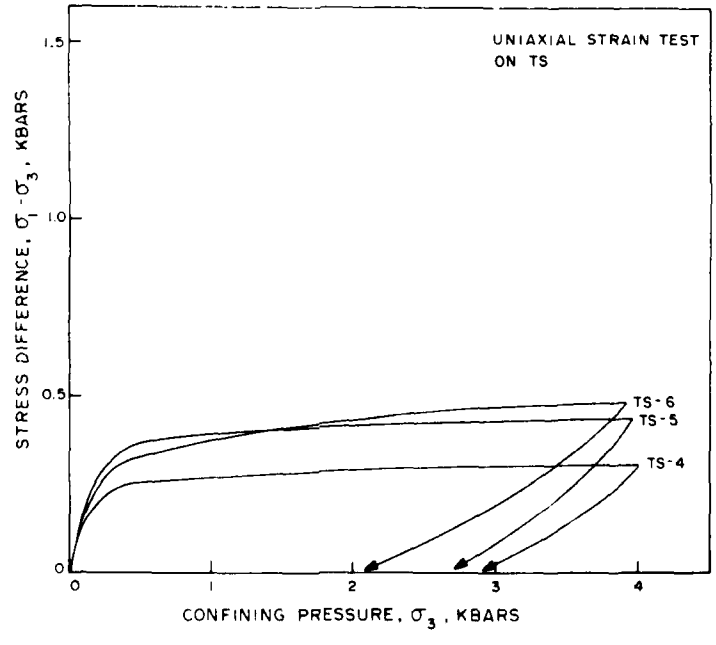

Figure C8b.

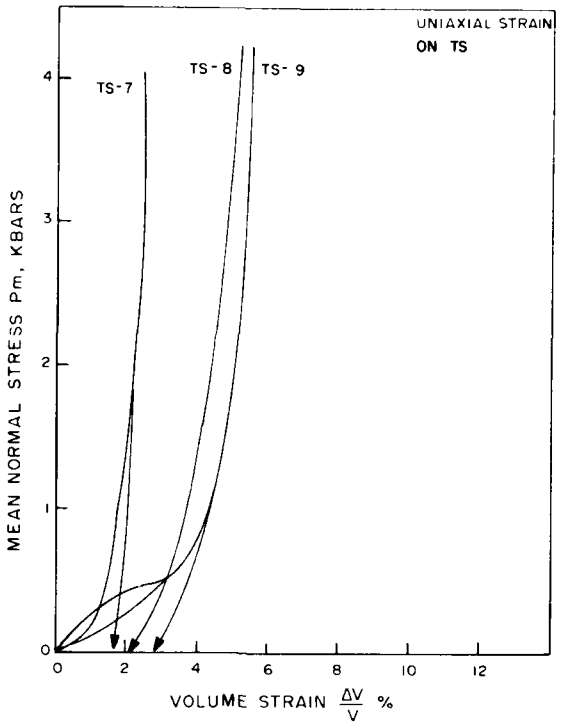

Figure C9a.

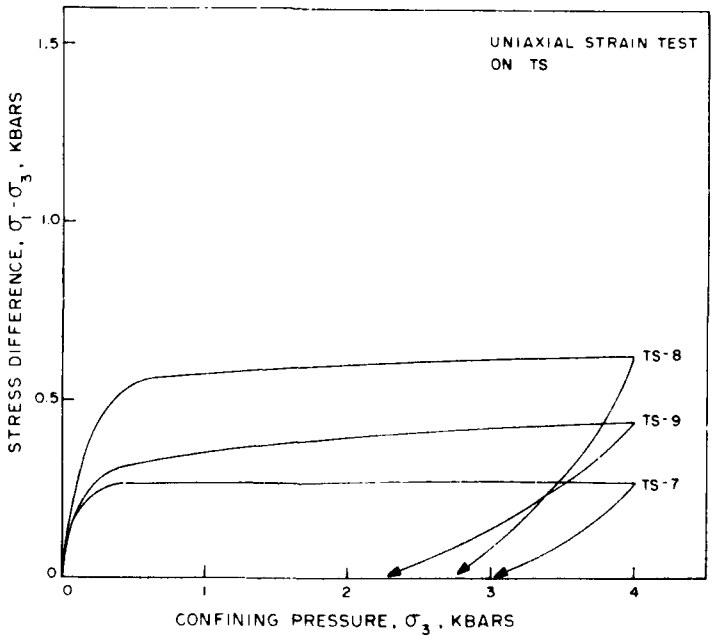

Figure C9b.

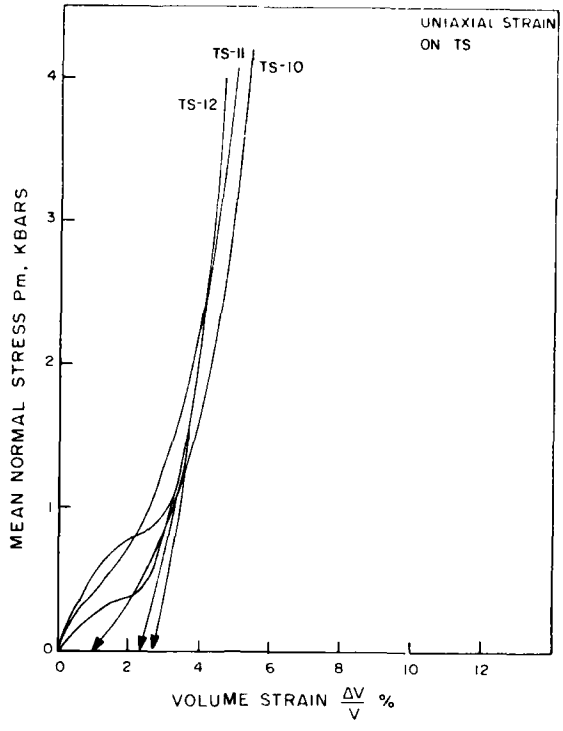

Figure C10a.

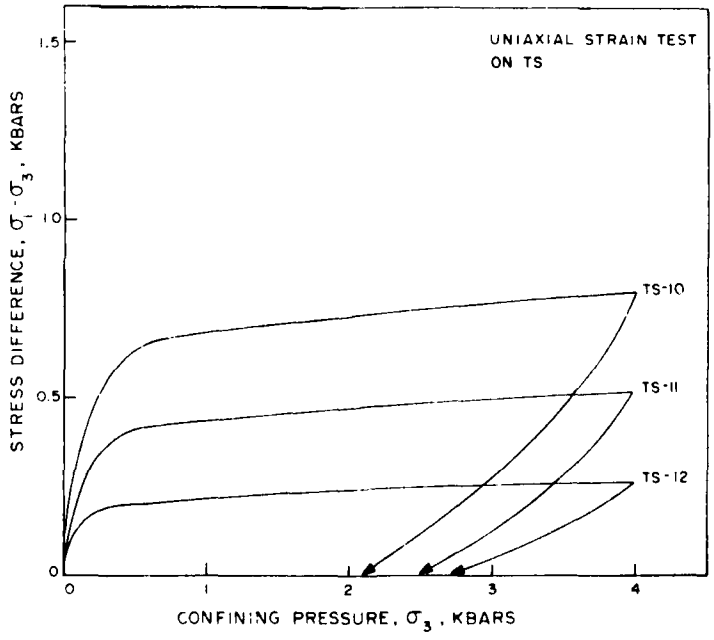

Figure C10b.

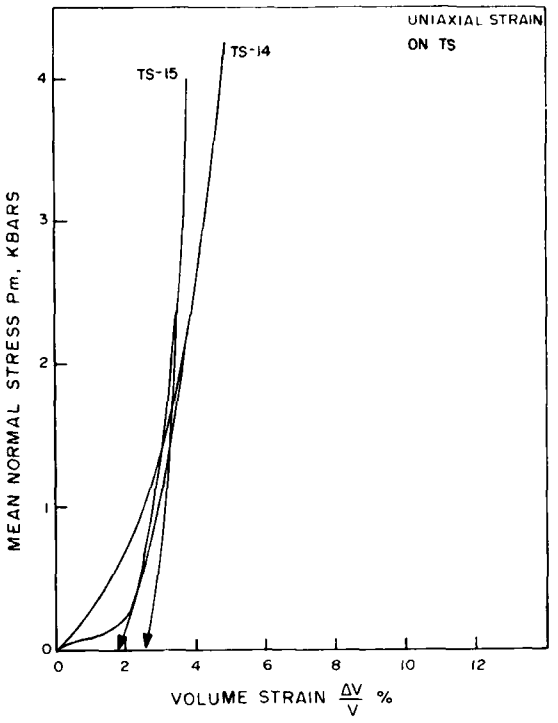

Figure C11a.

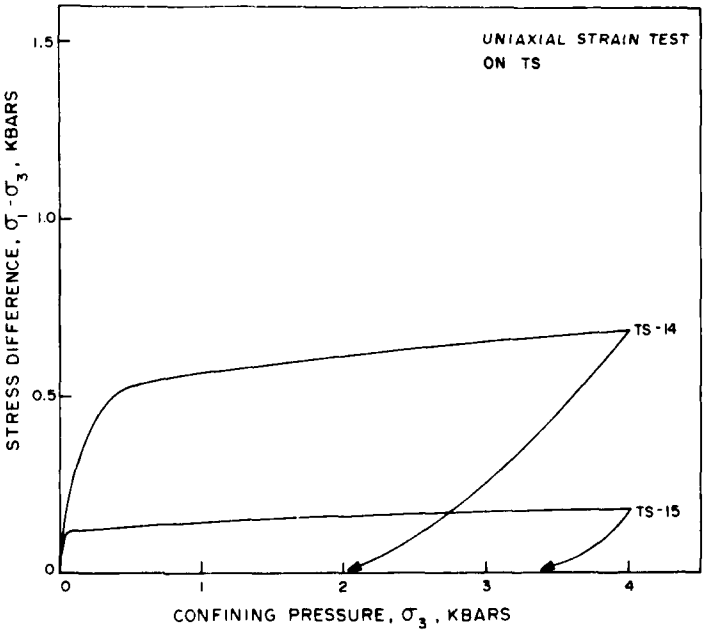

Figure C11b.

APPENDIX D

LABORATORY TESTING PROCEDURE

SAMPLE HANDLING AND PREPARATION TECHNIQUES

Tuff samples were received wrapped in foil and sealed in beeswax. Cores were between 1.85 and 2.5 inches (4.7 and 6.4 cm) in diameter and ranged in length from approximately 8 to 20 inches (20.3 to 50.8 cm). Density and moisture content were determined with small pieces (i.e. ~50 cc) chipped from the core. Mechanical test specimens were cut to 2.5 inch (6.4 cm) length using a diamond cut-off saw and water coolant. The ends were subsequently ground parallel to within 0.001 inches (0.0025 cm). After cutting and grinding, specimens were wrapped in a urethane jacket and mounted to steel endcaps. The jacket was then sealed to the endcaps with rubber tape and wire.

TEST PROCEDURES

Physical Properties Determination

The "as-received" density is determined by weighing the cut-off test specimen and measuring the volume using a mercury displacement technique. The same specimen is then stripped of the wax, weighed and dried in an oven at 105°C for 24 hours. From the dried sample weight, the percentage water by wet weight (% H_2O) can be determined. The piece is then crushed and pulverized (100 mesh) for use in determining the grain density. Grain volume is measured by water immersion and gas evacuation technique. All weights are measured to ±0.05 percent accuracy; volumes are accurate to ±1.0 percent.

The symbols and equations used for the measured and calculated physical properties are as follows:

Symbols

$*\rho_w$ = in situ bulk density (wet or "as-received" density) (gm/cm^3)

$*\rho_g$ = grain density (density of solids) (gm/cm^3)

ρ_{H_2O} = density of water (gm/cm^3)

$*$ w = moisture content (percent by total weight)

ρ_d = dry bulk density after oven drying (gm/cm^3)

η_t = total porosity (percent by total volume)

S_r = degree of saturation (percent by void volume)

V_{av} = air void content (percent by total volume)

$*$ Measured parameters

Equations

$$\rho_d = \rho_w \left(1 - \frac{W}{100}\right)$$

$$\eta_t = 100 \times \left(1 - \frac{\rho_d}{\rho g}\right)$$

$$s_r = 100 \times \frac{(w \times \rho_w)}{(\eta_t \times \rho H_2 0)}$$

$$V_{av} = 100 \times [1 + \rho_d (1 - 1/\rho_g) - \rho_w]$$

Mechanical Tests

All mechanical tests were conducted using a servo-controlled press coupled to a servo-controlled intensifier shown in Figures D1 and D2 respectively. A variety of different tests are possible with this machine including hydrostatic and triaxial compression and uniaxial strain tests. The upper loading actuator has 130,000 pounds capacity and the pressure vessel is capable of 4 kilobars (400 MPa) internal pressure.

Data are recorded using X-Y recorders. Signal conditioning equipment and calibration methods provide an accuracy of ±2% on pressure and stress measurements.

Strain Measurements

Strains are measured using cantilevers inside the pressure vessel. A schematic of a mechanical test specimen with axial and transverse strain cantilevers is shown in Figure D3. A photograph of a test specimen is shown in Figure D4.

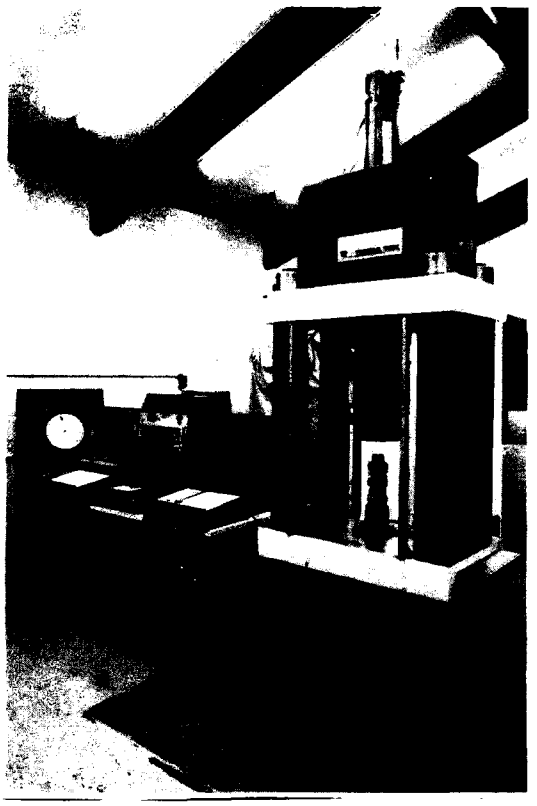

Figure D1. 4 Kbar test machine with associated servo-controlled electronic equipment.

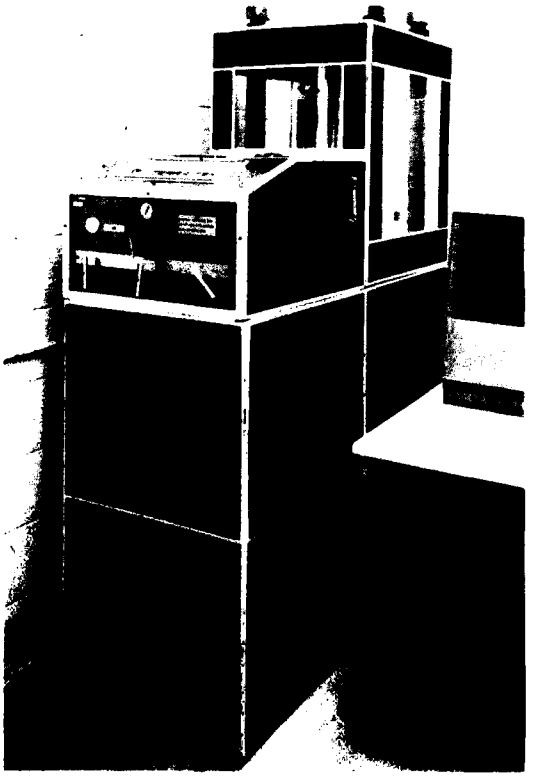

Figure D2. 4 Kbar pressure intensifier.

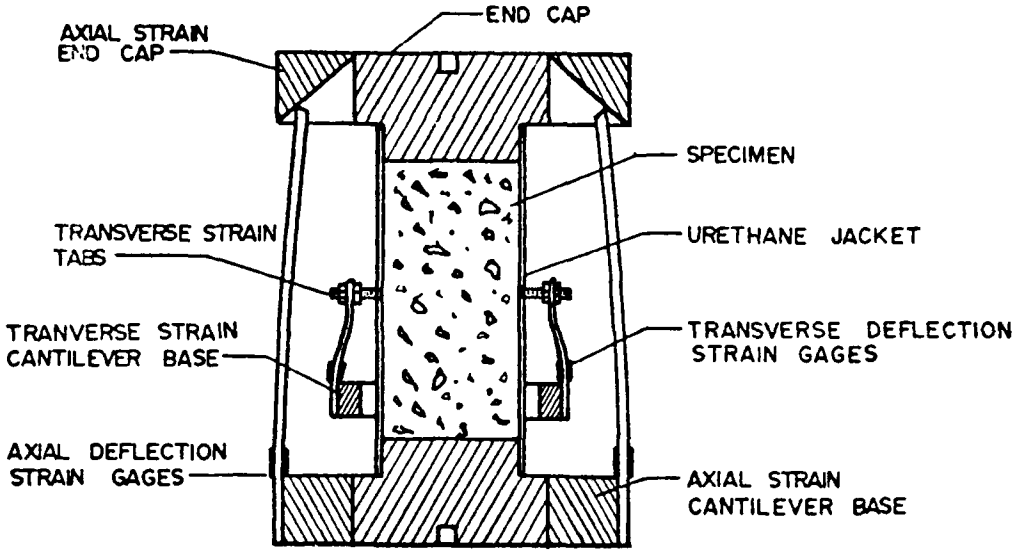

Figure D3. Schematic drawing of a specimen with the axial and transverse strain transducers.

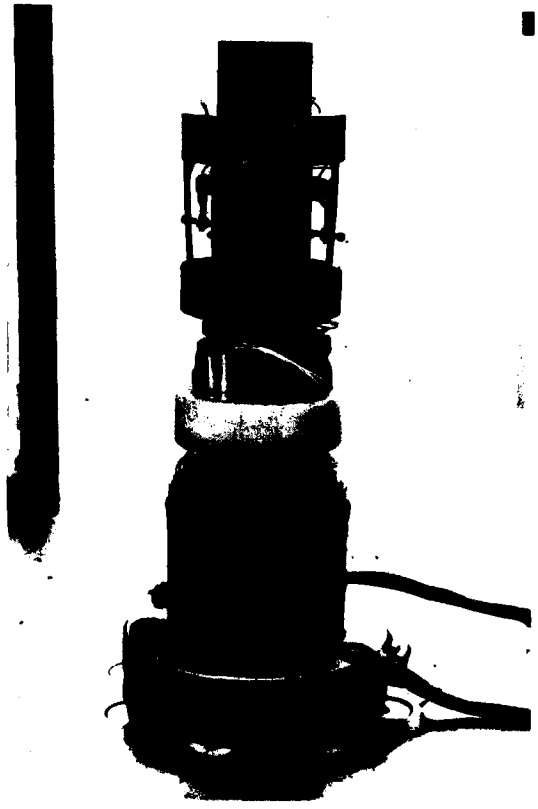

Figure D4. Test sample with axial and transverse strain measured cantilevers.

Data Presentation

Data are plotted as either hydrostatic pressure or mean normal stress versus volume change, stress difference versus individual strains, or stress difference versus confining pressure where compressive stresses and shortening strains are positive. Here σ_1, σ_2, σ_3 and ε_1, ε_2, ε_3 refer to principal stresses and strains, respectively. For all tests, σ_1 and ε_1 refer to axial direction, and $\sigma_2 = \sigma_3$ are the lateral stresses applied by the liquid pressure. The term ε_2, which for an isotopic material is assumed equal to ε_3, refers to the transverse strain. Other terms frequently used in the text are defined as follows:

$$\text{Mean normal stress} = \frac{(\sigma_1 + \sigma_2 + \sigma_3)}{3}$$

$$\text{Volume strain} = \varepsilon_1 + \varepsilon_2 + \varepsilon_3$$

$$= \varepsilon_1 \text{ (for uniaxial strain loading)}$$

$$\text{Stress difference} = \sigma_1 - \sigma_3$$

$$\text{Confining pressure} = \sigma_3$$

Ultrasonic Velocities

The through-transmission technique was employed to obtain the ultrasonic velocity data; the system used to obtain the data is shown schematically in Figure D5. The main advantage of this technique is the high accuracy with which wave transit time can be measured. The received signal is viewed (on the oscilloscope) alternately with the signal from the variable frequency synthesizer after it has passed through a shaper.

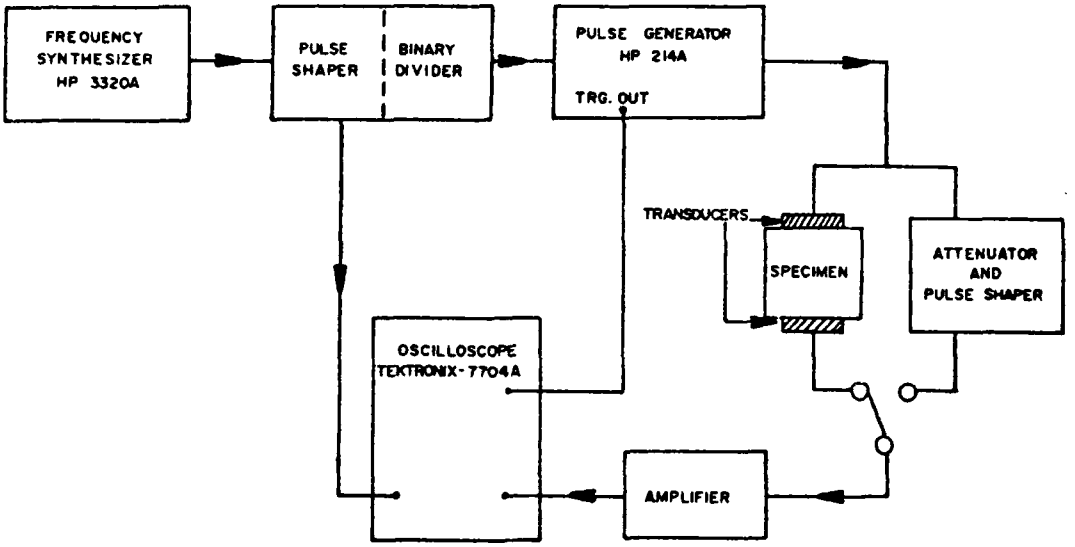

Figure D5. Schematic of ultrasonic velocity measuring equipment.

The shape of the latter is adjusted for an exact match of the initial wave arriving through the specimen. The pulse that excites the transmitting transducer is next viewed and its shape matched to that of the comparison wave. Once this is done, the frequency of the synthesizer is adjusted for an exact number of cycles between the transmitted and received waves. The number of cycles divided by the frequency is the transit time through the specimen.

The ultrasonic longitudinal and shear wave transit times are measured and, along with the specimen length and density, can be used to calculate the apparent Poisson's ratio, ν, and Young's modulus, E, as follows:

$$\nu = \frac{(V_l^2) - 2\,(V_s^2)}{2\,(V_l^2 - V_s^2)}$$

V_l = longitudinal velocity

V_s = shear velocity

$$E = 3\rho V_s^2\,(V_l^2 - \frac{4}{3}\,V_s^2)/(V_l^2 - V_s^2)$$

where ρ is the specimen density.

APPENDIX E

COMMUNICATION TO DR. ALEXANDER FLORENCE, SRI, JULY 8, 1977

TerraTek

July 8, 1977

Dr. Alexander Florence
Stanford Research Institute
333 Ravenwood Ave.
Menlo Park, CA 94025

Dear Alex:

As per your request, we have conducted material property testing on the samples of rock matching grout (RMG 2C4) that you supplied. Physical property and ultrasonic wave velocity measurements were conducted on samples from batches 1A, 2A, and 3A to verify batch consistency. Mechanical property tests were conducted on batches 1A and 3A. Mechanical tests included triaxial compression and uniaxial strain tests to 0.5 kbars confining pressure. Tests were conducted on 1 July 1977 to coincide with your test date.

Triaxial test results are shown in Figure 1 as stress difference versus individual strains. Uniaxial strain test results are shown in Figures 2 and 3. Table I lists the physical properties and ultrasonic wave velocities.

Test results show that both mechanical and physical properties are similar to the rock matching grout (RMG 2C3) previously tested[1]. Maximum stress difference at 0.5 kbar confining pressure is 0.32 kbars for the triaxial compression test which is in good agreement with the stress difference during the uniaxial strain test. Permanent volume strain resulting from the uniaxial strain test is 0.7 percent by volume.

Physical property measurements show the grout batches to be totally saturated with similar densities and porosities.

Sincerely,

Don Gardiner

D. S. Gardiner
Project Engineer

DSG/jlg

---

1. TR 76-41, "Material Properties of Stanford Institute Grout, July 1976.

UNIVERSITY RESEARCH PARK · 420 WAKARA WAY · SALT LAKE CITY, UTAH 84108 · (801) 582-2220

TABLE I

Stanford Research Institute Rock Matching Grout

SAMPLE DESIGNATION	DENSITY (gm/cc)			WATER BY WET WEIGHT (%)	POROSITY (%)	SATURATION (%)	CALC. AIR VOIDS (%)	MEAS. PERMANENT COMP. (%)	VELOCITY (km/sec)	
	AS-RECEIVED	DRY	GRAIN						LONG	SHEAR
2C4-1A	2.15	1.76	2.90	18.1	39.4	98.9	0.5	---	3.30	1.82
2C4-2A	2.15	1.75	2.87	18.6	39.2	100.0	0	---	3.23	1.81
2C4-3A	2.18	1.79	2.88	17.7	37.7	100.0	0	---	3.28	1.82

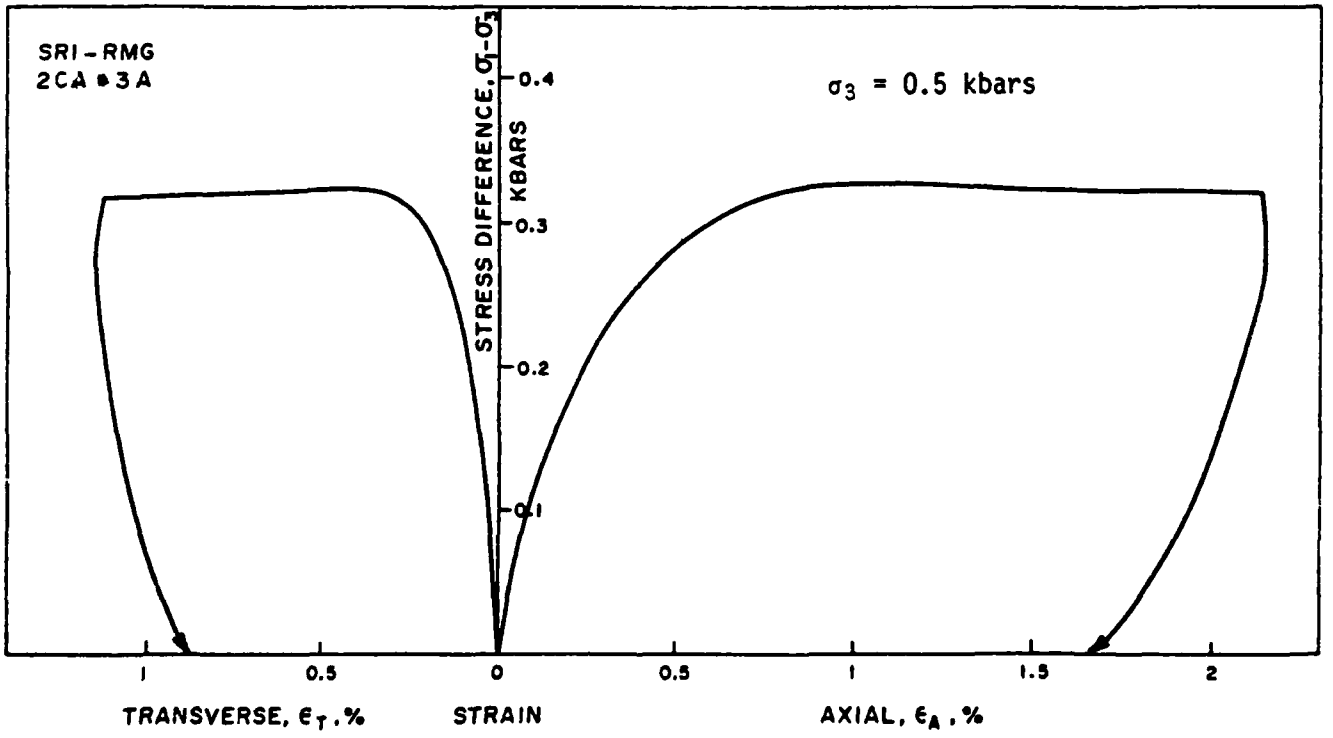

Figure 1. Triaxial compression test--stress difference versus individual strains.

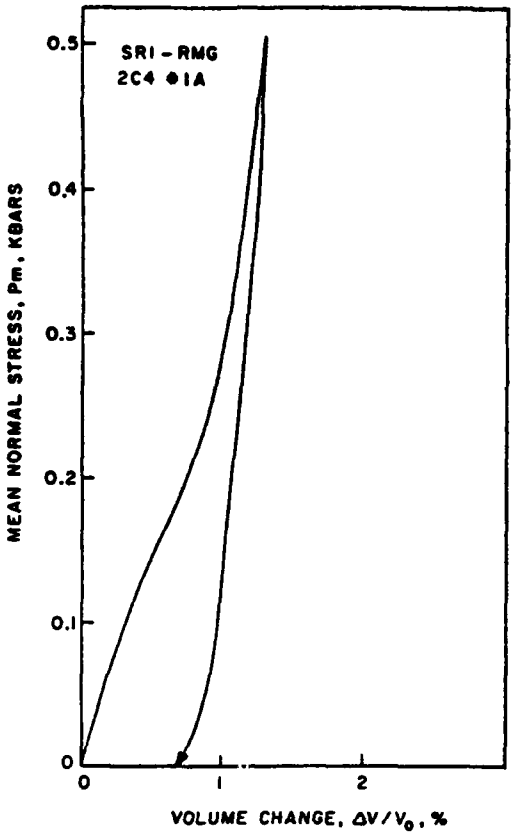

Figure 2. Uniaxial strain test--mean normal stress versus volume change.

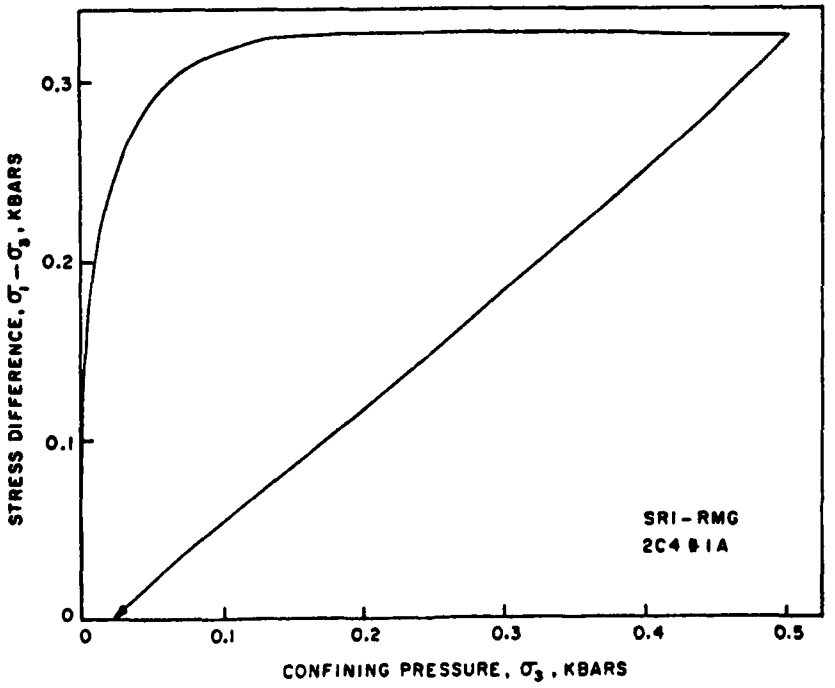

Figure 3. Uniaxial strain test--stress difference versus confining pressure.

DISTRIBUTION LIST

DEPARTMENT OF DEFENSE

Defense Nuclear Agency
ATTN: SPTD
ATTN: STSP
4 cy ATTN: TITL
4 cy ATTN: SPSS

Defense Technical Information Center
12 cy ATTN: DD

Field Command
Defense Nuclear Agency
ATTN: FCT, W. Tyler
ATTN: FCTO
ATTN: FCTE, B. Johnson
ATTN: FCTK, B. Ristvet
10 cy ATTN: FCTK, C. Keller
10 cy ATTN: FCTC, J. Lacomb

Field Command
Defense Nuclear Agency
Livermore Branch
ATTN: FCPRL
ATTN: Library

DOD/IDA Management Office
ATTN: J. Statler

DEPARTMENT OF THE ARMY

U.S. Army Engineer Center
ATTN: ATSEN-SV-L

U.S. Army Engr Waterways Exper Station
ATTN: D. Day
ATTN: J. Boa
ATTN: J. Zelasko
ATTN: W. Flathau
ATTN: Rsch Center Lib
ATTN: L. Ingram
ATTN: P. Hadala
ATTN: J. Jackson
ATTN: J. Ehrgot

Harry Diamond Laboratories
Department of the Army
ATTN: DRXDO-N-P, F. Wimenitz

Explosive Excavation Rsch Laboratory
Department of the Army
ATTN: FCPRL
ATTN: Library

Headquarters
Department of the Army
ATTN: W. Murry

DEPARTMENT OF THE NAVY

Naval Construction Battalion Center
ATTN: J. Allgood
ATTN: Code L31

Naval Ordnance Station
ATTN: Code 121

DEPARTMENT OF THE NAVY (Continued)

Naval Research Laboratory
ATTN: Code 2627 for Code 1065
ATTN: Code 2627 for Cont Branch

Chief of Naval Research
Department of the Navy
ATTN: Technical Library

DEPARTMENT OF THE AIR FORCE

Air Force Weapons Laboratory
Air Force Systems Command
ATTN: DE-I
ATTN: DEV-G, J. Bratton
ATTN: NTE, M. Plamondon
ATTN: SES, R. Henning
ATTN: Technical Library
ATTN: DEX

Air Force Cambridge Research Labs
Air Force Systems Command
ATTN: LWW, K. Thompson

DEPARTMENT OF ENERGY CONTRACTORS

Fenix & Scisson
ATTN: F. Waltman
ATTN: D. Townsend

Geotechnical Instrumentation & Grouting, Inc
ATTN: Technical Library

Structural Mechanics Assoc
ATTN: R. Kennedy

Los Alamos National Scientific Lab
ATTN: J. McQueen
ATTN: A. Davis
ATTN: Report Library
ATTN: F. App
ATTN: R. Brownlee
ATTN: B. Killian
ATTN: L. Germain
ATTN: J. House

Sandia National Laboratories
ATTN: C. Gulick
ATTN: C. Smith
ATTN: C. Broyles
ATTN: C. Mehl

Lawrence Livermore National Lab
ATTN: J. Hearst
ATTN: V. Wheeler
ATTN: McKague
ATTN: H. Rodean
ATTN: R. Terhune
ATTN: J. Shearer
ATTN: B. Hudson

Nevada Operations Office
ATTN: R. Newman
ATTN: Technical Library

OTHER GOVERNMENT AGENCIES

Bureau of Mines
Twin Cities Research Center
ATTN: T. Ricketts
ATTN: T. Atchison

Department of the Interior
Bureau of Mines
ATTN: G. Waddell/L. Obert

Department of the Interior
U.S. Geological Survey
ATTN: R. Carroll
ATTN: W. Twenhofel
ATTN: B. Ellis

DEPARTMENT OF DEFENSE CONTRACTORS

Agbabian Associates
ATTN: Technical Library
ATTN: C. Bagge

Boeing Company
ATTN: K. Fridell

General Electric Company—TEMPO
ATTN: DASIAC

Shock Hydrodynamics, Inc
ATTN: L. Zernow/K. Kreyenhagen

H Tech
ATTN: B. Hartenbaum

Holmes & Narver, Inc
ATTN: J. Calovini

Ken O'Brien & Associates, Inc
ATTN: D. Donegan

Massachusetts Inst of Technology
ATTN: W. Brace

Merritt CASES, Inc
ATTN: J. Merritt

DEPARTMENT OF DEFENSE CONTRACTORS (Continued)

R & D Associates
ATTN: R. Shaeffer
ATTN: J. Lewis
ATTN: P. Haas

SRI International
ATTN: A. Florence
ATTN: H. Lindberg

Pacifica Technology
ATTN: D. Patch
ATTN: J. Kent

Reynolds Electrical & Engr Company, Inc
ATTN: FOD/DOD, H. Edwards

Structural Mechanics Assoc
ATTN: R. Kennedy

Systems, Science & Software, Inc
ATTN: R. Duff
ATTN: Technical Library
ATTN: E. Peterson

Terra Tek, Inc
ATTN: S. Green

TRW Defense & Space Sys Group
ATTN: R1/2162, M. Schrader

Weidlinger Assoc, Consulting Engineers
ATTN: M. Baron

University of Illinois
ATTN: N. Newmark

University of Nevada
Desert Research Institute
ATTN: P. Fenske
ATTN: C. Case